Dissertation

Master of Computer Engineering

Indoor Positioning System with Smart Wi-Fi Antennas

Student: Marko Gašparović
Supervisor: João Da Silva Pereira

Leiria, March 2018.

Acknowledgements

I would like to express my gratitude to my supervisor João da Silva Pereira for his continuous support, guidance, knowledge and patience with me while working on this project. Without his help, the completion of this project would not be possible.

Special thanks go to Instituto Politécnico de Leiria and Escola Superior de Tecnologia e Gestão for providing me all the needed resources to work on and finish my dissertation. Also, a big thanks go to Instituto de Telecomunicações where I made high number of research which greatly helped me for my dissertation work.

And without a doubt my biggest support while working on this dissertation, my sister Ana and parents Ante and Jelena Gašparović, who supported all my actions. Thank you!

Abstract

The advancements of the indoor positioning system (IPS) in the recent years have been immense, yet we do not see the standardization of any solution. The system which is being used in many public scenarios is the Wi-Fi technology and the solution which we propose in this dissertation would not require change of infrastructure, but rather reusing existing one and simply enhancing it. This solution is low-cost and with relatively high precision considering current precision of Global Positioning System (GPS) of five meters. In this dissertation prototype is designed with motorized directional antennas using signal strength of two ESP8266. These position measurements are calculated and presented via micro controller and a Wi-Fi enabled device – ESP8266. Together with Yagi antenna, this solution has shown extremely good IPS characteristics and possibility to be implemented in real-case scenarios.

Key words: low-cost, Wi-Fi, access point, smartphone application, GPS, indoor localization.

Index of Figures

Index of Tables

List of Acronyms

2D	2-dimensional
3D	3-dimensional
AOA	Angle-of-arrival
AP	Access Point
ARM	Advanced RISC Machine
CDMA	Code-Division Multiple Access
CPU	Central Processing Unit
FM	Frequency Modulation
GPS	Global Positioning System
IT	Information Technology
LFSR	Linear-Feedback Shift Register
LIDAR	Light Detection and Ranging
LOS	Line-of-sight
LSR	Linear Recursive Sequences
OPDG	Orthogonal Perfect DFT Golay
RF	Radio Frequency
RSS	Received Signal Strength
TDOA	Time-difference-of-arrival
TOA	Time-of-arrival
WPS	Wi-Fi Positioning System

Index

Contents

1. Introduction

By seeing the world around, it is obvious that technology has permeated our lives. Every daily action we do, most of the time has some type of interaction with the technology. It is hard to imagine even one day without our phone or a computer and just thirty years ago all that was minimal or nonexistent. Computing has involved drastically in the recent years and the technical changes are happening exponentially faster. There was a lot of development and contribution of researchers around the world to help us to get to the point where we are now.

This dissertation is based on a research about indoor positioning system [1]. The methodology and approach of implementing the IPS is explained in detail. All the devices and technologies will be elaborated together with testing scenarios and results.

The goal of this dissertation is an implementation of a low cost indoor positioning system using two major components: Wi-Fi (Wireless Fidelity) micro controllers ESP8266 and smart motorized directional antennas. Global positioning system (GPS) is widely used in the unobstructed line of sight (LOS). As it is well known, GPS does not work inside the buildings. In addition, a problem of a GPS is that accuracy is far too big to consider it, when implementing it into indoor scenarios. In this dissertation, the new indoor localization system is made using a network of ESP8266, Wi-Fi emitter devices that work inside the buildings. A prototype is designed with directional antennas using signal strength of two micro controllers ESP8266. These signal strengths are measured and the position is calculated using the triangulation method. Finally, this gives us an opportunity for further development of an application where the user would be able to navigate through certain indoor scenario such as big shopping centers, airports etc.

This work was based on my research published in the following publications:

[P1] - J. Pereira, M. Gasparovic, M. P. M. Ferreira, INDOOR POSITIONING SYSTEM AND METHOD, 109950, March 2017, Portuguese Pending Patent.

[P2] - J. Pereira, M. Gasparovic, P. Pujari, G. Manjunath, Standing Wave Cancellation and Shadow Zone Reducing Wireless Transmitter, System and Respective Method and Uses, 109332, April 2016, Portuguese Pending Patent

[P3] - J. Pereira, M. Gasparovic, M. P. M. Ferreira, A TUNABLE FIBER BRAGG GRATING DEVICE, A SUPERSTRUCTURED TUNABLE FIBER BRAGG GRATING DEVICE AND RESPECTIVE USES AND OPERATING METHODS, 109554, July 2016, Portuguese Pending Patent.

[P4] - J. Pereira, M.P.M. Ferreira, M. Gasparovic, Tunable Super-Structured Fiber Bragg Gratings with Perfect Sequences Based on m-Sequence, Journal of Electronic Science and Technology, JEST, Vol. 15, No. 4, pp. 358 - 363, December 2017.

[P5] - J. Pereira, M.P.M. Ferreira, M. Gasparovic, Tunable super-structured fiber Bragg gratings with perfect sequences, OAHOST - Open Access Journal, Vol. 1, No. 1, pp. 1 - 15, October 2016.

[P6] - J. Pereira, M.P.M. Ferreira, M. Gasparovic, Tunable Super-Structured Fibre Bragg Gratings with Perfect Sequences, Energy Material Nanotechnology, Beijing, China, Vol. 1, pp. 29 - 29, April 2016.

[P7] - M. Gasparovic, P. Nicolau, A. Marques, C. Silva, L. Marcelino, On Privacy in User Tracking Mobile Applications, Information Systems and Technologies (CISTI), 2016 11th Iberian Conference, 16191805, 5-18 June 2016

2. State of the Art

Indoor positioning system has a significant impact in different aspects of life. With Indoor Positioning System (IPS) and positioning system in general, more solutions are being discovered with the importance of orientation in space. Nowadays, if we travel around the globe, rarely we can see people using standard maps to find directions. With the technology swiftly growing this has been revolutionized in a way that only a smartphone and an application is needed to abandon traditional maps. The development of the indoor positioning system doesn't mean it must necessarily be related only to the research and tests being discovered in this area. There are many research, patents and products which can help us in receiving more ideas and giving us an opportunity to have an approach from a different angle. In the following sections, we will describe some of the essential elements which can have a beneficial spot in indoor positioning system.

It is possible to calculate indoor positioning in a multitude of ways and we can choose from variety of wireless technologies. One of the methods which is gaining popularity and many of the systems try to use it is a Wi-Fi access point based to create a Wi-Fi Positioning System (WPS). In this dissertation we are also working with the mentioned technology, however, in the following paragraphs we will not only concentrate on Wi-Fi based research, but rather on different technologies to discover more ways on how to create a reliable indoor positioning system.

2.1. HTC Vive – Virtual Reality (VR)

Virtual technology is developing rapidly and research proves that VR technology is the development of all aspects of life and that will have a big impact on the life in the future [2]. We are all experiencing this impact while the technology is developing and it is important to research and observe the VR solutions discovered for positioning and orientation. HTC Vive is one of the examples where its technology requires high precision without errors and latency. Every VR typically consists of a head mounted display and a position and orientation tracking system. To understand better the setup of the VRs refer to the following paper [3] where they explain parts of another product from the VR technology – Oculus rift. In addition to general components, Vive has two controllers and two infrared laser emitter units which are designed to track an observer who freely moves through space of up to 4 x 4 meters [4].

Figure 1 - HTC Vive with its components [5]

Relatively expensive head-mounted display (HMD) and position and orientation tracking system could enable a far larger number of researches to conduct experiments with moving observers in VR environments. The first commercially available system that has the promise to fulfil this ambition is the HTC Vive. In the tests performed [4] we see position and orientation tracking capabilities. Tracking is subjectively fast and supports good presence, the system end-to-end latency is low at 22 ms, and the noise level in the tracker output is low. This example serves as an important point for its insights in the interaction between one point which is acting as an information receiver and the other which is information transmitter. We were unable to find a specific value for a HTC Vive precision, however, knowing its capabilities in tracking in-game experience, precision is measured in millimeters.

2.2.MIT - Chronos

Researchers from Massachusetts Institute of Technology (MIT) have developed technology which can locate the Wi-Fi enabled devices within centimeters [6]. Their invention/technology is called Chronos [7] and relies on making the devices emulate multi-gigahertz wideband radios.

Chronos works in a way where two Wi-Fi devices, a transmitter and a receiver, change all 35 frequency bands every 2 to 3 microseconds calculating the distance and the angle between the devices. At each band receiver is comparing the phase difference so it can calculate the time of flight, therefore, determine the distance between the devices. In other words, Chronos stitches the measurements from different Wi-Fi bands to calculate signal's travel distance, by multiplying the time of the flight by the speed of the light [8]. Please refer to the Figure 2 to understand better the ration between frequency and the distance and how the travel distance is calculated. Knowing both the distance and the angle allows to compute the user's position using just one access point.

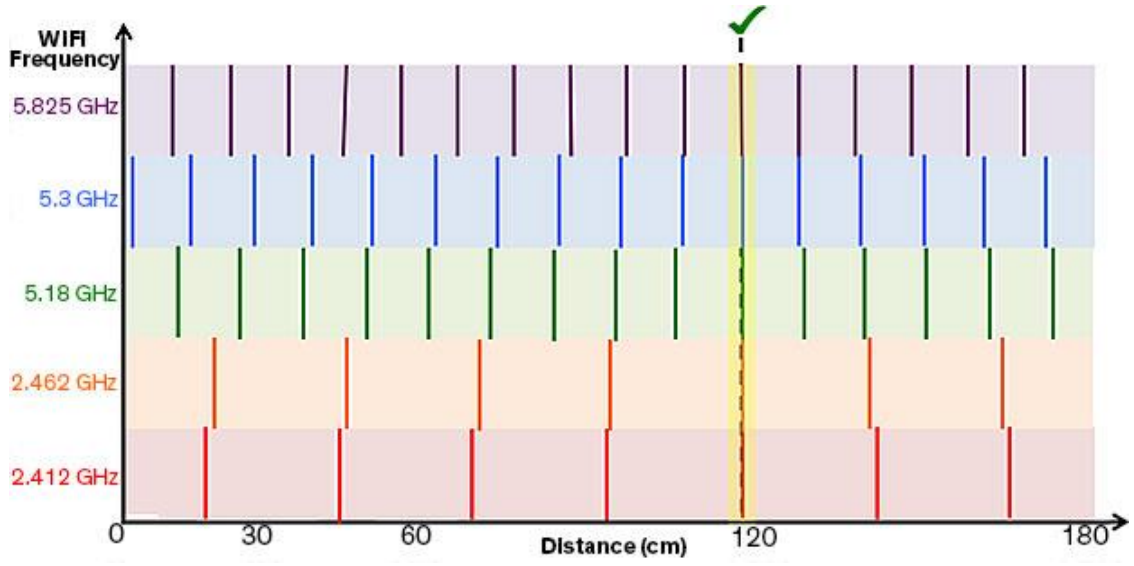

Figure 2 - MIT Chronos determining the distance [6]

The accuracy of this invention is about 10 times the accuracy of the GPS since in testing the MIT researchers could locate the device within 65 cm using the devices from everyday environment using only an application. However, there are few limitations of this invention. Each device must perform a one-time distance calibration and at that time, both devices need to be in a still position. If the devices are moving relative to each other, accuracy drops significantly. Additionally, there are issues with the delay of the transmitting packet signal and it can bounce of different objects for not satisfying accuracy results.

2.3.Broadcom chip - BCM47755

Company Broadcom has announced testing of the first chip which can have an advantage as a new technology in global navigational system. Its accuracy should enable smartphones improved 30 cm accuracy, which is exceptionally better than today's 5 meters. Moreover, Broadcom is stating that the chip will be able to work even in the streets which are surrounded by tall concrete buildings with usage of only half of the power which today's era of chips are using.

Figure 3 - Broadcom BCM47755 chip [9]

Name of the chip is BCM47755 and it has been told that it will be incorporated in some of the smartphones in 2018, however, there is no info which smartphones model could include this chip [10]. The BCM47755 supports two frequencies (L1+L5) see Figure 4 highlighted area, and as a result, achieves lane-level accuracy outdoors and much higher resistance to multipath and reflected signals in urban scenarios, as well as higher interference and jamming immunity [9].

System	Signal	Frequency (MHz)	Wavelength λ_i (m)	Signals combined	Widelane λ_W (m)	Narrowlane λ_N (m)
	i	f_i	$\lambda_i = c/f_i$	ij	$c/(f_i - f_j)$	$c/(f_i + f_j)$
GPS	$L1$	1575.420	$\lambda_{L1} = 0.190$	$L1, L2$	0.862	0.107
	$L2$	1227.600	$\lambda_{L2} = 0.244$	$L1, L5$	0.751	0.109
	$L5$	1176.450	$\lambda_{L5} = 0.255$	$L2, L5$	5.861	0.125
GLONASS (k=0)	$G1$	1602.000	$\lambda_{G1} = 0.187$	$G1, G2$	0.842	0.105
	$G2$	1246.000	$\lambda_{G2} = 0.241$	$G1, G3$	0.760	0.107
	$G3$	1204.704	$\lambda_{G3} = 0.249$	$G2, G3$	7.827	0.122
Galileo	$E1$	1575.420	$\lambda_{E1} = 0.190$	$E1, E5b$	0.814	0.108
	$E5b$	1207.140	$\lambda_{E5b} = 0.248$	$E1, E5a$	0.751	0.109
	$E5a$	1176.450	$\lambda_{E5a} = 0.255$	$E5b, E5a$	9.768	0.126

Figure 4 - GPS signal different frequencies [11]

Furthermore, the BCM47755 incorporates numerous technologies that enable ultralow power consumption in both the location function and the sensor hub function. The device features a low-power Radio Frequency (RF) path, a Big/Little Central Processing Unit (CPU) configuration composed of an Advanced RISC Machine (ARM)-based 32-bit Cortex-M4F (CM4), an ARM-based Cortex-M0 (CM0), and is built in a 28 nm process [9].

2.4. Other findings

In this section we describe some of the findings which are related to this work and can be of a potential value for the future of indoor positioning system development.

2.4.1. Tesla

According to the Vice article [12] where it says that Tesla's system estimates the position of the car in the tunnel by the steering wheel rotation and speed of the wheels, with the Broadcom chip (2.3) where the GPS precision would be narrowed to 30 cm it could detect the person with the smartphone exact position when entered into enclosed space and it can track the user by counting the steps made using accelerometers and position of the phones using gyroscope.

2.4.2. Light Detection and Ranging (LIDAR) and GPS signal

In the paper [13] the aim is to introduce the GPS positioning results into indoor environment and to combine ultra-wide band (UWB) indoor positioning method with the coordinate information of point cloud data. Their method combines GPS signals and point cloud data effectively, taking advantage of the characteristics of point cloud such as high density, high precision and containing geographic information. According to the results of their experiments, the precision of indoor positioning achieves level which is sub-meter.

2.4.3. Exploring Vision-Based Techniques

This paper describes investigation of utilizing image-based techniques together with context information to provide an outdoor positioning system. They named the system Human-centric Positioning System, i.e., HoPS. The system revolves around humans rather than machines. As described, humans can conveniently trigger the system as necessary by leveraging wearables like Google Glass [14].

2.5. Josip Bagaric - Indoor Positioning System for Mobile Devices

Proposed solution for IPS for mobile devices in the thesis by Josip Bagaric was based on the communication of the FM transmitters and receivers [15]. This communication was tested using four different codes – Golay, Chu, OPDG and ZigBee, from which only Orthogonal Perfect DFT Golay (OPDG) and ZigBee showed satisfying results. The OPDG coding sequences have perfect autocorrelation properties therefore they are a good candidate to be used in asynchronous communication systems. The properties of the OPDG coding sequences allow for enhanced detection of codes. On the other hand, a key component of the ZigBee protocol is the ability to support mesh networking. In a mesh network, nodes are interconnected with other nodes so that multiple pathways connect each node. Connections between nodes are dynamically updated and optimized through sophisticated, built-in mesh routing table [16].

Table 1 - Average indoor location estimation error between two transmitters - Golay, Chu, ZigBee and OPDG [15]

Code Family	Average estimation error
Golay	13.48 m
Chu	14.28 m
ZigBee	7.99 m
OPDG	3.67 m

Research done in this thesis shows us following results, displayed in Table 1 shows that using the OPDG codes was possible to estimate the position of the receivers between two transmitters with an error near 3.5 meters, when a frequency carrier around 100 MHz is used. Also, this shows better estimation properties than ZigBee, Golay and Chu codes, which had an error higher than 7, 13 and 14 meters respectively [15].

We wanted to continue the work and try to acquire better results, but this showed us that different approach might be needed to obtain better results. With use of Wi-Fi technology and directional antennas precision is narrowed down to centimeters.

2.6.Daniela Taipe - Sistema de Localización Indoor y Outdoor

In order to use the Angle of Arrival (AoA) technique explained in the section 4.5, we will use the mathematical method described in the dissertation of Daniela Taipe [17]. Figure 5 shows the arrangement of antennas, which allows estimating the Received Signal Strength (RSS) in a certain angular interval through the AoA method. Each reference node (A, B) must have a known location with coordinates (X_i, Y_i) (i = 1, 2, ...). These nodes are making scan movement and locating the maximum intensity of the signal emitted by the target. This is measured by angles representing the direction of propagation α and β. [17]

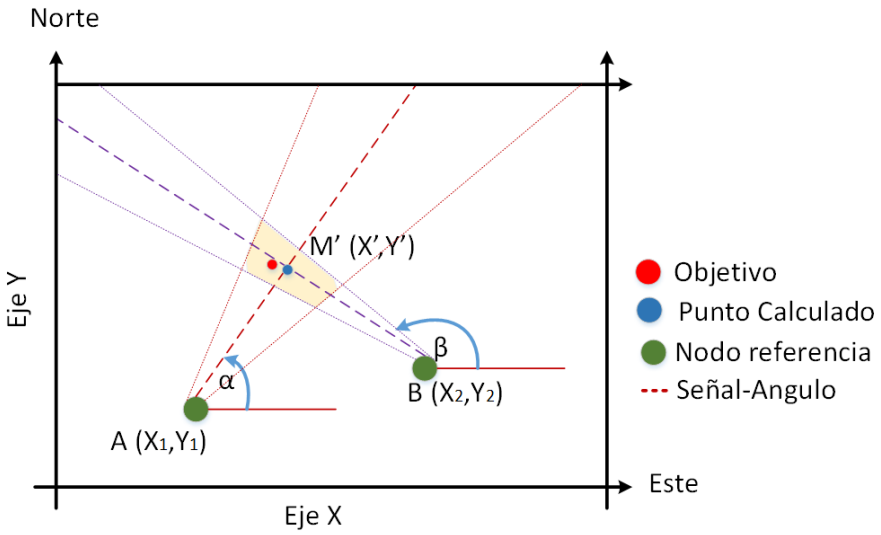

Figure 5 - Positioning RSSI-AOA [17]

To understand the explanation, we used image from Daniela's dissertation Figure 5, and below is the English version.

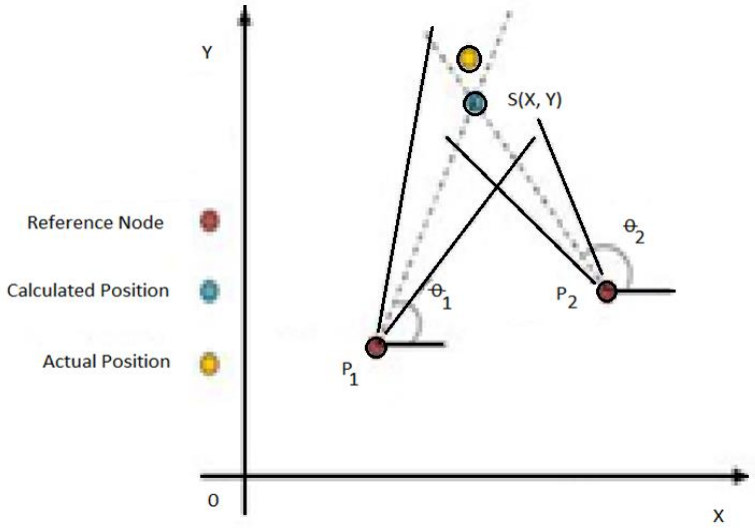

Figure 6 – AoA method

2.6.1. Mathematical method – Triangulation

After the angle measurements, it is necessary to find the line that symbolizes the direction of maximum propagation. This calculation is made to each of the reference points or nodes (P_R) in this case A and B, with previous information of their coordinates (X_i, Y_i) and their respective angles (α and β), in addition to the point of intersection between them ($M' = (X', Y')$), through the equation of the line (1) (2) (3).

Line AM'

$$m = Slope = \tan\alpha = \frac{Y' - Y_1}{X' - X_1} \quad (1)$$

$$\tan\alpha\,(X' - X_1) = Y' - Y_1 \quad (2)$$

Where

$$X' \tan\alpha - X_1 \tan\alpha = Y' - Y_1 \quad (3)$$

Then we obtain following equations which represent X' and Y':

$$Y' = X' \tan\alpha - X_1 \tan\alpha + Y_1 \quad (4)$$

$$X' = \frac{Y' - Y_1 + X_1 \tan\alpha}{\tan\alpha} \quad (5)$$

Line BM'

$$m = Slope = \tan\beta = \frac{Y' - Y_2}{X' - X_2} \quad (6)$$

$$\tan\beta\,(X' - X_2) = Y' - Y_2 \quad (7)$$

Where

$$X' \tan\beta - X_2 \tan\beta = Y' - Y_2 \quad (8)$$

Then we obtain following equations (9) (10), which represent X' and Y':

$$Y' = X' \tan\beta - X_2 \tan\beta + Y_2 \quad (9)$$

$$X' = \frac{Y' - Y_2 + X_2 \tan\beta}{\tan\beta} \quad (10)$$

With previously obtained equations, we calculate X' and Y'. Using X' using equations from (4) and (10), we acquire equation (11).

$$X' = \frac{X_1 \tan\alpha - X_2 \tan\beta + Y_2 - Y_1}{\tan\alpha - \tan\beta} \quad (11)$$

Similarly, equations (5) and (11) are used, which returns Y' in equation (12).

$$Y' = \frac{(X_1 - X_2)\tan\alpha \tan\beta - Y_1 \tan\beta + Y_2 \tan\alpha}{\tan\alpha - \tan\beta} \quad (12)$$

Finally, equations (11) and (12) allow the localization of the node M' (X', Y'), as shown in Equation (13):

$$M' = \frac{X_1 \tan\alpha - X_2 \tan\beta + Y_2 - Y_1}{\tan\alpha - \tan\beta}, \frac{(X_1 - X_2)\tan\alpha \tan\beta - Y_1 \tan\beta + Y_2 \tan\alpha}{\tan\alpha - \tan\beta} \quad (13)$$

The advantage of using AoA position estimation is that it does not need to use many devices for both 3D and 2D measurement, in addition it doesn't require a time synchronization.

2.7. Positioning System (PS)

A PS is a system for determining the location of an object in space. It is a way to identify the location of certain object using specific positioning system technologies. There are variety of technologies, which are used regarding several factors. Is the system made for outdoor or indoor scenarios and what level of precision does the system need? Technologies for this task exist ranging from worldwide coverage with kilometer accuracy to workspace coverage with centimeter accuracy. In the next paragraph, we will explain the Global Positioning System (GPS), since it is the most used outdoor geo-localization system, its strengths and weaknesses and most importantly how it is related to this work.

2.8. Global Positioning System

A global positioning system (GPS) is used for estimating the position of a mobile object such as a mobile phone in a global geometrical region which includes a GPS satellites and a GPS receiver for receiving radio waves from the satellites [18]. As it is well known GPS to function properly needs satellite and receiving GPS device to be in a line of sight (LOS). If this is not accomplished satellites are unable to locate device, thus, we are unable to estimate the position of the device. In the next paragraph, we will point out the advantages and disadvantages of GPS.

- Advantages of GPS
    - Used worldwide
    - Available in almost every point on earth (see Figure 7)
    - Relatively small error rate for outdoors (avg. ≤7.8 m with 95% probability) [19]
- Disadvantages of GPS
    - Error rate too high for precise location estimation
    - Attenuated by solid objects
    - Cannot work without LOS

The GPS sounds like a perfect solution for determining location, however there is one big weakness of this technology that prevents being used in closed spaces. The signals of the GPS are using wave frequency which until it reaches the ground it attenuates and scatters by roofs,

walls and other objects so it becomes unusable without LOS. A GPS device to work properly needs LOS with the satellites to precisely determine where the device is physically located. Besides problem of LOS due to walls and rooftops when using GPS inside of a building, there are also numerous other barriers which can interfere and make it impossible to locate device precisely or even to locate device at all. Signals which are using short wavelengths the energy is very high, like x-rays and gamma rays. These signals go through things solely because of their high energy. At lower energies (longer wavelengths) such as RF signals, the waves interact with the material in various ways so that they can get absorbed, refracted, reflected, and re-emitted. The frequencies of Wi-Fi and GPS does not differentiate by much (see Table 2), however here is also important the energy of the signal and how close is the emitter from the receiver.

On the Figure 7 we can see the position of the satellites around the globe. There are 24 GPS satellites from which 21 active and 3 passive ones (spare) which are in the orbit approx. 17.000km above the ground. They are positioned so that from any point on earth four satellites will be above the horizon. Every satellite consists of:

- Computer
- Atomic clock
- Radio

Each satellite broadcasts the position change and time, and on the ground, every GPS receiver on smartphones, gadgets etc. calculates triangulation between 3 of the 4 satellites and the result is provided in the geo-position as latitude and longitude.

Figure 7 - GPS coverage [20]

Table 2 - Frequency comparison

	Radio Frequency	GPS	Wi-Fi	X-ray
Low	0.000003 GHz	1.23 GHz (L2)	2.4 GHz	3×10^{16} Hz
High	300 GHz	1.57 GHz (L1)	5 GHz	3×10^{19} Hz

2.9. Indoor Positioning System

An indoor positioning system is a method of localizing a person/object in an indoor environment by identifying the orientation and direction of a person/object to provide a true location of the person/object without navigation errors [21].

2.10. Wireless technologies

Here we describe one of the most common wireless technologies which are being used for IPS among others.

2.11. Wi-Fi

In this section, we will cover about Wireless Fidelity (Wi-Fi) since this is the main technology used in this dissertation. We used Wi-Fi as a base to this project, where we use it as a main source of communication and positioning system.

Wi-Fi technology is mainly used for wireless local area networking which is based on the IEEE 802.11 standards. There are numerous devices which are using Wi-Fi technology including smartphones which nowadays every person has at least one and this is one of the reasons why this technology is suitable option for indoor positioning system. Devices which are Wi-Fi compatible can connect to the wireless access point (AP) and in our case, we used it as a transmitter of the Wi-Fi signal. When there are objects which could interfere with the signal such as walls, tables, etc. the range of AP is usually around 20 meters to 70 meters depending on the exact standard shown in Table 3. This value increases outdoors or in open spaces and signal can reach much further distance as shown in the table. These 20 to 70 meters indoor can be increased by using directional Yagi antenna which uses frequency carrier of 2.4 gigahertz.

Table 3 - 802.11 protocol comparison [22]

802.11 Protocol	Freq (GHz)	Bandwidth (MHz)	Approximate indoor range	Approximate outdoor range
-	2.4	20	20 m	100 m
a	3.7/ 5	20	35 m	120 m
b	2.4	20	35 m	140 m
g	2.4	20	38 m	140 m
n	2.4/5	20 - 40	70 m	250 m

2.12. Frequency modulation (FM) signal

FM broadcasting is a method of radio broadcasting using frequency modulation (FM) technology. To generate a frequency modulated signal, the frequency of the radio carrier is changed in line with the amplitude of the incoming audio signal [23]. Some of the advantages of using FM signals above others is their resilience to noise, easiness to apply modulation at a low power stage of the transmitter and a possibility to use efficient RF amplifiers with frequency modulated signals: There have been several attempts to create and IPS using this technology and one of them is presented here [15].

3. Devices and Methodology

In this chapter we are going to describe devices and application which were used in this project and explain how they work as well as the technologies related to this work.

3.1.ESP8266

ESP8266 is a low-cost Wi-Fi chip with full TCP/IP stack and MCU (Micro Controller Unit) capability. The ESP8266 is capable of either hosting an application or offloading all Wi-Fi networking functions from another application processor. On the image below, you can see the pins structure and this board can be directly connected to a computer via micro USB cable to power it up and to transfer the written programs in it. The IDE for this board is Arduino application.

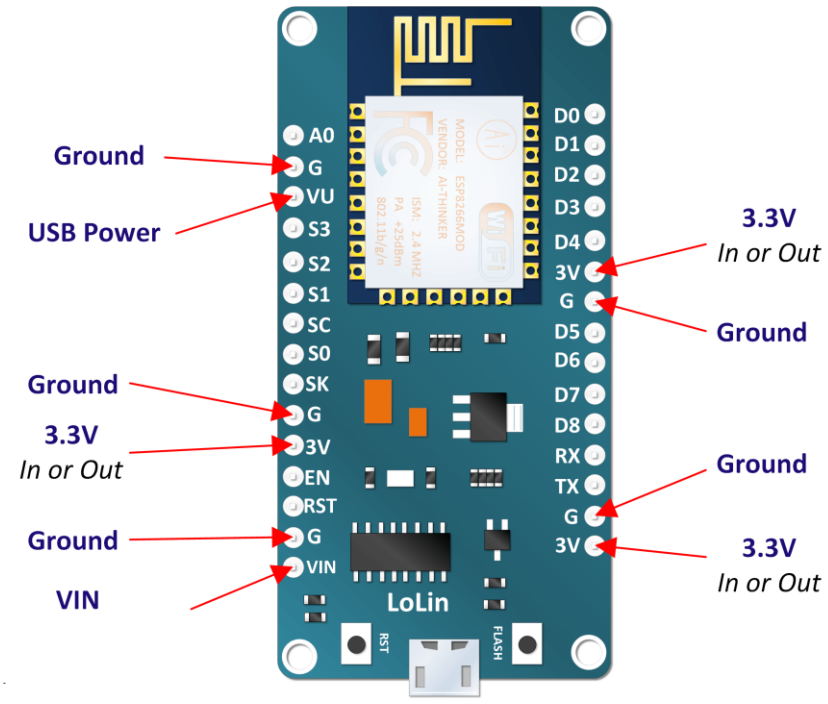

Figure 8 - ESP-12E Board with ESP8266 chip - pinout [24]

The exact model used in this project is ESP8266 ESP-12E NodeMCU which we can see on the Figure 8 and Figure 9.

.

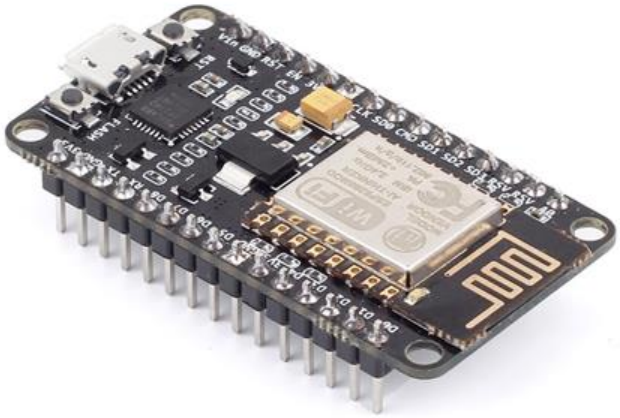

Figure 9 - ESP-12E NodeMCU

3.2. Yagi antenna

A Yagi–uda antenna, commonly known as a Yagi antenna, is a directional antenna consisting of a driven dipole, a parasitic dipole reflector and one or more parasitic dipole directors. All the elements usually lie on the same plane and can be distributed symmetrically [25]. The Yagi antenna consists of a single driven element, typically a dipole. This is the only part of the antenna where the signal is applied. The other parts are parasitic elements, meaning they either reflect or help transmitting the energy in particular directions [26]. Yagi antenna is an example of a multielement parasitic array [27]. A parasitic array consists of one or more parasitic elements with a driven element. The amount of power gain depends on the lengths of the parasitic elements and the spacing between them such as in Yagi antenna [28]. The Yagi antenna shown in Figure 10 has three directors. The greater number of parasitic elements used, the greater the gain. However, a greater number of such elements causes the array to have a narrower frequency response as well as a narrower beam width. Therefore, proper adjustment of the antenna is critical. The gain does not increase directly with the number of elements used. For example, a three-element Yagi array has a relative power gain of 5 dB. Adding another director results in a 2 dB increase. [27]

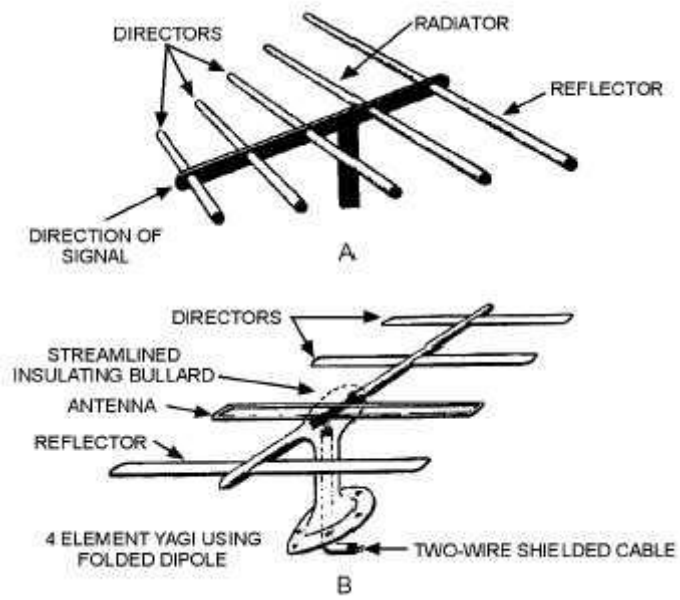

Figure 10 - Yagi antenna parts [26]

On the image below, we can see the type of Yagi antenna used for this project. As shown in the Figure 11 this Yagi antenna consists of six elements where element A is being a reflector, element B the radiator and C-F directors.

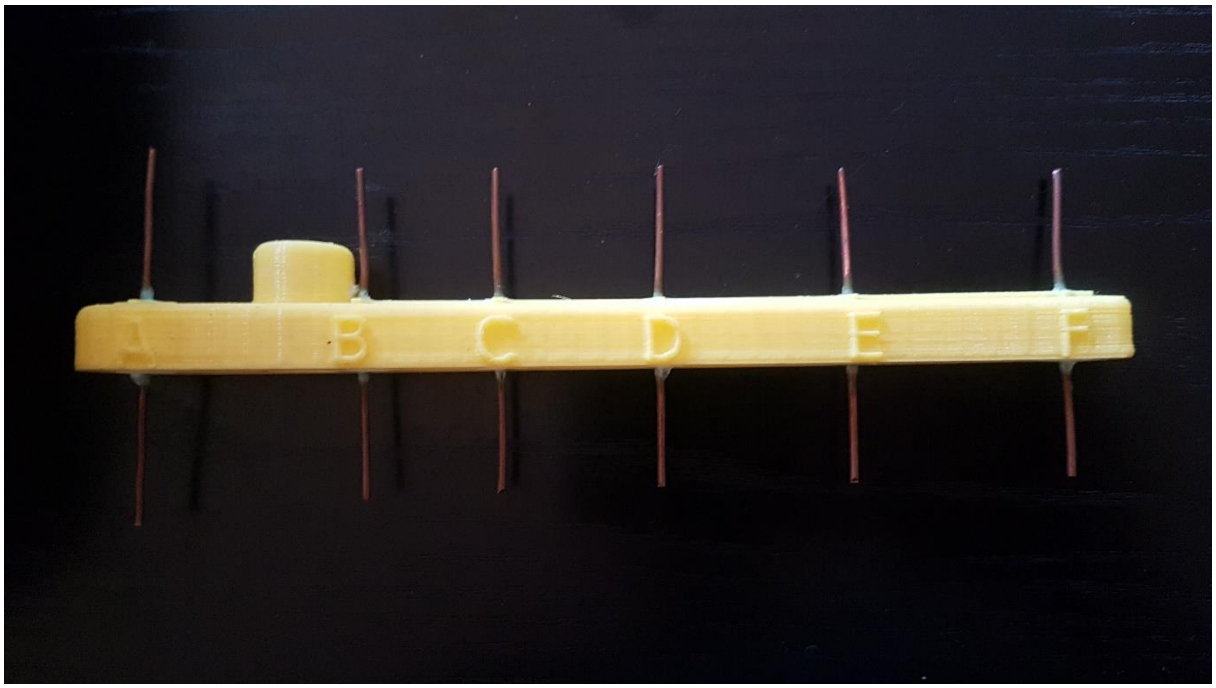

Figure 11 - Yagi Antenna

On the Figure 12 is shown custom made directional Yagi antenna for 3D printed which is used for WLAN signal. It is adjusted for 2.4 Ghz WLAN and optimizing the Wi-Fi environment

[29]. Uses 1 mm diameter copper rods.

Position - Length:

- A - 59 mm
- B - 52 mm
- C - 51 mm
- D - 50.5 mm
- E - 50 mm
- F - 49 mm

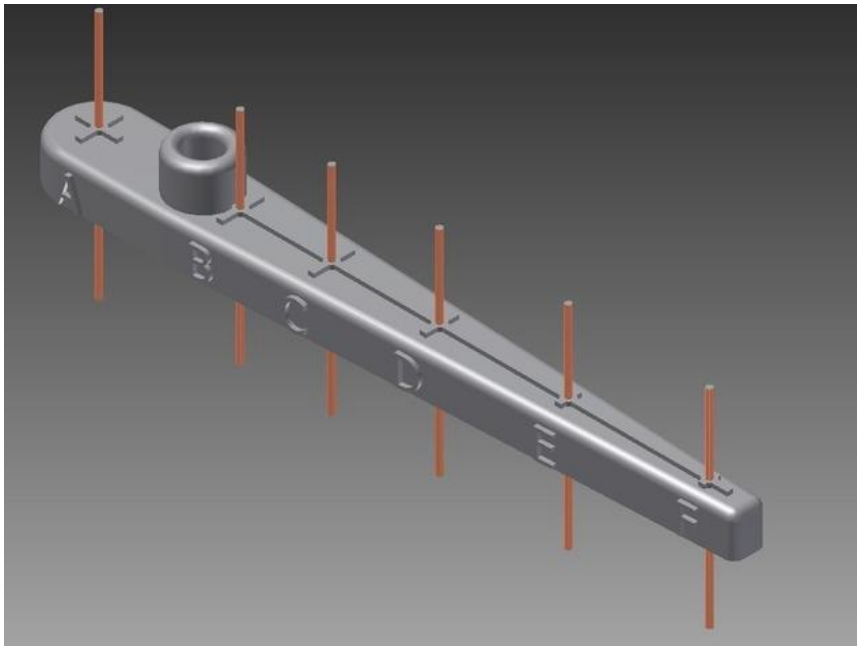

Figure 12 - 3d printed Yagi antenna [29]

3.3. Servo motor

A servo motor is a rotary actuator that allows precise control of angular positions, velocity and acceleration. The pulse is fed to the servo via a control line. The control line does not supply power to the motor directly it is an input to a control chip inside the servo and as such it does not have to supply much current to the servo [30]. For our project, servo motor is receiving an input signal from control device to scan the room as well as an output device to send its current angle value. Also, we used servo as facilitating device to automate some of the measurements. On the Figure 13 is shown the type of the servo used in this project.

Figure 13 - Servo motor [31]

This servo motor has very good specifications and that is the reason why it was used in this project to motorize Yagi antennas. These specifications are shown in the table below.

Table 4 - Servo motor specifications [31]

Specifications	
Modulation:	Analog
Torque:	**4.8V:** 25.00 oz-in (1.80 kg-cm)
Speed:	**4.8V:** 0.12 sec/60°
Weight:	0.32 oz (9.0 g)
Dimensions:	**Length:** 0.91in (23.0 mm) **Width:** 0.4in (12.2 mm) **Height:** 1.14 in (29.0 mm)
Motor Type:	3-pole
Gear Type:	Plastic
Rotation/Support:	Bushing
Pulse Width:	1.1.

3.4. Wi-Fi analyzer app

The ’Wi-Fi analyzer app’ application detects all existing Wi-Fi networks in the environment, with their corresponding signal strength and channels. As shown in Figure 14 we see ESP139610 network – the network of our ESP8266 is detected with all other Wi-Fi signals in range. Also, there are a different view options which can help us in detecting the correct signal and performing measurements.

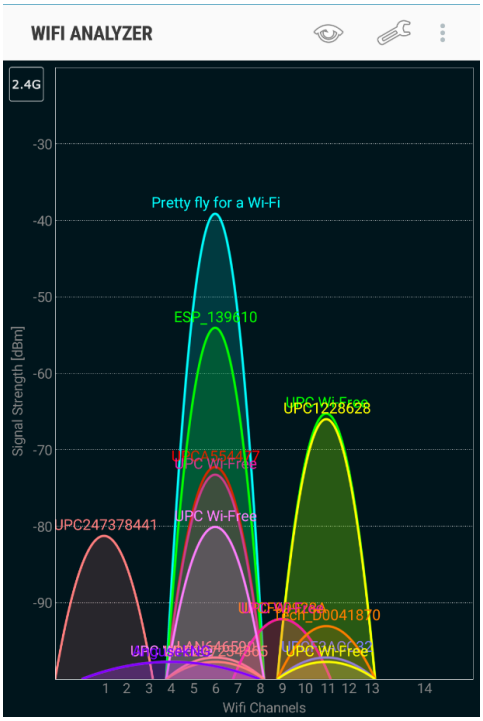

Figure 14 - Wi-Fi analyzer - mobile application to detect Wi-Fi signal strength

Below in the Figure 15 we can see the graphical representation of the Wi-Fi signal shown in real-time with its oscillations. This type of graphical interface helped us to get the precise graphs without margin for errors.

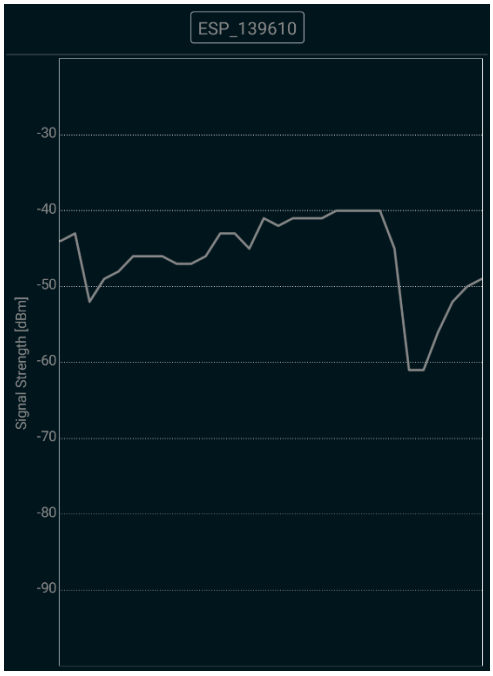

Figure 15 - Wi-Fi analyzer - graphical time view in seconds of the ESP8266 signal

3.5. Triangulation

Triangulation is the technique using the geometric properties of triangles to compute objects' location. The location is estimated relatively to some known framework. Triangulation has two derivations; Lateration and Angulation.

3.5.1. Lateration

Lateration is the technique to locate an object by measuring its distance from multiple reference positions, while angulation is the technique used to locate an object by computing angles or bearings relative to multiple reference positions. This technique must have at least three non-collinear nodes that form a 2-dimensional calculation, called trilateration. See Figure 16.

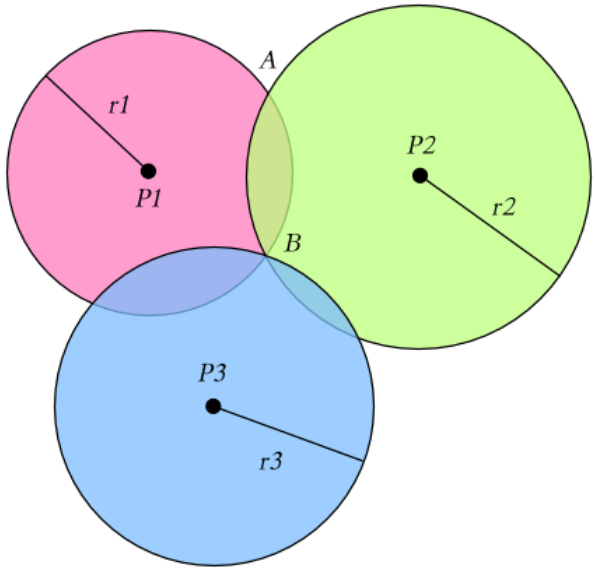

Figure 16 - Trilateration [32]

As shown in Figure 16 the black points represent the reference nodes (P1, P2, P3) with their respective radius the distance (r1, r2, r3). By relating them, the objective is estimated (B). This method is based on following techniques: Time of Arrival (ToA) / Time of Flight (ToF), Time Difference of Arrival (TDoA), Round-Trip Time of Flight (RToF), Received Signal Strength Indication (RSSI).

- **ToA/ToF** - is the travel time of a radio signal from a single transmitter to a remote single receiver.
- **TDoA** - is the technique in which the time of arrival of a specific signal, at physically separate receiving stations with precisely synchronized time references, are calculated.
- **RToF** - This technique measures the round-trip time by the signal from the transmitter to the receiver, and complies with the same measurement mechanism as ToA.

- **RSSI** - is a measurement of the power present in a received signal.

3.5.2. Angulation

Angulation is a technique like lateration with the difference that it uses angles to estimate the position. It is known as the direction of arrival (Direction of Arrival, DoA) or angle of arrival (AoA). This localization method is used in this project in correlation with Wi-Fi. The system consists of Yagi antennas placed around the room to be able to be implemented together with this technique. These antennas are rotary and directional that sweep in a certain range, to receive the strongest signal from a mobile device.

3.6. Sequences

The autocorrelation function of a sequence is a measure for how much the given sequence differs from its translates. Periodic binary sequences with good correlation properties have important applications in various areas of engineering [33]. Golay, Chu, OPDG, ZigBee codes are sequences that have been used previously in an indoor position system.

3.6.1. CDMA

CDMA (Code-division multiple access) is an example of multiple access, where several transmitters can send information simultaneously over a single communication channel. This allows several users to share same bandwidth. There is no restriction on time and frequency in this scheme. All the users can transmit at all times and at all frequencies. Because users are isolated by code, they can share the same carrier frequency, eliminating the frequency reuse problem encountered in other technologies [34]. CDMA deals with minimizing the multiuser interference by allowing them to share the same bandwidth at the same time. For this purpose, specific set of codes is used to encode and decode the sending value. On the image below Figure 17, we can see the difference between Frequency Division Multiple Access (FDMA), Time Division Multiple Access (TDMA) and Code Division Multiple Access (CDMA).

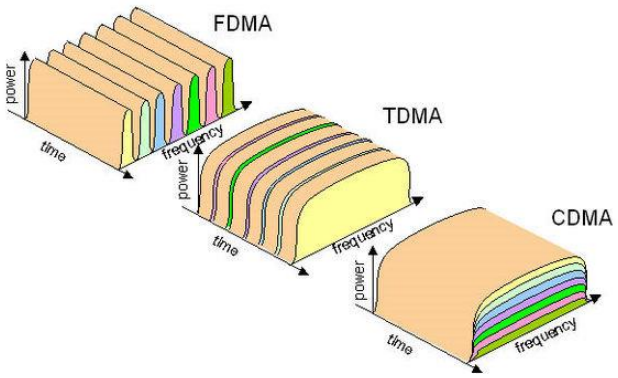

Figure 17 - FDMA, TDMA and CDMA graph comparison [34]

3.6.2. M-sequences

M-sequences are used in CDMA systems. Linear-feedback shift register LFSR generators produce what are called linear recursive sequences (LRS) because all operations are linear. LFSR is a shift register whose input bit is a linear function of its previous state. The length of the sequence before repetition occurs depends upon two factors, the feedback taps and the initial state [35]. An LFSR of any given size m (number of registers) can produce every possible state during the period $N=2^m-1$ shifts, but will do so only if proper feedback taps have been chosen. For example, such an eight stage LFSR will contain every possible combination of ones and zeros after 255 shifts. Such a sequence is called a maximal length sequence, maximal sequence, or less commonly, maximum length sequence. It is often abbreviated as m-sequence. The most commonly used linear function of single bits is exclusive-or (XOR). If an m-sequence is mapped to an analog time-varying waveform, by mapping each binary zero to -1 and each binary one to +1, then the autocorrelation function for the resulting waveform will be unity for zero delay [36].

In the previous Josip Bagaric's dissertation [19], the m-sequences have been integrated in an Indoor Positioning Solution with CDMA. For this reason, the m-sequences have been object of a study as a coding source for a new AoA Indoor Positioning System. In our case, there are two ways how m-sequences could be integrated. We can have a Yagi antenna which would turn off and on in the m-sequence pattern or to have the movement which resembles the pattern of m-sequences. The outcome of implementing m-sequence would be minimizing the interference due to a high number of Yagi antenna signals and other mobile devices. This solution is not implemented. However, the study of new AoA IPS coding methods with m-sequence resulted in 3 new papers "Pereira, M. P. M. Ferreira, M. Gasparovic, Tunable Super-Structured Fiber Bragg Gratings with Perfect Sequences Based on m-Sequence, Journal of Electronic Science and Technology, JEST, Vol. 15, No. 4, pp. 358 - 363, December 2017", " J. Pereira, M. P. M. Ferreira, M. Gasparovic, Tunable super-structured fiber Bragg gratings with perfect sequences, OAHOST - Open Access Journal, Vol. 1, No. 1, pp. 1 - 15, October 2016", and "J. Pereira, M.P.M. Ferreira, M. Gasparovic, Tunable Super-Structured Fibre Bragg Gratings with Perfect Sequences, Energy Material Nanotechnology Beijing, China, Vol. 1, pp. 29 - 29, April 2016" that can be applied in optical CDMA systems. These 3 research papers, with m-sequence application, have been placed in appendix of this dissertation.

4. Results

To have a better visibility in the outcome of this project we needed to perform several simulations of a real world indoor test scenarios. Starting with the real-time graphical measurements of the ESP8266 with integrated motorized Yagi antenna, then moving to the 2D scenarios using different methods for increasing the Wi-Fi signal and comparing it.

4.1. Real-time graphical measurements

For the first measurement, we had to create an environment with following devices:

- ESP8266 – ESP12
- Servo motor
- Arduino Uno
- 3D printed ESP8266+Servo stand
- Smartphone with Wi-Fi analyzer application

On the image below Figure 19 it is shown how these devices were positioned in the room. In front we have mobile phone with an application and in the distance rest of the equipment. To understand how the mechanism is made and how it is working it is shown on Figure 18. We are using the stand for the servo motor which was moving the mount with ESP8266 in a certain direction.

NOTE: Use of Arduino Uno was only for testing purposes.

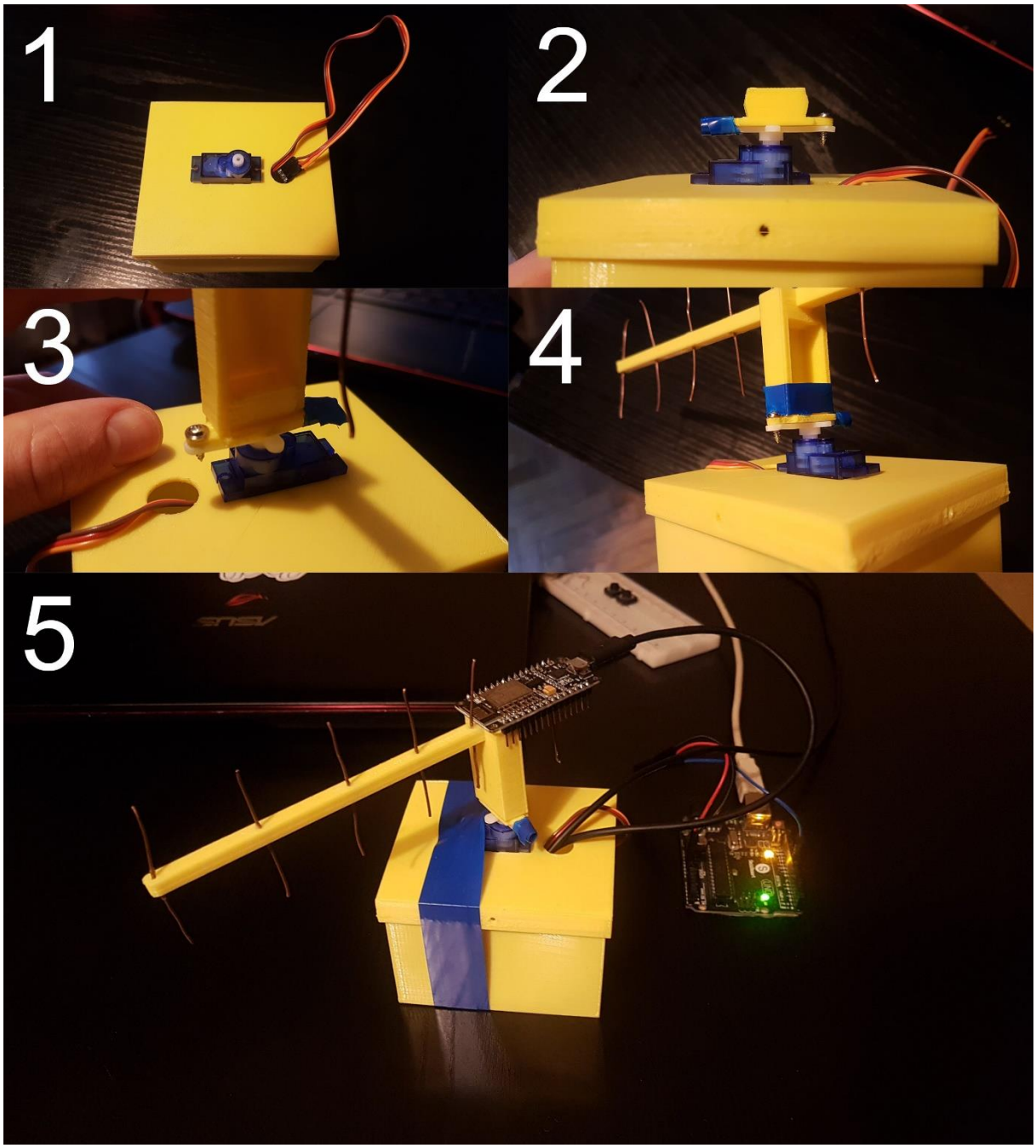

Figure 18 - ESP8266 with servo motor mechanism

Figure 19 and Figure 20 represents the simulation of a real-life scenario and testing phase of the measurements done via phone while ESP8266 with the antenna was moving 180°. The purpose of this test was to demonstrate the advantage of using directional Yagi antenna and to determine the difference of the signal strength with and without the antenna.

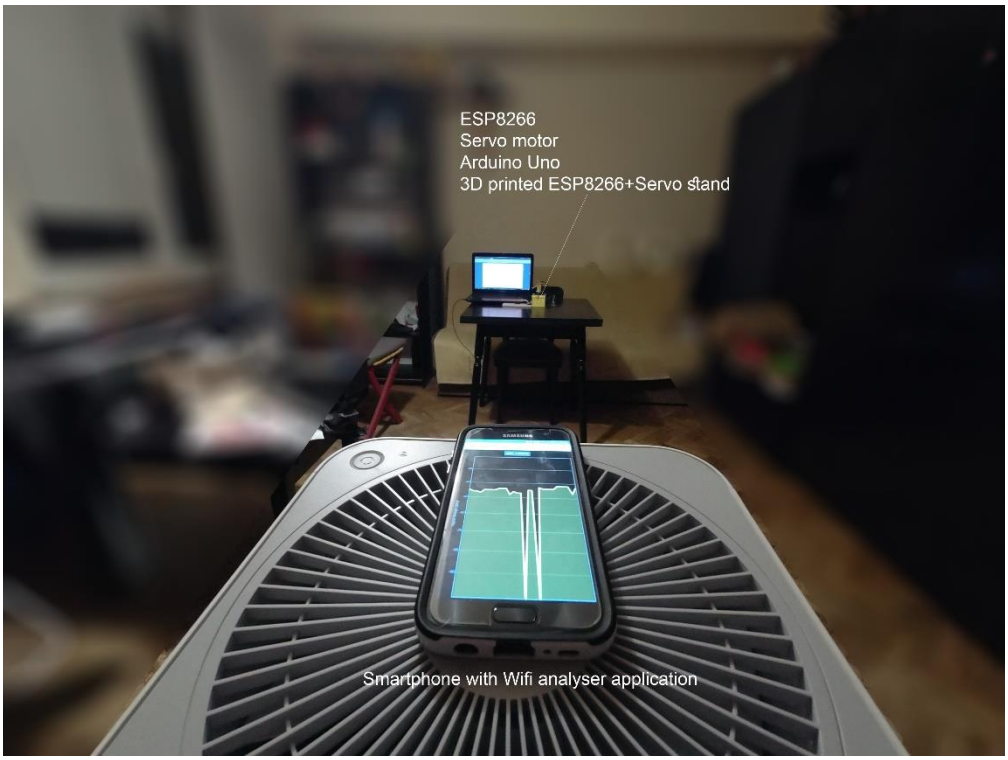

Figure 19 - Real-world simulation testing scenario

To assess the power of using directional Yagi antenna the following tests were performed. Using Arduino Uno, we programmed servo motor to change the angle of the antenna (Figure 18 - 5) after 'x' number of seconds. First position of the antenna was *Position 1* as shown in Figure 20. After the position 1, antenna would make a scanning movement from left to right - from *Position 1* to *Position 7* and back. An application would be running as shown in Figure 19 to note the change in the signal strength while antenna is scanning the room.

The results can be seen on Figure 21, Figure 22. Since the scan interval (speed of receiving the signal) on the application can be changed we decided to perform two tests to have more accurate results. The application has an option to change the scan interval from L0 (shortest) to L5 (Longest) and this is very important for the end goal of this project. We want to have the fastest possible signal readings – scan, to have fast calculations for IPS. For that reason, we kept the scan interval on L0 which is approximately 4 seconds between each scan. Just for a comparison the longest scan interval L5 is around 14 seconds which is not acceptable for IPS. The update rate of GPS for most devices is 1 Hz (once per second). [37]

On the Figure 20 we can see the testing environment, the room 5x5 m with ESP8266 device at the top, Yagi antenna in different positions and a smartphone. This test was used to determine

the improvement of the Wi-Fi signal while using directional antenna. The scan movement of the antenna was automated using Arduino Uno and servo motor.

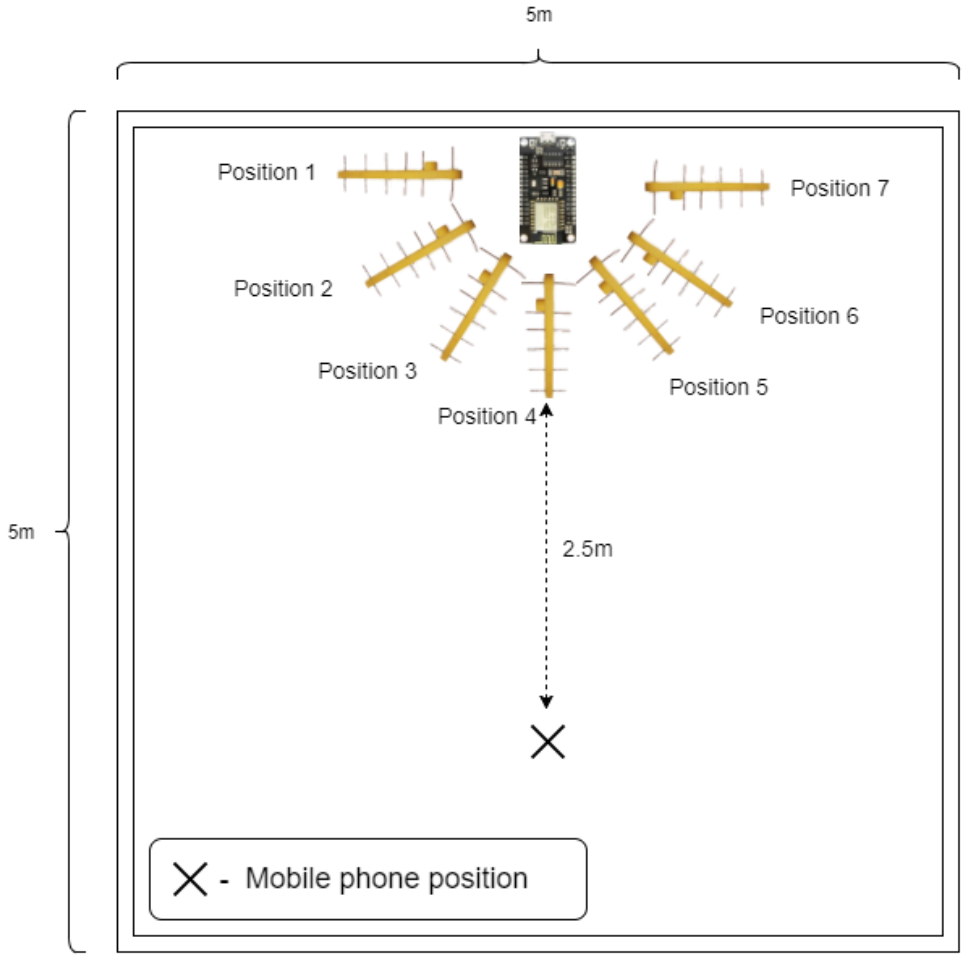

Figure 20 - Antenna angles test

Figure 21 shows the movement of the Yagi antenna from the previous figure in diagram with strength of the signal in time. With the help of Arduino, Yagi antenna was changing its positions every 10 seconds. The antenna was moving from left to right (from position 1 to position 7) and we can see that the signal is the highest in the middle position where Yagi antenna is directed towards to smartphone which was receiving the signal. Important to note here is that the difference between end positions and middle position is 6 dB, which makes this satisfying mean to detect the direction of the smartphone.

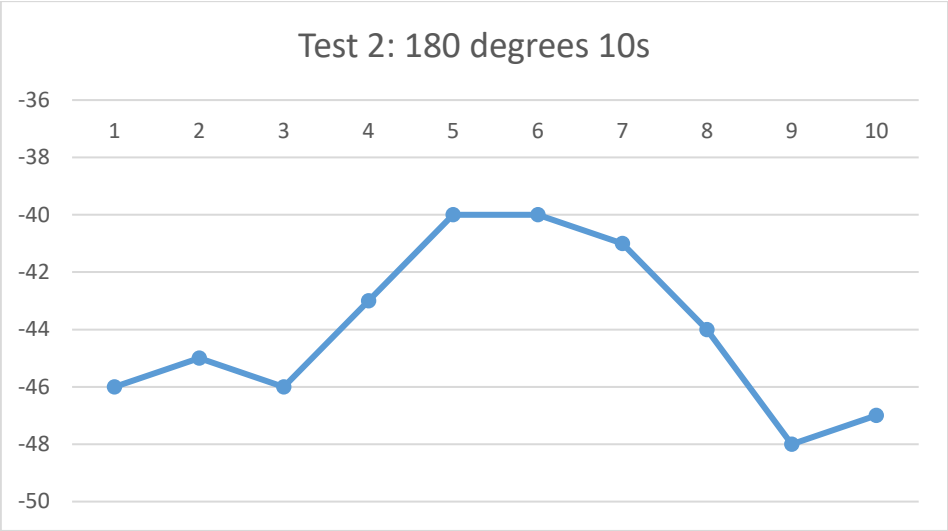

Figure 21 - Signal strength (1)

Figure 22 shows the same scenario and measurements as for the previous figure except for changing the time value of the Yagi antenna scan, which was set to 20 seconds. The reason to change this value is because the more time antenna is directed in one position the more time there is for the signal to stabilize. This gave us slightly more accurate result. In the perfect scenario the detection of the person/smartphone would be easily detected with small movements, but of the position of the person/smartphone is changing rapidly it becomes a challenge. The improvement we got with 20 seconds was 12 dB which is double than on previous test.

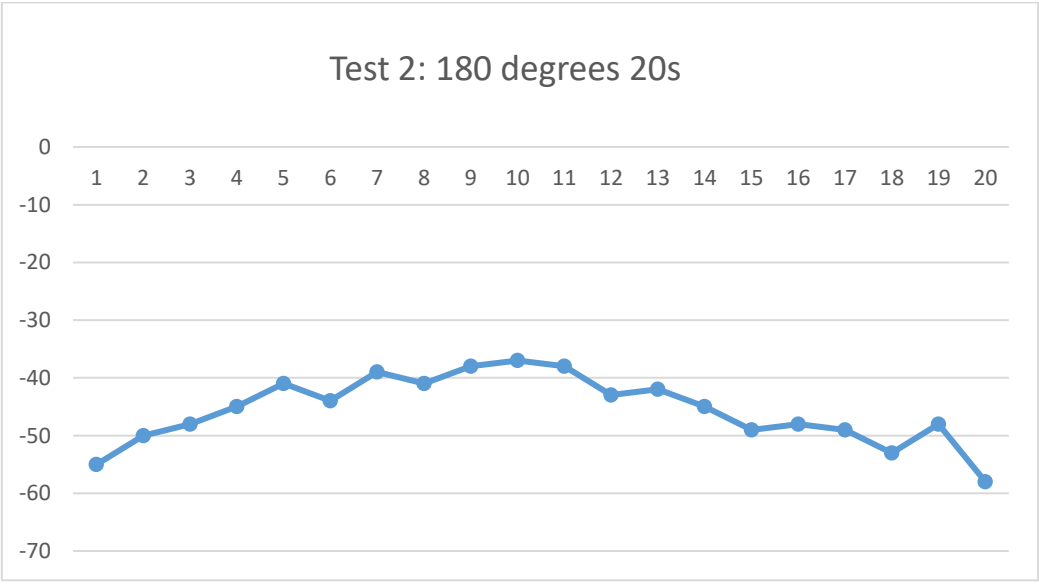

Figure 22 - Signal strength (2)

In the research presented here [38] we obtained similar results. As shown in the Figure 23 and Figure 24 we can see a graphical representation of the signal strength from the AP to the smartphone in a range of 60 degrees and the testing scenario is shown in the Figure 24. The peak reading is -45 dB. Other APs signal shown in the image are present only for real scenarios and interferences in testing environment. The range of the rotation was 60 degrees (P2 < - > P6). The maximum wireless peak appears with error less than 10 degrees. When triangulation calculations are performed the outcome, result is an error less than 1.5 meter if the distance of the Yagi antennas are approximately 10 meters.

With this comparison we confirmed positive results acquired in the tests performed for this dissertation as the results appear with the same error which is below 10 degrees when using only one AP.

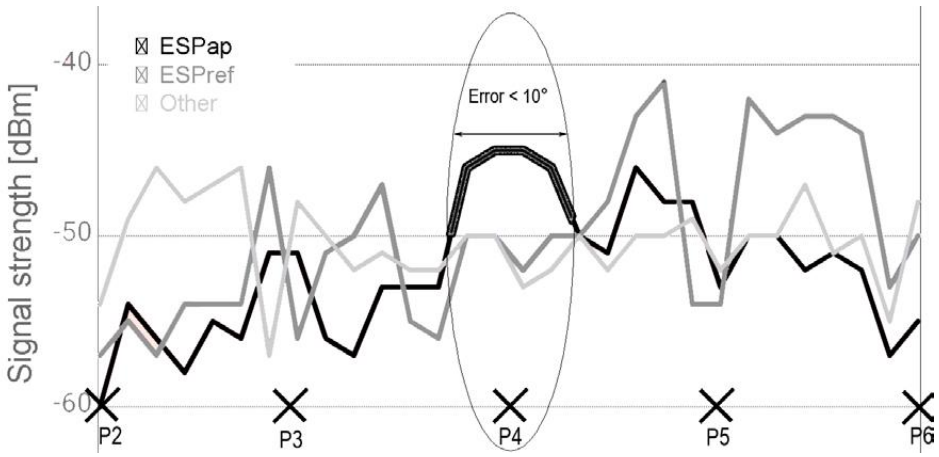

Figure 23 - Signal strength (3) [38]

On the Figure 25 is a graphical demonstration of angle of rotation of the scenario made for measurements in the Figure 24. All rotations are only made between angles P2 and P6, represented by the grey area. With this scenario, we demonstrated that the error is only 10 degrees and when all three APs are included the error would be significantly reduced.

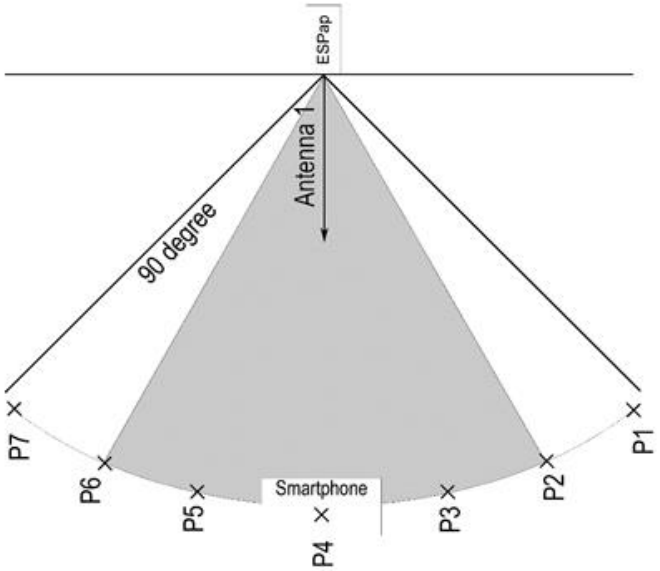

Figure 24 - Graphical representation [38]

Comparing the results to the ones presented on Figure 25, the signal increased 7 dB which gave us confidence in achieving excellent results when a full scenario is implemented. Below on the Figure 25 we can see the scan movement of the antenna 360 degrees and the error being under 1 m [38].

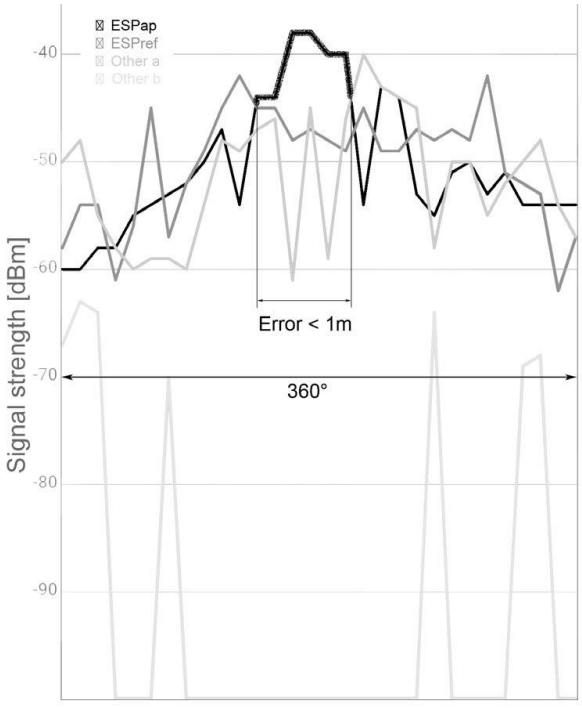

Figure 25 - Graphical representation of a 360 degrees test [38]

4.2. Standing wave

One of the challenges for this project if implemented in real-world scenario would be interference with another devices and signals. One of them being an issue with a standing wave which causes a wave being sent from the transmitter to the receiver propagates through space and gets reflected in different kinds of surfaces. These reflections cause the receiving end to receive multiple instances of the same wave, some of them arriving directly, while others arriving after being reflected from certain objects [39].

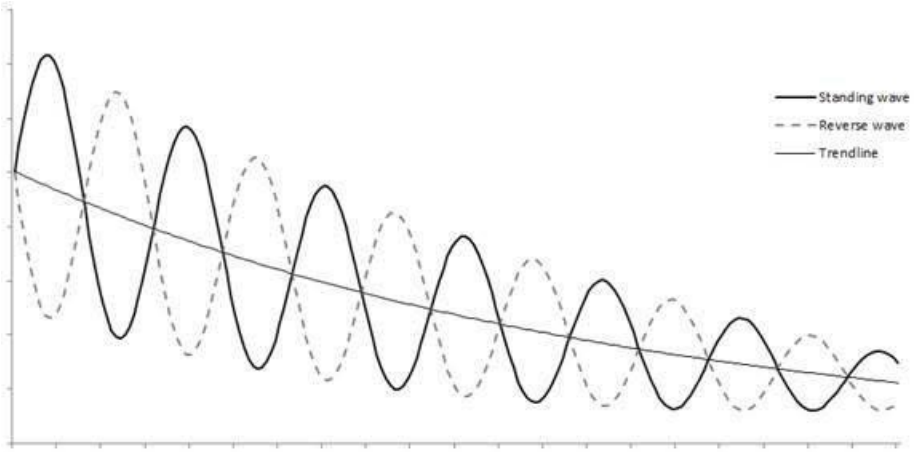

Figure 26 - Effect of a standing wave [39]

On the Figure 26 is a graph describing the effect of the standing wave in indoor positioning systems. The continuous line corresponds to a standing wave with a full wavelength of λ and the dashed line corresponds to a standing wave with a wavelength of λ, but with a shift of λ/2. In this patent [35] we presented the solution to reduce the negative impact of standing waves. To improve the accuracy of the solution presented in this dissertation, a future work can be performed.

4.3.Two-dimensional test scenarios

Here on the Figure 27 we can see the ESP8266 on the top without Yagi antenna and measurement points which were performed with the smartphone. We have a slightly better result in the middle lower point since ESP's integrated antenna is located on the bottom side and it is transmitting stronger signal in that direction. Each value shown on the figure is negative and in dB. Since it is important to know the range, because of the possible oscillations. Peaks were not considered in this testing.

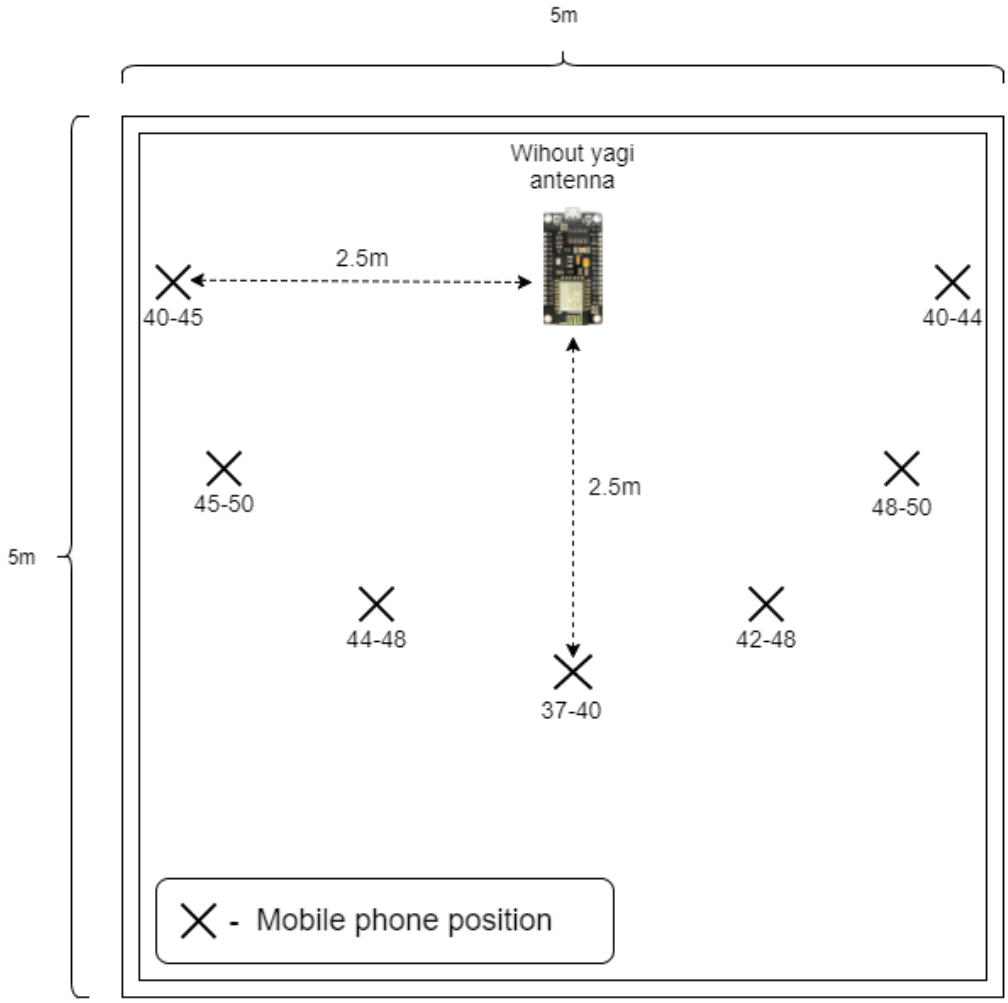

Figure 27 - Measurement 1 - without Yagi antenna (with negative dBm measurements)

On the Figure 28, ESP8266 was equipped with the Yagi antenna and the same test as on previous figure was performed. Since we were using directional antenna better results were obtained. Because of the possible fluctuations due to interference of other APs, it is important to note the average range of the signal e.g. 37-40. Using antenna, the results were better for 3 dB (average).

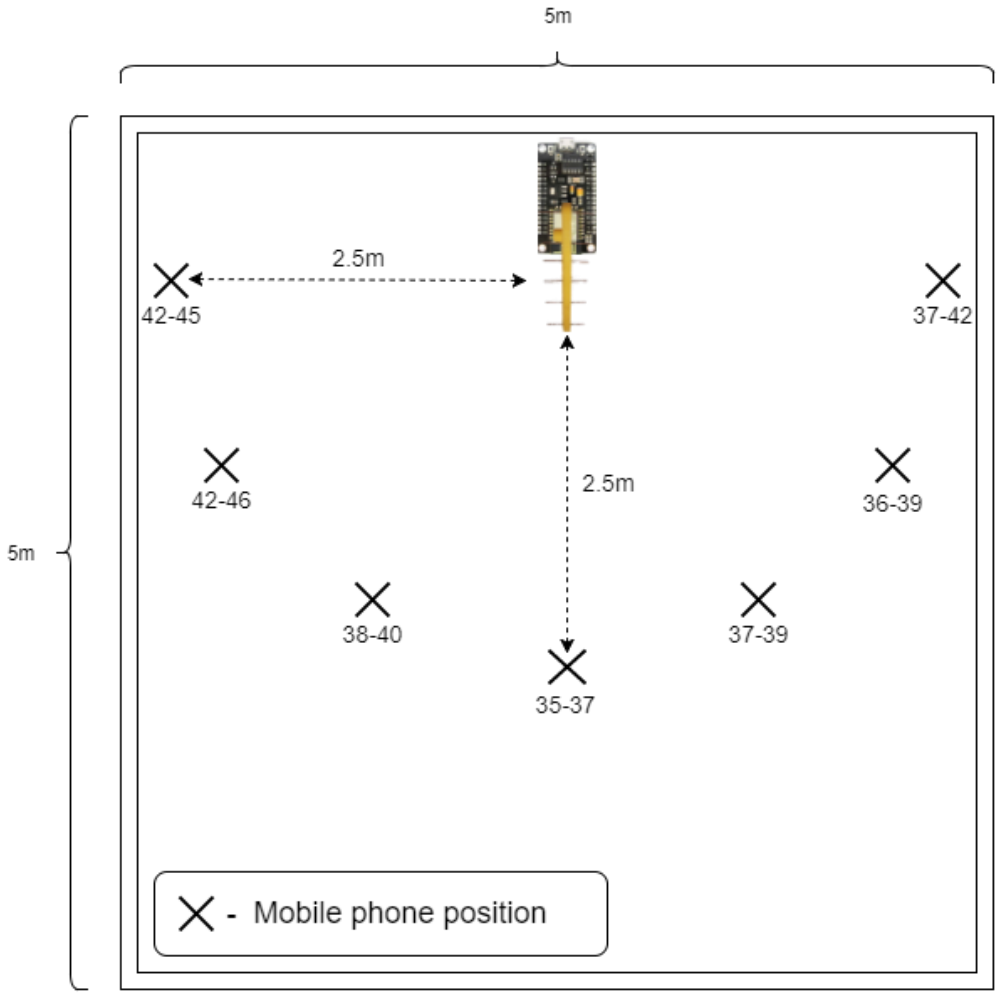

Figure 28 - Measurement 2 - with Yagi antenna (with negative dBm measurements)

Figure 29 shows three different scenarios with ESP8266 and smartphone 2.5 m apart. The value differs from the previous testing since here we were taking only the average value with all the oscillations (considering peak values). Also, here the first value is pure signal from the AP without any amplifiers. The second one is with one antenna on the ESP directed towards to smartphone and the third one is with antennas on both side. As shown on the figure, we can notice significant improvement when using Yagi antenna. With antenna only on one side we have an improvement of 9 dB and when on both sides, delta reaches 10 dB.

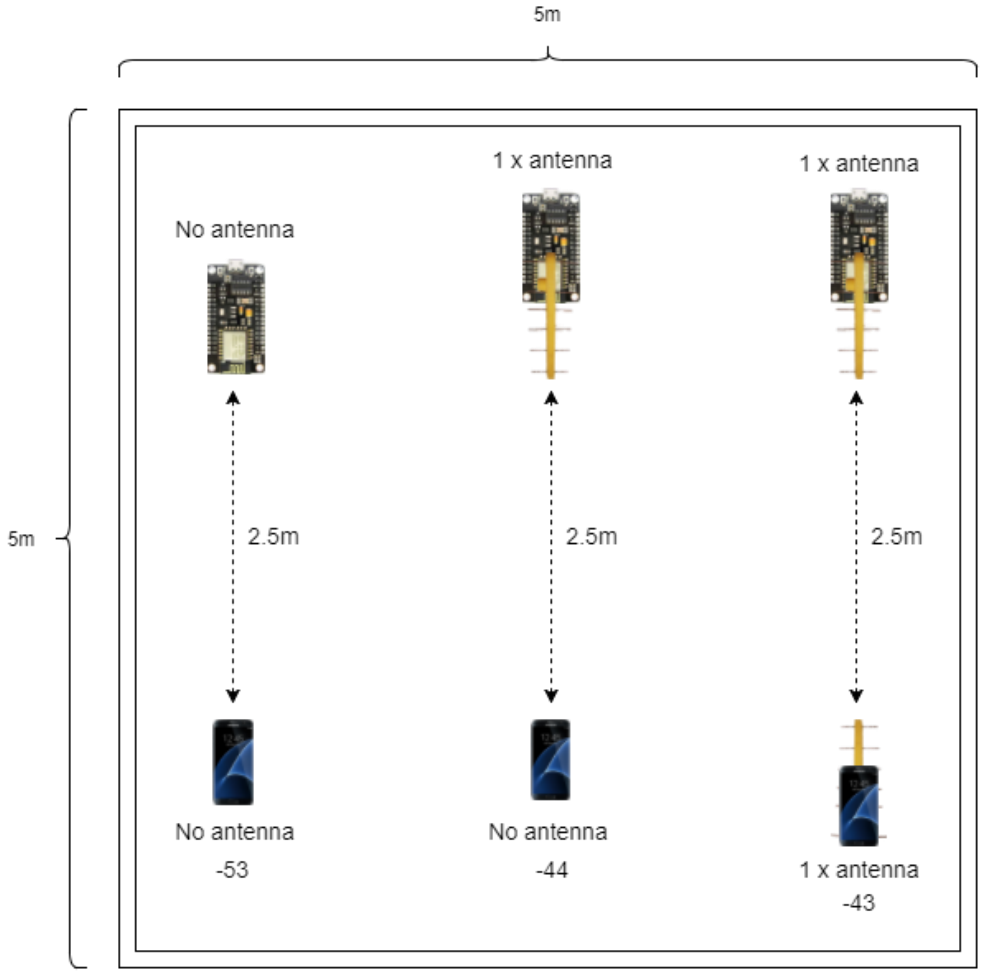

Figure 29 - Measurement 3 - combining antennas

On the Figure 30 is shown an analysis of the signal when we have double antenna on the ESP8266. These tests shown that adding another antenna to the AP it improves the signal by 7 dB from using only one. The added antenna was 90 degrees angled in a relation to existing antenna. If two antennas on the AP are used and one antenna on the smartphone, this signal reaches a very strong signal of -35 dB.

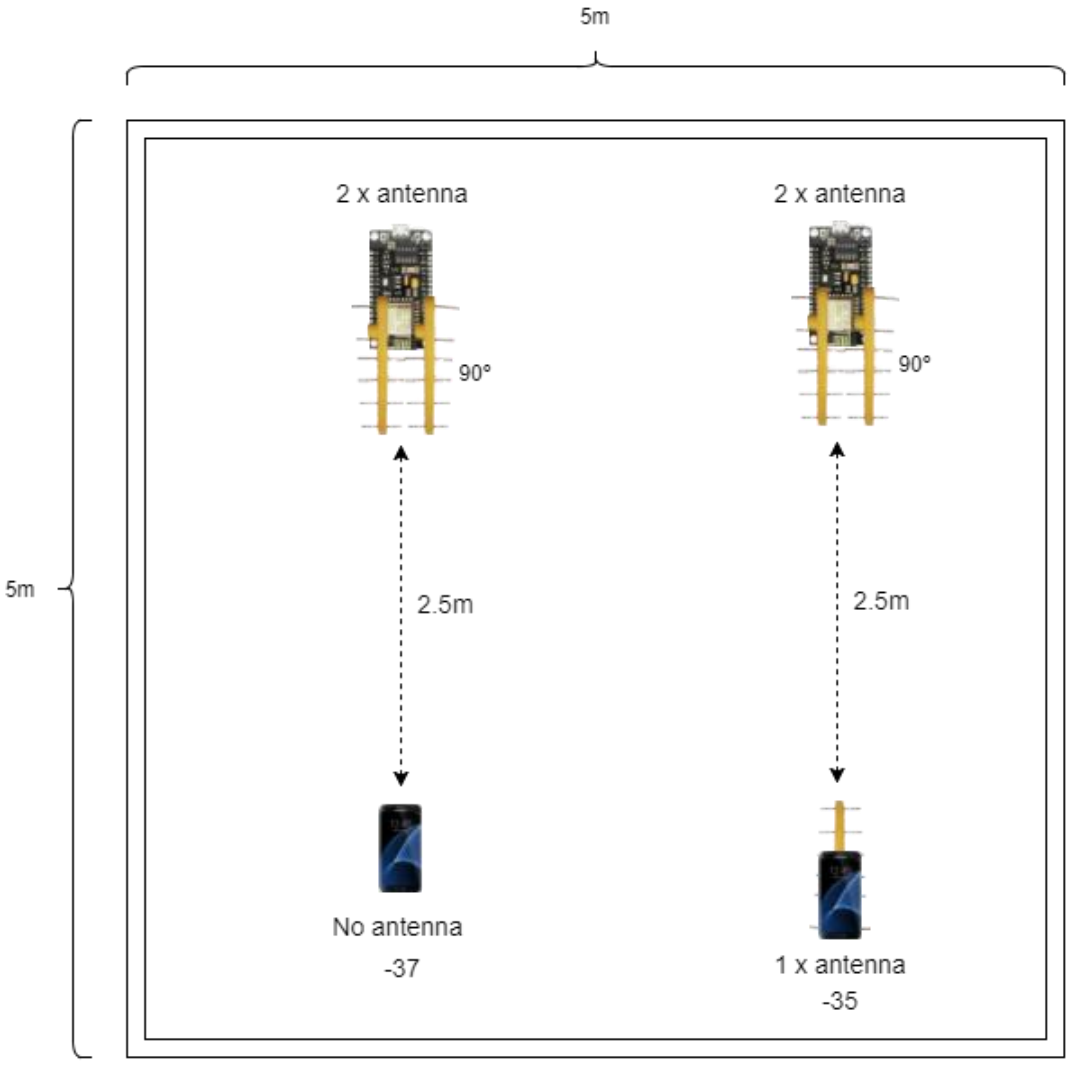

Figure 30 - Measurement 4 - double Yagi antennas

4.4. Simulation of a real-case scenario

To demonstrate this simulation, we were using ESP8266 as a main device which was calculating the strength of all the Wi-Fi signals (APs) in reach. To test the solution, Wi-Fi signal from Android device was used, to have more movement control of the mobile device.

First, we set up Android phone (Samsung S7) to act as an access point (hotspot) and were using mobile data to broadcast the Wi-Fi signal.

On the Figure 31 we can see the *AndroidMG_AP* with no devices connected to the it. ESP8266 was reading the signal strengths of all the APs in reach, including the one from the mobile phone.

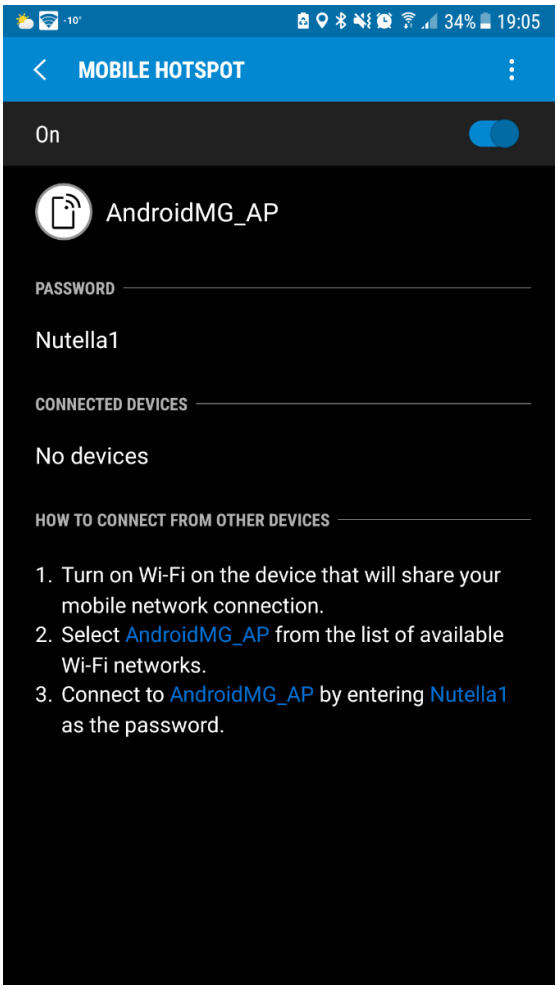

Figure 31 - Android mobile hotspot

Secondly, we created a software code which was uploaded to the ESP8266 which goal was to scan the Wi-Fi network in the area and return their signal strength value. For this matter we were using ESP8266WiFi library [40]. The Wi-Fi library for ESP8266 has been developed basing on ESP8266 SDK, using naming convention and overall functionality philosophy of

Arduino Wi-Fi library. The ESP8266WiFi library provides wide collection of C++ methods (functions) and properties to configure and operate an ESP8266 module in station and/or soft access point mode. For this project we were not using station nor access point mode, but rather only as a mechanism to scan the networks which is described in more details in the section below.

4.4.1. Network scan

Scanning for networks takes hundreds of milliseconds to complete. This may be done in a single run when we are triggering scan process, waiting for completion, and providing result - all by a single function. Another option is to split this into steps, each done by a separate function. This way we can execute other tasks while scanning is in progress. This is called asynchronous scanning [41]. In this project we were using the single run method as we did not need the asynchronous tasks, since the whole code is in the loop mode, we were using that to adjust the antenna position and send the value in serial communication.

Below method was used to scan the Wi-Fi networks in the area.

Code 1 - Network scan

```
// WiFi.scanNetworks will return the number of networks found
int n = WiFi.scanNetworks(false, false);
```

Method *scanNetworks* can accept two parameters which are *async* for the asynchronous scanning and *show_hidden* to include in scan result networks with hidden SSID. However, in our case we did not use neither of these functionalities so both values are set to false. Return the RSSI (Received Signal Strength Indication) of a network discovered during the scan.

Code 2 - RSSI

```
WiFi.RSSI(networkItem)
```

4.4.2. Logic

As shown in the Code 3 below, first the antenna makes a scanning movement of 180 degrees, while storing the value of the signal strength on each degree into an array. This array consists of position value in degrees and the signal strength received by the ESP8266. This can be explained more easily with the graphic example as shown below.

Example (random values):

Table 5 - Graphical explanation – finding the highest signal

psition[x]	0	1	2	**3**	4	5	6
Value	-49	-48	-47	**-45**	-47	-48	-49

As the antenna is making the scan movement each time it detects higher signal this value will be stored in the variable called *highest* together with its position – variable called *pssition.* Once the full scan is done we will have the highest signal and the position of the antenna. Variable name *position* could not be used since this is one of the key words in C++ language.

Code 3 - Finding the position of the highest signal

```
for (pos = 0; pos <= 180; pos += 1)           // goes from 0 degrees to 180 degrees
    { // in steps of 1 degree
        for (int i = 0; i < n; ++i)
            {
             if (i == 0)
             {
              myservo.write(pos);             // tell servo to go to position in variable 'pos'
              delay(15);                      // waits 15ms for the servo to reach the position
              Serial.println("");
              Serial.print("servo  position: ");
              Serial.print(pos);
              Serial.println("  degree");
              Serial.print("RSSI  net 1: ");
              Serial.print(WiFi.RSSI(indices[i]));
              Serial.println("");
              Serial.println("");


              pssition[x] = WiFi.RSSI(indices[i]); //saving each measurement into the array

              if (pssition[x] > highest) //checking if there is a higher value
              {
               highest = pssition[x]; //saving the highest value
               pstion = pos;
              }
               Serial.println(highest); //print the highest value
              x++;
            }
        }
```

4.4.3. Signal output value

On the image below, we can see the first output of the scan movement. We acquire the signal strength and store this value as the highest since it is the only value. After that, any value which is higher, it gets stored.

```
...---------------------------------START----------------------------------------
Setup done

MAC: 5C:CF:7F:13:96:10

servo position: 0 degree
RSSI net 1: -51

***
***
-51
***
01: (-51) AndroidMG_AP [01]
--------------------------------FINISH----------------------------------------
```

Figure 32 - Signal output value

Here we can see the signal strength in each position of the antenna. For testing purposes, we were using span of five degrees, but in the final tests we used 1-degree movements.

```
---------------------------------FINISH-----------------------------------------

servo position: 170 degree
RSSI net 1: -49


---------------------------------FINISH-----------------------------------------

servo position: 175 degree
RSSI net 1: -49


---------------------------------FINISH-----------------------------------------

servo position: 180 degree
RSSI net 1: -48


---------------------------------FINISH-----------------------------------------

servo position: 0 degree
RSSI net 1: -49


---------------------------------FINISH-----------------------------------------

servo position: 5 degree
RSSI net 1: -44


---------------------------------FINISH-----------------------------------------

servo position: 10 degree
RSSI net 1: -45


---------------------------------FINISH-----------------------------------------
```

Figure 33 - ESP8266 serial output and the scan movement of the antenna

4.4.4. Output – Phone's localization

To confirm previous tests, we created final scenario of the phone's localization which would resemble real-world situation. In the following Figure 34 we can see our 3D scenario in the 2D perspective. This shows positions of the mobile phone as well as positions of two ESP8266. Firstly, the Yagi antenna with ESP8266 would make a scanning movement across the room and it would save the position where the signal is the highest and that info would be the angle of the antenna. Since we only had one ESP8266 with antenna we needed to perform separate measurements for each point and write down the obtained angles.

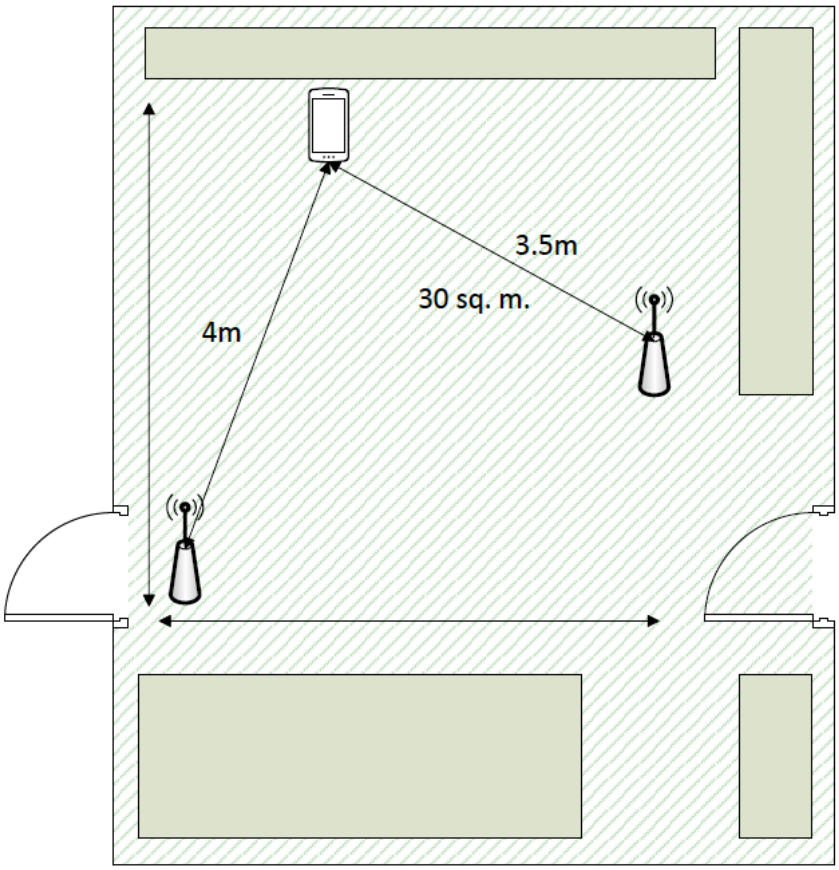

Figure 34 - Room layout

To understand better, we will explain this using Figure 35:

- Point A represents the position of the first ESP8266
- Point B represents the position of the second ESP8266
- α is an angle received from the first ESP8266
- β is an angle received from the second ESP8266
- Point C is an ideal localization point (perfect result) – the actual position of the smartphone (AP)
    - Position: (5.00, 10.00)
- Point M is our result of the phone's position
    - Position: (4.45, 11.26)

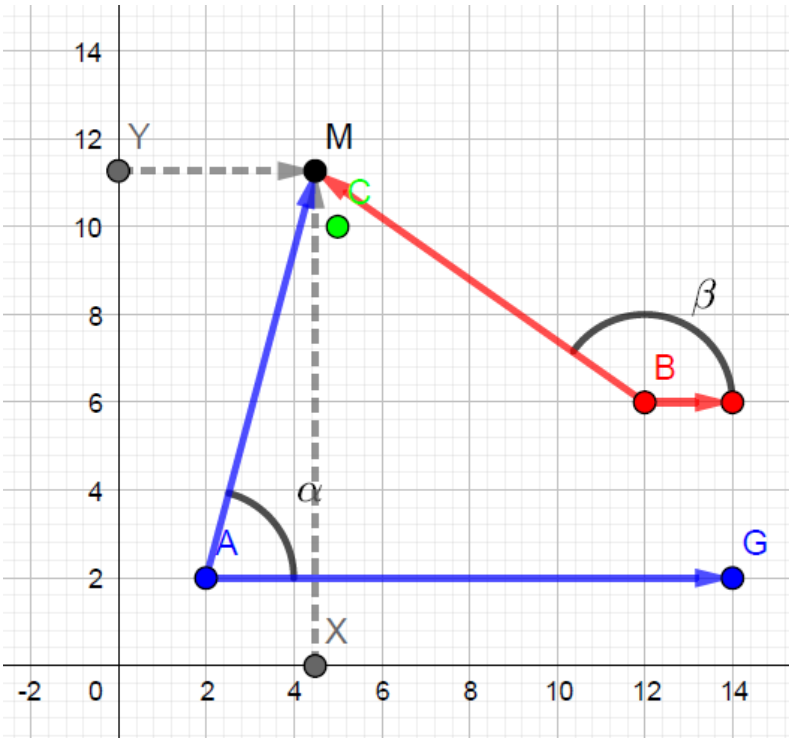

Figure 35 - APs and phone in the coordinate system

After we obtained to angles, α and β, we used formula from section Mathematical method – triangulation to calculate the position of the phone. Below you can find formulas with numbers from out test scenarios. In the formulae (14) and (15) we see the implementation of the formula (13) from the above-mentioned paragraph. We made a separation, to calculate *x* and *y* one at a

time. In the output (16) we can see the result of the calculations which are the coordinates of the mobile phone detected by our system.

$$\frac{2\tan(75°) - 12\tan(145°) + 6 - 2}{\tan(75°) - \tan(145°)} \quad (14)$$

$$\frac{(2 - 12)\tan(75°)\tan(145°) - 2\tan(145°) + 6\tan(75°)}{\tan(75°) - \tan(145°)} \quad (15)$$

$$\{4.48227,\ 11.264\} \quad (16)$$

In this measurement the error is the distance between the point M (result) and the point C (ideal) which is 1.37 according to our coordinate system, which translates into 0.68 m in the room space. As the tests were done on a shorter distance, it is a possibility that because of the shorter distance we have more interferences, so that prevents to have better results. In any case, the result is considerably below 1 m which makes it suitable for IPS system.

5. Conclusions

The direction where the Information Technology (IT) is headed it is inevitable that soon enough we will have the opportunity to use indoor positioning system in our everyday lives. Many large companies are working on the development of the IPS and standardizing the solution. While we can only observe these companies implementing solution, we switch our focus on practical low-cost devices such as ESP8266, servo motor, Yagi antenna. With combination of this inexpensive equipment we can create a lot of testing scenarios and make improvements with trial and error method. Results of testing the indoor positioning system in this project using the Wi-Fi and motorized directional antennas led to encouraging results. Having the ESP8266 as Wi-Fi emitter proved to be an ideal solution for IPS implementation due to its low cost and possibility to act as a web server and control different actuators such as servo motor in this case. Results obtained in this project showed us that the localization detection error can be less than one meter. When combining at least two ESP8266, with a motorized Yagi antenna, and using triangulation method these results showed us a high precision (comparatively to the GPS error) of a little bit more than half a meter. This gives us a lot of confidence in extending this project by implementing the end solution with a mobile application.

6. Future work

There are several different approaches on extending this project and improving the overall solution. Here we present two ideas on possible future work, what can be added and finally improved.

6.1. Mobile application

One of the key parts of the final solution would be creation of an Android or/and iOS app to have the possibility of testing the solution in places such as airports, shopping malls etc. This app could be integrated with existing ones, or it could have its own mapping system. To create this application, a communication between an ESP8266 and a mobile device would be needed. Since the ESP8266 can act as a web server, one of the possible ways to create a communication channel is to use jsoup which is a Java library for working with real-world HTML. It provides a very convenient API for extracting and manipulating data [42].

6.2. Performing tests in the real-world scenarios

In planned and controlled environment where there are not so many interferences, our system is performing very well. One of the next steps would be to perform some of the tests in the surroundings (shopping malls, airports) with challenges of signal interferences of other ESP8266 and mobile devices, wall obstructions, etc. It is likely that the error would increase, but we expect it would still have acceptable results to obtain good IPS measurements.

7. Bibliography

[1] H. Liu, H. Darabi, P. Banerjee, and J. Liu, "Survey of Wireless Indoor Positioning Techniques and Systems," *IEEE Trans. Syst. Man Cybern. Part C (Applications Rev.*, vol. 37, no. 6, pp. 1067–1080, Nov. 2007.

[2] F. Z. Su Meiling, "Virtual Reality Technology," 2015. [Online]. Available: http://en.cnki.com.cn/Article_en/CJFDTotal-SZJT201505058.htm. [Accessed: 08-Oct-2017].

[3] P. R. Desai, P. N. Desai, K. D. Ajmera, and K. Mehta, "A Review Paper on Oculus Rift-A Virtual Reality Headset," *Int. J. Eng. Trends Technol.*, vol. 13, no. 4, 2014.

[4] D. C. Niehorster, L. Li, and M. Lappe, "The Accuracy and Precision of Position and Orientation Tracking in the HTC Vive Virtual Reality System for Scientific Research," *Iperception.*, vol. 8, no. 3, p. 204166951770820, Jun. 2017.

[5] VIVE, "HTC Vive." [Online]. Available: https://www.vive.com/eu/product/. [Accessed: 08-Oct-2017].

[6] MIT, "MIT turns Wi-Fi Into Indoor GPS - IEEE Spectrum." [Online]. Available: http://spectrum.ieee.org/tech-talk/telecom/wireless/mit-turns-wifi-into-indoor-gps. [Accessed: 01-Apr-2017].

[7] D. Vasisht, S. Kumar, and D. Katabi, "This paper is included in the Proceedings of the 13th USENIX Symposium on Networked Systems Design and Implementation (NSDI '16). Decimeter-Level Localization with a Single WiFi Access Point Decimeter-Level Localization with a Single WiFi Access Point."

[8] MIT, "Wireless tech means safer drones, smarter homes and password-free WiFi | MIT News." [Online]. Available: http://news.mit.edu/2016/wireless-tech-means-safer-drones-smarter-homes-password-free-wifi-0331. [Accessed: 01-Apr-2017].

[9] Broadcom, "BCM47755," 2017. [Online]. Available: https://www.broadcom.com/products/wireless/gnss-gps-socs/bcm47755#overview.

[10] IEEE Spectrum, "Superaccurate GPS Chips Coming to Smartphones in 2018," 2017. [Online]. Available: https://spectrum.ieee.org/tech-talk/semiconductors/design/superaccurate-gps-chips-coming-to-smartphones-in-2018.

[11] "Combining pairs of signals and clock definition - Navipedia." [Online]. Available: http://www.navipedia.net/index.php/Combining_pairs_of_signals_and_clock_definition. [Accessed: 15-Mar-2018].

[12] Vice, “How Tesla’s Model S Tracks Your Location In a Tunnel Without GPS,” 2015.

[13] Yao Yao, Mingming Lou, Pengwei Yu, and Lei Zhang, “Integration of indoor and outdoor positioning in a three-dimension scene based on LIDAR and GPS signal,” in *2016 2nd IEEE International Conference on Computer and Communications (ICCC)*, 2016, pp. 1772–1776.

[14] M. Song, Z. Ou, E. Castellanos, T. Ylipiha, T. Kamarainen, M. Siekkinen, A. Yla-Jaaski, and P. Hui, “Exploring Vision-Based Techniques for Outdoor Positioning Systems: A Feasibility Study,” *IEEE Trans. Mob. Comput.*, vol. 16, no. 12, pp. 3361–3375, Dec. 2017.

[15] J. Bagarić, “Indoor Positioning System for Mobile Devices using Radio Frequency and Perfect Sequences,” no. September, 2016.

[16] Digi, “Zigbee Wireless Standard - Digi International.” [Online]. Available: https://www.digi.com/resources/standards-and-technologies/zigbee-wireless-standard. [Accessed: 04-Mar-2018].

[17] D. Katherine and F. Taipe, “Sistema de Localización Indoor y Outdoor para un Mini Vehículo Aéreo Autónomo No Tripulado utilizando Módulos Wi-Fi,” 2017.

[18] M. Yutaka, “Global positioning system,” 1992.

[19] U.S. Goverment, “GPS.gov: GPS Accuracy.” [Online]. Available: http://www.gps.gov/systems/gps/performance/accuracy/. [Accessed: 11-Mar-2017].

[20] Gis2gps, “GIS2GPS.” [Online]. Available: http://www.gis2gps.com/GPS/GPSDEF/SAT.HTM.

[21] T. C. Avik Ghose, Arpan Pal, Anirban Dutta Choudhury, Vivek Chandel, Chirabrata Bhaumik, “Indoor Positioning System,” 2017.

[22] “5 Wireless Wifi 802.11 a, b, g, n, ac, ad, ah, aj, ax, ay Router Range and Distance Comparison | GeckoandFly 2018.” [Online]. Available: https://www.geckoandfly.com/10041/wireless-wifi-802-11-abgn-router-range-and-distance-comparison/. [Accessed: 14-Mar-2018].

[23] Electronics-notes.com, “What is FM | Frequency Modulation | Electronics Notes.” [Online]. Available: https://www.electronics-notes.com/articles/radio/modulation/frequency-modulation-fm.php. [Accessed: 10-Mar-2018].

[24] Henrysbench, “ESP pinout image.” [Online]. Available: http://henrysbench.capnfatz.com/henrys-bench/arduino-projects-tips-and-more/powering-the-esp-12e-nodemcu-development-board/.

[25] R. F. Graf, *Modern Dictionary of Electronics*. 1999.

[26] "The Yagi-Uda Antenna - Yagi Antennas." [Online]. Available: http://www.antenna-theory.com/antennas/travelling/yagi.php. [Accessed: 17-Feb-2018].

[27] "YAGI ANTENNAS." [Online]. Available: http://electriciantraining.tpub.com/14182/css/Yagi-Antennas-205.htm. [Accessed: 17-Feb-2018].

[28] "PARASITIC ARRAY." [Online]. Available: http://electriciantraining.tpub.com/14182/css/Parasitic-Array-222.htm. [Accessed: 17-Feb-2018].

[29] Thingiverse, "directional YAGI WLAN Antenna EXTENSION for 2.4 GHz by photonix - Thingiverse." [Online]. Available: https://www.thingiverse.com/thing:19548. [Accessed: 17-Feb-2018].

[30] D. Sawicz, "Fundametals (of servo)."

[31] "SG90 TowerPro RC Micro Servo Motor For Arduino, RC Heli | Lazada Malaysia." [Online]. Available: https://www.lazada.com.my/sg90-towerpro-rc-micro-servo-motor-for-arduino-rc-heli-29683155.html. [Accessed: 17-Feb-2018].

[32] "File:Trilateration.png - Wikimedia Commons." [Online]. Available: https://commons.wikimedia.org/wiki/File:Trilateration.png. [Accessed: 04-Mar-2018].

[33] D. Jungnickel and A. Pott, "Perfect and almost perfect sequences," *Discret. Appl. Math.*, vol. 95, no. 1–3, pp. 331–359, Jul. 1999.

[34] Dolcera, "CDMA Basics - DolceraWiki." [Online]. Available: http://www.dolcera.com/wiki/index.php?title=CDMA_Basics. [Accessed: 16-Mar-2018].

[35] "LFSR Reference -- M-Sequence, Linear Feedback Shift Register, Feedback Taps for Maximal Length Sequences." [Online]. Available: http://www.newwaveinstruments.com/resources/articles/m_sequence_linear_feedback_shift_register_lfsr.htm. [Accessed: 16-Mar-2018].

[36] "LFSR Reference -- M-Sequence, Linear Feedback Shift Register, Feedback Taps for Maximal Length Sequences." [Online]. Available: http://www.newwaveinstruments.com/resources/articles/m_sequence_linear_feedback_shift_register_lfsr.htm#M-Sequence Properties. [Accessed: 10-Mar-2018].

[37] "GPS Basics - learn.sparkfun.com." [Online]. Available: https://learn.sparkfun.com/tutorials/gps-basics/gps-glossary. [Accessed: 28-Jan-2018].

[38] J. Pereira, M. Gasparovic, M. Ferreira. "INDOOR POSITIONING SYSTEM AND

METHOD," 2017.

[39] J. Pereira, M. Gasparovic, Pooja Pujari, GuruKiran Manjunath. "STANDING WAVE CANCELLATION AND SHADOW ZONE REDUCING WIRELESS TRANSMITTER, SYSTEM AND RESPECTIVE METHOD AND USES," 2016.

[40] ESP8266, "ESP8266WiFi library — ESP8266 Arduino Core 2.4.0 documentation." [Online]. Available: http://arduino-esp8266.readthedocs.io/en/latest/esp8266wifi/readme.html. [Accessed: 05-Mar-2018].

[41] ESP8266, "Scan Class — ESP8266 Arduino Core 2.4.0 documentation." [Online]. Available: http://arduino-esp8266.readthedocs.io/en/latest/esp8266wifi/scan-class.html. [Accessed: 05-Mar-2018].

[42] "jsoup Java HTML Parser, with best of DOM, CSS, and jquery." [Online]. Available: https://jsoup.org/. [Accessed: 10-Mar-2018].

8. Annex

[P1] - J. Pereira, M. Gasparovic, M. P. M. Ferreira, INDOOR POSITIONING SYSTEM AND METHOD, 109950, March 2017, Portuguese Pending Patent.

ABSTRACT

"INDOOR POSITIONING SYSTEM AND METHOD"

The present invention relates to an indoor position system combining three solutions: triangulation system, smart glove or smart case and wireless receiver device using access points with directional and motorized antennas. Global Positioning System (GPS) is accurate and reliable when used outdoors. However, in indoor spaces, due to the signal loss, caused by walls and rooftops, the detection of GPS signals becomes an impossible task. As a solution to the indoor area coverage problem, an indoor positioning system based on wireless triangulation is proposed. A wireless positioning is designed with directional motorized antennas that uses the signal strengths and the angle of arrival of at least three wireless access points. The positioning measurements are calculated and presented to the user via an application running on a mobile device. The present invention helps in the extension of indoor positioning system that requires small hardware additions to set up the solution inside buildings where the service with a specific software application is deployed.

DESCRIPTION

"INDOOR POSITIONING SYSTEM AND METHOD"

Field of the invention

In the field of Indoor Position System, a new approach has been implemented for facilitating orientation in closed spaces such as shopping centres, airports, hospitals, etc. Using wireless technology with different Access Points (AP) it is possible to receive signal strength (RSS) or an angle of the arrival (AOA) of the signal to estimate the current location of a person or a device, in real time.

Prior art of the invention

GPS receivers can work well when a line-of-sight (LOS) exists. However, they cannot work properly in closed spaces where LOS is not available. Another problem is that GPS accuracy has a precision error between 3 and 10 meters, which is too high for implementing it on the majority of indoor scenarios.

Summary of the invention

This approach enables expansion of Global Position System (GPS) due to the fact that devices cannot detect GPS satellites in an enclosed area and the precision

is not acceptable, meaning that this patent is a highly valuable base to make a full system for navigation in closed spaces with a much higher precision. This patent present three parts connected to one whole: triangulation system (1), smart glove/bracelet or device case with a grade of Yagi antenna pattern (2) and a wireless receiver (a smartphone, a RFID reader or any computerized device with wireless access) (3).

In the present invention the triangulation system (1) comprises at least three Wireless Access Points (AP) with motorized directional antennas are used to scan an open or closed room and to receive the highest Wireless power signal where the person is.

A smart glove/bracelet or a specific device case with a grade of Yagi antenna pattern (2) is used to amplify a wireless signal in one specific direction. For example, when a person uses a smartphone with a case or a glove with this specific grade pattern, the smartphone is able to receive the AP signal with a higher strength. The received peak power occurs when the grade Yagi pattern is oriented to the correct direction toward the AP.

The antenna is embedded in the glove, in a bracelet or in the device case. This antenna is a grade of metallic wires. Each metallic wire has a specific length and each wires are parallel and separated by a distance of approximately 1/4 wavelength of the AP frequency. For example, when the Wireless frequency is 2,4GHz this value is approximately 3cm. When the AP frequency is 5GHz this value (the distance between the metallic grade pattern) is

approximately 1,5cm. If a much higher frequency is used, than the metallic grade pattern would not be visible to the human eye. Since radio waves travel at a speed of 299,792,458 meters per second, the distance between the metallic grade pattern can be calculated as distance = 299792458/(4 x frequency), in meters.

The Wireless receiver (3) – smartphone or a RFID reader or any computerized device with wireless access – has an application that detects the power level of each wireless AP. After collecting data from all APs, a signal is sent to each corresponding AP. With the use of servo motor, these APs will have the ability to rotate their antenna to the right direction, toward the person (or the device) that made the location request. In order to do that, the APs can use the direction sent by the device to get a general direction and then fine-tune it by analysing which direction has the highest signal strength.

The peak power will be measured with a higher level when one of the AP antennas is aligned with the grade of the glove/bracelet or with the grade of the case.

A 360º rotation of the person who hand the wireless receiver device with the smart glove or the smart case would provide at least three Radio Frequency (RF) peak detections, during one full rotation.

For example, a smartphone user (or a robot) can make a 360º rotation when he wants to improve the precision of his location inside the room. The full rotation is not necessary when a higher precision is not required. The

smart glove or the smart case with the Yagi grade antenna pattern is essentially useful when the 360º rotation is made.

When the three highest signals are received by the smartphone, a triangulation application calculates the position based on the RSS and the AOA. All the three AP send periodically their data to the smartphone where the calculations of the triangulation process are performed. This data is composed by the three angles where each peak signal strength was detected. While the AOA is sufficient to perform the triangulation and detect the devices location, the combination of RSS and AOA are fundamental to increase the precision of the smartphone location.

Smart antennas based localization is performed using the AoA technique. To find the location, the antennas measure the RSS and calculate the angle at which the maximum value is found. With this information, a line can be traced between the antenna and the wireless receiver. By grouping at least one more antenna it is possible to find the intersection of two of those lines which should indicate the position of the wireless receiver.

Assuming that there are two antennas A and B with coordinates (a_x, a_y) and (b_x, b_y), and angles θ_A and θ_B respectively and that P is the calculated intersection point with coordinates (p_x, p_y), its position can be found using the following system of equations:

$$p_x = \frac{a_x \times \tan\theta_A - b_x \times \tan\theta_B + b_y - a_y}{\tan\theta_A - \tan\theta_B}.$$

$$p_y = \frac{(a_x - b_x) \times \tan\theta_A \times \tan\theta_B + b_y \times \tan\theta_A - a_y \times \tan\theta_B}{\tan\theta_A - \tan\theta_B}.$$

Multiple intersections can be found and an average aggregation method can be used. With this method, assuming that we have a set of *N* intersection points represented by a pair of coordinates (x_i, y_i), where $i=1,2,\ldots,N$, the average point (x, y) of all intersections can be found using the following equations:

$$x = \sum_{i=1}^{N} x_j / N \quad ,$$

$$y = \sum_{i=1}^{N} y_j / N \quad .$$

The average point indicated by the two previous equations will estimate the location of the wireless receiver.

An additional glove rotation of 360º (with the wireless receiver device) will further increase this precision. That is because now the AP antennas are directed towards the device, resulting in a higher signal amplification when the antennas are facing each other, which reduces the error in the angle estimation, as shown in Figure 5.

Description of the drawings

Figure 1 – represents a triangulation with three access points with Yagi antennas and a smartphone in a hand/glove of a user with an application for estimating the position. It is shown three Wireless Access Points (AP) which have motorized directional antennas and they are used to scan a room and to receive the highest wireless power signal where the person (or a generic device) is. In the centre is a smartphone with an application which reads the signal strength of the APs. The highest signal received is obtained when the motorized antennas point to the direction where the smartphone is.

Figure 2 – graphical representation of a wireless signal pattern radiation with a signal propagation from the antenna itself – preferably Signal pattern of Yagi antenna – to the direction where antenna is pointed. As shown, the distance between the metallic wires on the Yagi antenna is around ¼ the wireless wavelength. The wireless emitter should be positioned close to the point C of the metallic grade. All the metallic wires should have a length around ¼ the wireless wavelength. The reflector is a metallic wire and must always exist. The metallic director elements (the director elements are metallic wires of the Yagi antenna) should exist in a minimum quantity of two wires and should be closer to the point C. When more driven elements exist, the antenna becomes more directional and the positioning system accuracy improves. It is possible to use a calculator to define the exact positions and the lengths of

all metallic wires. Some calculations can be found in this site: http://www.changpuak.ch/electronics/yagi_uda_antenna_DL6WU.php. However, the shape of the metallic grade of the proposed Yagi pattern is not limited to the exact theoretical lengths.

Figure 3 - graphical representation of the strength of a signal from the AP to the smartphone in a range of 60 degrees and the scenario is shown in the Figure 4. More specific is a graph showing wireless signal readings of an AP (ESPap) on a smartphone when it is aligned with the Yagi antenna. The peak reading is -45 dB. Other APs are present only for simulating real scenarios and interferences. The range of the rotation was 60 degrees (P2 <-> P6). Using 5 director Yagi wires, the maximum wireless peak appears with an error less than 10 degrees. When triangulation calculations will be performed the outcome should result in an error less than 1.5 meter if the distance of the Yagi antennas are around 10 meters.

Figure 4 - visual demonstration of Angle of rotation of the scenario made for measurements in the Figure 3. All rotations are only made between angles P2 and P6, represented by the grey area. With this scenario, we demonstrate that the error is only 10 degrees and when including all three APs the error will be significantly reduced.

Figure 5 - graphical representation of the strength of the received wireless signal after a full rotation of the smartphone (or another wireless device) in

the presence of a wanted wireless AP and some other wireless unwanted AP signals (acting as interferences). Shows the signal measurement of the full rotation of the smartphone around itself in the vicinity of an AP (ESPap). Also, as in Figure 3, other APs are only present to simulate real scenarios and interferences. In this case we have put the Yagi pattern antenna under the smartphone (glued with its plastic case) to amplify a wireless signal in one specific direction. This Yagi antenna was in the direction of the AP and we made a full turn of 360 degrees. When two antennas, from the AP and under smartphone are aligned towards each other the signal is noticeably higher. Comparing the results to the ones presented on Figure 3, the signal increased 7dB which gives us confidence in achieving excellent results when a full scenario is implemented. We estimate that the new indoor location error could be lower than 1 meter, with a Wi-Fi signal of 2.4 GHz, when 3 Aps are used.

In our real indoor scenario with 30 APs, the results were quite positive. We obtained a maximum positioning error of approximately 37 cm. The average Euclidean distance of all estimated points to the wireless received was approximately 20 cm. The distance between the centroid point of all measurements and the real position of the wireless receiver was only 5.7 cm.

Leiria, 07 of March 2017

CLAIMS

1. Indoor position system characterized in that it comprises three parts connected to one whole:
    a) triangulation system (1), which comprises at least three Wireless Access Points (AP) with motorized directional antennas;
    b) at least one receiving means (2) for receive the Wireless Access Points signal with a higher strength;
    c) at least one computerized device with wireless access (3) with means for read the signal strength of the Wireless Access Points;
    d) AP wireless signal emitters that provide values to the a) triangulation method;
    e) Reflector centred with at least one receiving means (2) that increase the power signal received.

2. Indoor position system according to claim 1 where in the means (2) are smart glove or bracelet with an embedded antenna.

3. Indoor position system according to claim 1 where in the means (2) are devices cases with an embedded antenna.

4. Indoor position system according to claims 2 and 3 where in the antenna is a grade of at least two metallic wires, each one parallel and separated by a distance of approximately 1/4 wavelength of the AP frequency, from each other.

5. Indoor position system according to claim 1 where in the computerized device with wireless access (3) is a wireless receiver, or a smartphone or a RFID reader.

6. Indoor position system according to claim 4 where in the metallic wires have a length around ¼ the wireless wavelength.

7. Indoor position method characterized by the following steps:
    a) the receiving means (2) read at least three Radio Frequency (RF) peak detections of the Wireless Access Points (AP) of the triangulation system (1);
    b) the highest Wireless power signal is amplify a wireless signal in one specific direction;
    c) The received peak power occurs when the grade Yagi pattern is oriented to the correct direction towards the Wireless Access Points;
    d) When the three highest signals are received by the receiving means (2) calculates the position based on the receive signal strength and the angle of the arrival;
    e) After collecting data from all Wireless Access Points a signal is sent to each corresponding Wireless Access Points. These AP will have the ability to rotate their antenna to the right direction, towards the point that made the location request;
    f) The peak power will be measured with a higher level when one of the AP antennas is aligned with

the grade of the glove/bracelet or with the grade of the case.

Leiria, 07 of March 2017

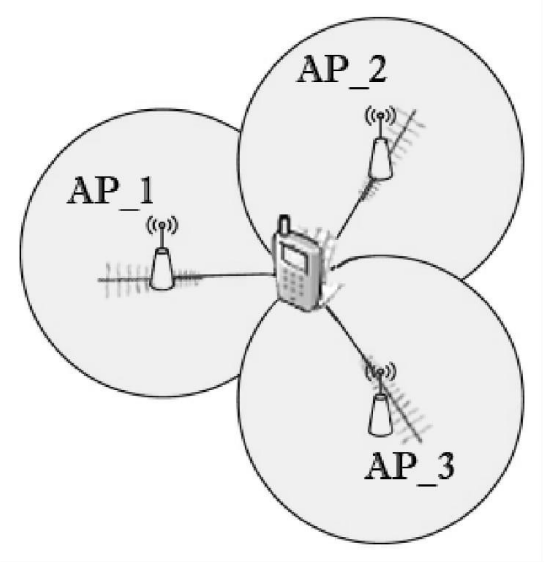

Figure 1

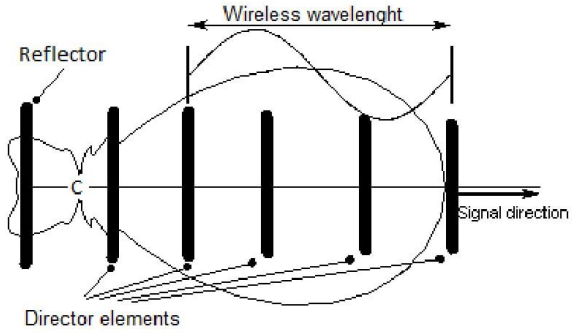

Figure 2

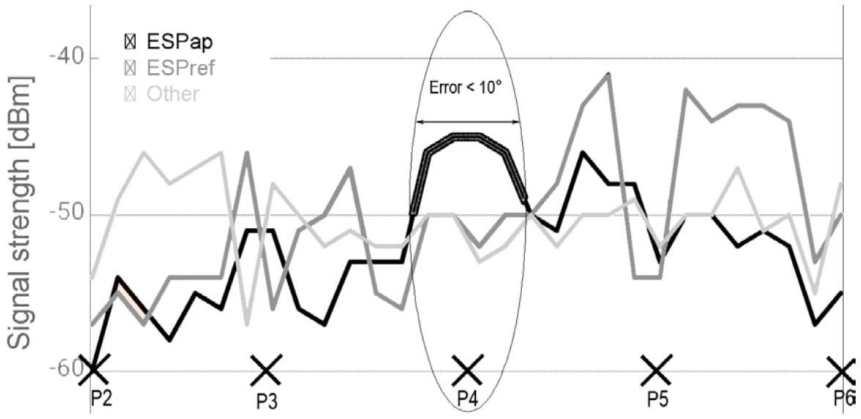

Figure 3

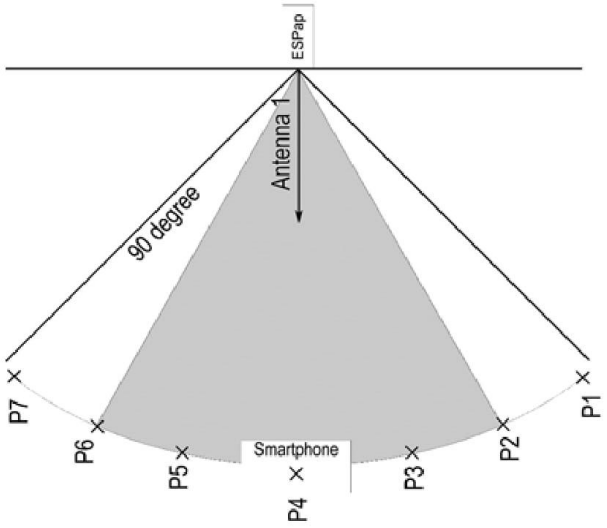

Figure 4

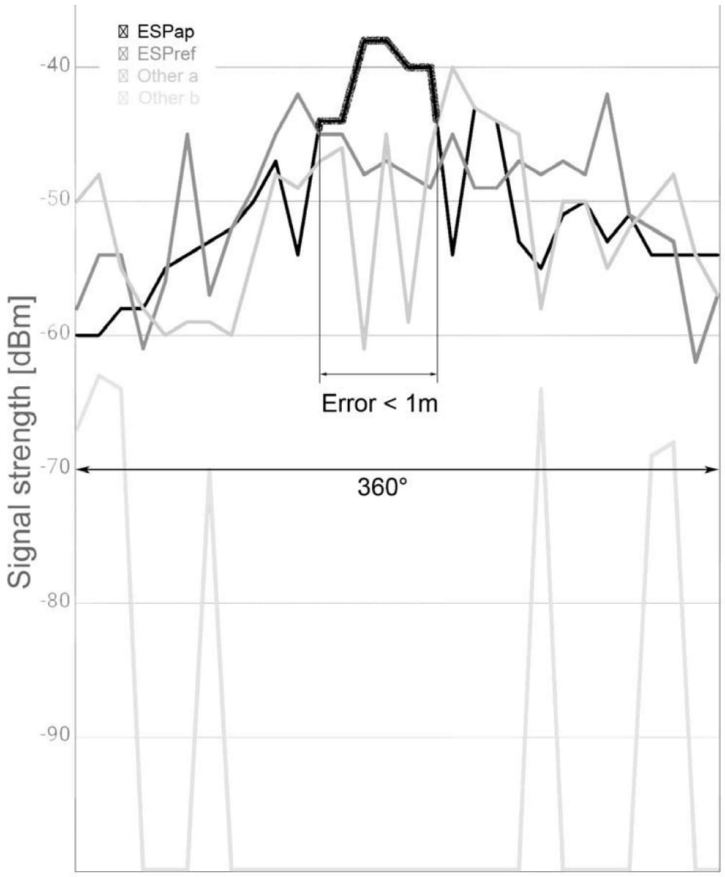
ESPap
ESPref
Other a
Other b
-40
-50
-60
-70
-80
-90
Signal strength [dBm]
Error < 1m
360°

Figure 5

[P2] - J. Pereira, M. Gasparovic, P. Pujari, G. Manjunath, Standing Wave Cancellation and Shadow Zone Reducing Wireless Transmitter, System and Respective Method and Uses, 109332, April 2016, Portuguese Pending Patent.

ABSTRACT

STANDING WAVE CANCELLATION AND SHADOW ZONE REDUCING WIRELESS TRANSMITTER, SYSTEM AND RESPECTIVE METHOD AND USES

This invention is enclosed in the area of wireless communication systems, generally directed towards the problem of multipath interference, and specifically towards mitigating the effect of the standing wave and shadow zone effect in indoor positioning systems.

It is an object of the present invention a standing wave cancellation wireless transmitter configured to transmit a first wave and a second wave with wavelength λ, with automatic displacement means configured to physically move emitting means at least from a first emission point to a second emission point, wherein (i) the first wave is emitted in the first emission point and (ii) the second wave is emitted in the second emission point.

A system which comprises said wireless transmitter, a method implemented by said system and uses of said wireless transmitter and system are also part of the present invention.

DESCRIPTION

STANDING WAVE CANCELLATION AND SHADOW ZONE REDUCING WIRELESS TRANSMITTER, SYSTEM AND RESPECTIVE METHOD AND USES

FIELD OF THE INVENTION

This invention is enclosed in the area of wireless communication systems, generally directed towards the problem of multipath interference, and specifically towards mitigating the effect of the standing wave in indoor positioning systems, as well as to the problem of reducing the shadow zone effect in environments with physical obstacles. It relates to the impact of standing waves in wireless communication and proposes a solution to reduce the negative impact of standing waves when wireless communication is used in indoor positioning systems (IPS) while synergistically reducing the shadow zone effect.

Therefore, it consists of an innovative approach suitable for easy to mount and maintain global low cost IPS. This approach enables to solve the issue of standing wave and to diminish the shadow zone effect, providing an IPS with higher precision.

PRIOR ART

A common occurrence in the field of wireless communication is the standing wave. Especially in environments that contain many obstacles, such as closed

spaces, a wave being sent from the transmitter to the receiver propagates through space and gets reflected in different kinds of surfaces. These reflections cause the receiving end to receive multiple instances of the same wave, some of them arriving directly, while others arriving after being reflected from a certain object. This occurrence is commonly called multipath interference (MPI), and represents a common issue in indoor positioning systems that use wireless technology.

The MPI has another side-effect, which is called the standing wave. When a wave is reflected in a surface, it generates another wave that propagates back in the opposite direction. If one puts a receiver somewhere between the transmitter and the reflective surface, detecting the strength of the signal will vary depending on the position in which the receiver is placed, because of the standing wave effect. Certain positions, particularly those that are half wave length apart, would show no oscillations in the signal strength when measured multiple times. These points along the medium are called nodes (N). Some other points along the medium would yield different results, showing high oscillations in signal strength. The points that contain the highest amount of oscillations are called the antinodes (AN).

In order to achieve accurate and consistent indoor positioning estimation using signal strength, inside closed spaces, mitigating the effect of the standing wave is one of the problems that needs to be addressed. A technical solution to this problem is disclosed in Portuguese patent application PT 109137, and the present application introduces an innovative way to solve the

problem of the standing wave when wireless communication is used in indoor positioning systems, providing also an advantageous solution by mitigating the shadow zone effect.

Because of the standing wave effect and having in consideration the position in which a receiver is placed, strength of the signal will vary from point to point, and due to the shadow zone created by possible obstacles the signal will not cover certain parts of a space.

In order to provide a reliable IPS in closed spaces, it is important to achieve accurate estimation of the signal strength and to have signal spreading without interference. Mitigating the problem of both the standing wave and shadow zone greatly increases the precision and accuracy of the IPS.

The solution of Portuguese patent application PT 106755 addresses the cancelling of multipath interference through a CODEC of orthogonal perfect DFT of Golay codes (OPDG). However this CODEC does not address the standing wave issue nor the shadow zone effect. The OPDG autocorrelation peak follows the standing wave fluctuation.

SUMMARY OF THE INVENTION

It is an object of the present invention a standing wave cancellation wireless transmitter configured to transmit a signal with wavelength λ to be transmitted, transmit a first wave and a second wave, being that the wireless transmitter of the present invention comprises emitting means and automatic displacement means, in which the automatic displacement means are configured to

physically move the emitting means at least from a first emission point to a second emission point, wherein the wireless transmitter is further configured to:

- emit the first wave through the emitting means in the first emission point and
- emit the second wave through the emitting means in the second emission point,

being that the emitted first wave has wavelength λ and the emitted second wave has wavelength λ and a shift equal to the distance between the first and second emission point.

Referring to Figure 1, a graph displays the effect of the standing wave in an indoor positioning system which includes a wireless transmitter as that previously described. The standing wave effect has a major impact on the accuracy of location estimation in the wireless mechanism, due to the constant change in amplitude of the wave that affects signal strength readings, and thus, location accuracy. To mitigate the effect of the standing waves, hardware-based techniques are implemented to generate two different standing waves.

The first standing wave is a wave with a full wavelength of λ. The second standing wave also has a wavelength of λ, but with a shift of equal to the distance from the second to the first emission point, when the emitting means are positioned in the second emission point. The curve gained from summing up the two waves proves to be better for usage, for example, in location estimation scenarios when considering that an X-axis is the distance and a Y-axis is the power of the signal received. It may be used both in radio waves and ultrasonic waves.

The wireless transmitter of the present invention enables to minimize the average fluctuation of the standing wave effect by forcing the emitting means to move in different directions, as shown in figures 2 to 4 (cancelling standing wave fluctuations over one period movement time). A possible receiver will be reading two values of the received waves, when a complete movement of the emitting means occurs. This movement may be provided in any direction. However, the two values of the received waves should occur when the emitting means make a minimum translation, in any direction, equal to the distance between the first and the second emission point. The two values of the received waves should be used to calculate an average.

This average value is the summed value of the two signals, at the receiver, divided by two. By doing so, the standing wave problem is solved because there are less standing waves fluctuations.

At the same time, the transmitter of the present invention enables to mitigate the problem of the shadow zone.

If the wireless transmitter is in a stationary position, the transmitted waves cannot go through possible obstacles positioned between the transmitter and a possible receiver, such as metal objects (closets, desks) and the signal is reflected by these objects. This may generate a problem, since the transmitted signals might not reach points behind these objects, hindering the receiver to

correctly receive the transmitted signal and creating a shadow zone.

Therefore, the wireless transmitter of the present invention improves direct visible angles behind these objects and reduces shadow zone, which causes IPS to have a high precision in those areas.

In an advantageous embodiment of the present invention, combinable with any of the previously described, the first and second emission points are at a minimum distance equal to $\lambda/2$.

This configuration permits to partially transmit a wireless signal behind certain obstacles. A possible wireless receiver positioned near the external borders of a shadow zone will be able to receive more incoming transmitted waves – corresponding to a signal – than in the case in which the wireless transmitter is static. This effect is represented in Figure 5.

In another preferred embodiment of the wireless transmitter of the present invention, combinable with any of the previously described, the second emission point is at a distance of $\lambda/2$ from the first emission point.

In the present configuration transmission occurs while making symmetric movements originating two opposite waves in one period of the movement.

It is also an object of the present invention a standing wave cancellation wireless system which comprises

the previously described wireless transmitter and at least a wireless receiver.

It is yet an object of the present invention a method for the cancellation of standing wave in wireless communications implemented by the previously described system, and which comprises a transmission stage and a receiving stage, wherein the transmission stage precedes the receiving stage and:

- in the transmission stage:
  - i. the wireless transmitter transmits a first wave with wavelength λ through the emitting means in a first emission point;
  - ii. automatic displacement means move the emitting means to a second emission point;
  - iii. the wireless transmitter transmits a second wave with wavelength λ through the emitting means in the second emission point;
- in the receiving stage:
  - i. a wireless receiver, for a received first wave with wavelength λ and a received second wave with wavelength λ and a shift equal to the distance between the first and second emission points, calculates their average on power or amplitude, obtaining a single signal.

This method provides the same advantages and effects of the previously described wireless transmitter and the corresponding system which comprises said wireless transmitter, being the method implemented by such devices.

In a preferred embodiment of the described method, the second emission point is at a distance of λ/2 from the first emission point.

DESCRIPTION OF DRAWINGS

In all of the following figures, the emitting means are indicated as "emitter" and the automatic displacement means as "motor".

Figure 1 - a graph describing the effect of the standing wave in indoor positioning systems. It displays a standing wave effect reduction obtained through the present invention. The continuous line corresponds to a standing wave with a full wavelength of λ and the dashed line corresponds to a standing wave with a wavelength of λ, but with a shift of λ/2. The curve gained from the sum of the two waves has better performance for usage in location estimation scenarios. The sum is equal to the trend line, without the undesirable standing wave fluctuations.

Figure 2 - a schematic representation which describes the connection of the automatic displacement means with the emitting means in a linear movement between two positions, with respect to time instants T1 and T2, in order to cancel standing waves (in opposite phases, when the transmitter distance between the two time-positions is half wavelength).

Figure 3 – physical connection of emitting means moving in a pendulum-like way through the action of the automatic displacement means, with respect to time instants T1 and T2 (in opposite phases, when the emitting means distance between the two time-positions is half wavelength).

Figure 4 – representation of the automatic displacement means to which the emitting means are physically connected, moving the emitting means in a circular-like way, and with respect to time instants T1 and T2 (in opposite phases, when the emitting means distance between the two time-positions is half wavelength).

Figure 5 – representation of the difference between stationary wireless transmitter (A) and a circular-like wireless transmitter (B), suitable for reducing a shadow zone.
In the case (A) a stationary wireless transmitter is presented, radiating a signal towards a wall, and in which a metal object does not allow the signal to reach certain points close to a part of the wall. Instead, the metal object sends a signal back to the emitting means/emitter, making a large shadow zone in the area behind it, not allowing to estimate satisfying IPS measurements.

In the case (B), in which the wireless transmitter of the present invention is used, the shadow zone effect is mitigated. The wireless transmitter is circular-like, wherein the emitting means are rotated by the automatic displacement means around the center of a circle (+ sign).

This allows the wireless transmitter to have a greater angle towards the wall and reducing the shadow zone effect, which was being created behind the metal object. With this type of solution, higher precision and satisfying IPS measurements are provided. The same effect is present in pendulum or linear-like solutions.

Figure 6 – representation of the technical solution of the present invention, mitigating standing wave and shadow zone effects. It consists of a closer view of Figure 5B, with the circular-like solution of Figure 4. The shift of the transmitted second wave is equal to the diameter of the circle formed by the movement of the emitting means.

DETAILED DESCRIPTION OF THE INVENTION

The most general configurations of the present invention are defined in the Summary of the invention. These configurations may be further detailed as follows.

In a detailed configuration of the wireless transmitter of the present invention, combinable with any of the previously described, it is further configured to detect the position of a possible receiver and reconfigure the first and second emission points so that the first and second emission points are at the same distance from a possible receiver.

This enables a dynamic reconfiguration of the device, so that the conditions of transmission may remain the same for any possible receiver in any possible point of space.

In several detailed configurations of the wireless transmitter object of the present invention, combinable with any of the previously described, the automatic displacement means are suitable for moving the emitting means between the first and the second emission points in a pendulum, circular or linear-like way.

With reference to figure 2, a linear-like motion is presented. In this figure the emitting means are connected to the automatic displacement means, represented as a motor and a bar. When the motor is working, the emitting means/emitter moves forward and backward with a period equal to the difference between T2 and T1. At the time instant T1, corresponding to the first emission point, a first wave is transmitted with wavelength equal to λ. At the time instant T2, corresponding to the second emission point, a second wave is transmitted with wavelength equal to λ and a shift of $\lambda/2$. By calculating the mean of these two values, in a possible receiver, an increase the strength of the signal is provided.

With reference to figure 3, a pendulum-like motion is presented. The natural frequency of oscillation of a compound pendulum is obtained from the ratio of the torque imposed by gravity on the mass of the pendulum to the resistance to acceleration defined by the moment of inertia. In this figure, as in figure 2, the emitting means are connected to the automatic displacement means, represented as a motor and a bar. When the motor is working, the emitting means swing between a first and a second emission point, respectively corresponding to the time instant T1 and the time instant T2. In the time instant T1, emitted first wave has a wavelength λ and at

the time instant T2 the emitted second wave has a wavelength λ with a shift of λ/2. By calculating the mean of these two values, in a possible receiver, an increase the strength of the signal is obtained.

By calculating the average of the two values, a solution for the reduction of standing wave issues is provided. With reference to Figure 4, a circular-like motion is presented. The emitting means are connected to an electrical motor to generate, at least, two values of a certain radio frequency. In this case the emitting means will be moving in circular motion to generate the two values. When the emitting means, at the time instant T1, emit a first wave, its wavelength is λ. When the emitting means, at the time instant T2, emit a second wave, its wavelength is λ with a shift of λ/2.

By calculating the average of these two values, a solution for the reducing of the standing wave issue is provided.

Correspondingly, in a specific configuration of the method of the present invention, the movement between the first and second emission points is pendulum, circular or linear-like.

The wireless transmitter of the present invention, as in any configuration previously or subsequently described, may be used in positioning systems, preferably indoor positioning systems.

The wireless system of the present invention, as in any configuration previously or subsequently described, may be used as a positioning system, preferably an indoor positioning system.

EMBODIMENTS

In a preferred embodiment of the wireless transmitter of the present invention, combinable with any of the previously described, the automatic displacement means comprise a motor and a rigid bar physically connecting the motor to the emitting means.

In an embodiment of the wireless transmitter of the present invention, suitable for ultrasonic communication and combinable with any of the previously described, the emitting means comprise a speaker and the first and second waves are ultrasonic waves.

In another embodiment of the wireless transmitter of the present invention, suitable for electromagnetic communication and alternative to the ultrasonic solution previously described, the emitting means comprise an antenna and the first and second waves are electromagnetic waves.

In specific embodiment of the electromagnetic communication solution, the antenna is suitable for radio communications.

In corresponding specific embodiments of the system of the present invention, said at least one wireless receiver comprises an antenna and electromagnetic wave transducer means or a microphone and ultrasound transducer means.

In corresponding specific embodiments of the method of the present invention, the first and second waves are electromagnetic waves or ultrasound waves.

The several embodiments described are combinable.

Each of the claims of the following set of claims defines specific embodiments.

Lisboa, 12.04.2016

CLAIMS

1. Standing wave cancellation and shadow zone reducing wireless transmitter configured to, for a signal with wavelength λ to be transmitted, transmit a first wave and a second wave with wavelength λ **characterized in that** it comprises emitting means and automatic displacement means, being the automatic displacement means configured to physically move the emitting means at least from a first emission point to a second emission point, wherein the wireless transmitter is further configured to:

– emit the first wave through the emitting means in the first emission point and

– emit the second wave through the emitting means in the second emission point.

2. Wireless transmitter according to the previous claim **characterized in that** the first and second emission points are at the same distance from the automatic displacement means.

3. Wireless transmitter according to any of the preceding claims **characterized in that** the second emission point is at a distance of λ/2 from the first emission point.

4. Wireless transmitter according to any of the preceding claims **characterized in that** it is further configured to detect the position of a possible receiver and reconfigure the first and second emission points so that the first and second emission points are at the same distance from a possible receiver.

5. Wireless transmitter according to any of the preceding claims **characterized in that** the automatic displacement means are suitable for moving the emitting means between the first and the second emission points in a pendulum, circular or linear-like way.

6. Wireless transmitter according to any of the preceding claims **characterized in that** the automatic displacement means comprise a motor and a rigid bar physically connecting the motor to the emitting means.

7. Wireless transmitter according to any of the preceding claims **characterized in that** the emitting means comprise a speaker and the first and second waves are ultrasonic waves.

8. Wireless transmitter according to any of the claims 1-6 **characterized in that** the emitting means comprise an antenna and the first and second waves are electromagnetic waves.

9. Standing wave cancellation wireless transmitter according to the previous claim **characterized in that** the antenna is suitable for radio communications.

10. Standing wave cancellation wireless system **characterized in that** it comprises the wireless transmitter of any of the preceding claims and at least one wireless receiver.

11. Wireless system according to the previous claim **characterized in that** said at least one wireless receiver comprises an antenna and electromagnetic wave transducer means **or** a microphone and ultrasound transducer means.

12. Method for the cancellation of standing wave in wireless communications **characterized in that** it is implemented by the system of any of the claims 10-11, and which comprises a transmission stage and a receiving stage, wherein the transmission stage precedes the receiving stage and:

- in the transmission stage:
  - i. the wireless transmitter transmits a first wave with wavelength λ through the emitting means in a first emission point;
  - ii. automatic displacement means move the emitting means to a second emission point;
  - iii. the wireless transmitter transmits a second wave with wavelength λ through the emitting means in the second emission point;
- in the receiving stage:
  - i. a wireless receiver, for a received first wave with wavelength λ and a received second wave with wavelength λ and a shift equal to the distance between the first and second emission points, calculates their average on power or amplitude, obtaining a single signal.

13. Method according to the previous claim **characterized in that** the second emission point is at a distance of λ/2 from the first emission point.

14. Method according to any of the claims 12-13 **characterized in that** the movement between the first and second emission points is pendulum, circular or linear-like.

15. Method according to any of the claims 12-14 **characterized in that** the first and second waves are electromagnetic waves or ultrasound waves.

16. Use of the wireless transmitter of any of the claims 1-9 in positioning systems, preferably indoor positioning systems.

17. Use of the wireless system of any of the claims 10-11 as a positioning system, preferably an indoor positioning system.

Lisboa, 12.04.2016

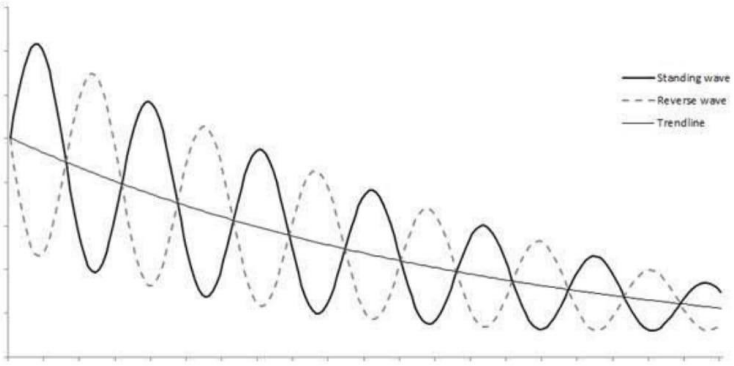

Figure 1

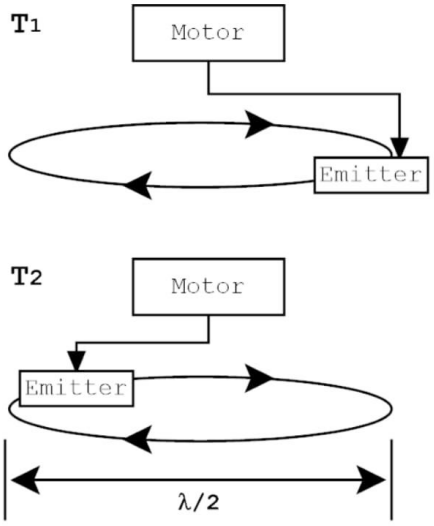

Figure 2

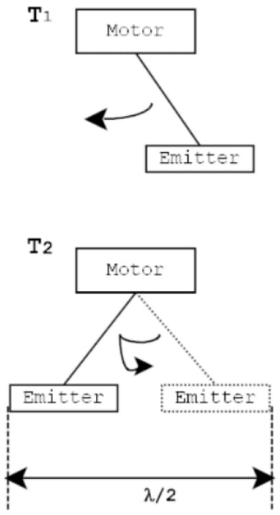

Figure 3

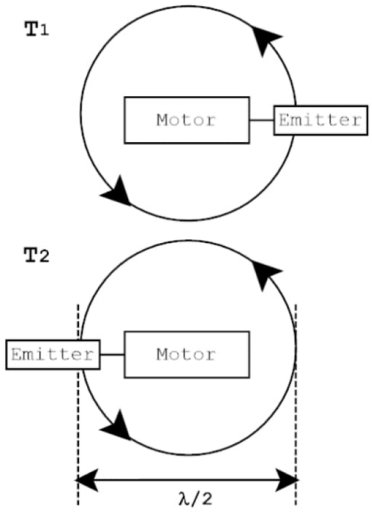

Figure 4

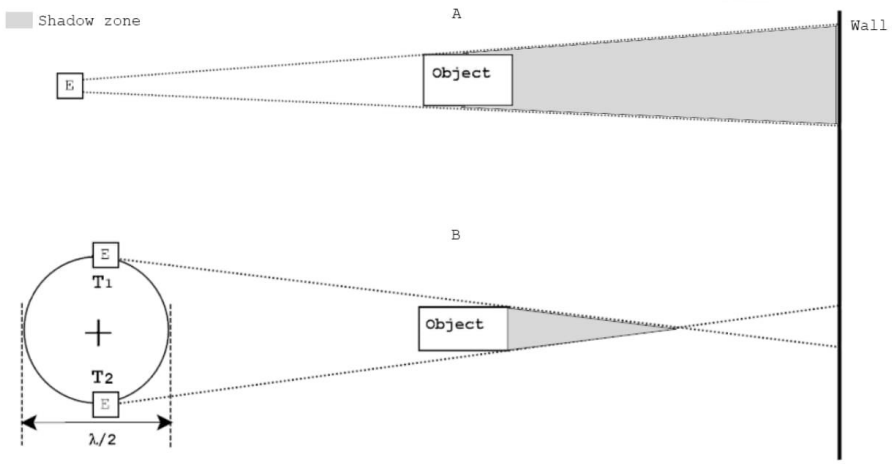

Figure 5

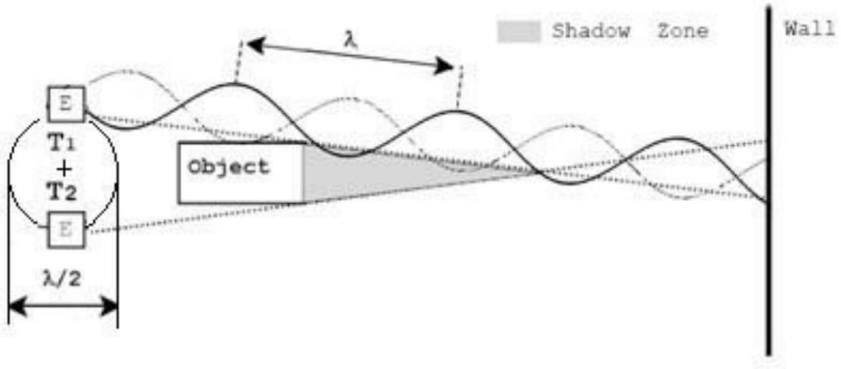

Figure 6

[P3] - J. Pereira, M. Gasparovic, M. P. M. Ferreira, A TUNABLE FIBER BRAGG GRATING DEVICE, A SUPERSTRUCTURED TUNABLE FIBER BRAGG GRATING DEVICE AND RESPECTIVE USES AND OPERATING METHODS, 109554, July 2016, Portuguese Pending Patent.

DESCRIPTION

A TUNABLE FIBER BRAGG GRATING DEVICE, A SUPERSTRUCTURED TUNABLE FIBER BRAGG GRATING DEVICE AND RESPECTIVE USES AND COMMUNICATION METHODS

FIELD OF THE INVENTION

The present invention is enclosed in the field of communication systems based in fiber optics, specifically based in tunable fiber Bragg grating.

The approach of the present invention enables the adaptation of installed physical optical fiber communication systems to the changing communication environment, optimizing properties such as reducing cross-correlation with multiple codes and increasing the auto-correlation of the code.

PRIOR ART

Closer references to the present invention may be found in coherent time spreading optical code-division multiple-access systems with tunable wavelength-division multiplexing (WDM-OCDMA), where a unique code can be reused and mixed with different wavelengths to obtain a system.

For these applications, tunable fiber Bragg grating devices, specifically in superstructured fiber Bragg grating devices, have been used for passive encoders and decoders of the transmitted signals.

These traditional superstructured fiber Bragg grating devices are configured to a specific static encoding, which remains unaltered for the rest of its useful life. If a new encoding is needed, for a new client, for instance, new superstructured fiber Bragg grating devices must be encoded dynamically. Also, a degradation in the signal's quality can occur when there are temperature differences between both ends of the optical fiber, which cannot be corrected without small

changes to the superstructured fiber Bragg grating devices. These small changes can be accomplished by tuning the devices.

Patent application with publication number CN101604053 allows such tuning by changing the gap distance between the fiber Bragg grating and a reflection mirror, although that approach only allows for the tuning of the signal's phase.

Published research also presents tuning the signal's wavelength by means of compression and/or tension on article Analysis and Development of a Tunable Fiber Bragg Grating Filter Based on Axial Tension/Compression (N. Mohammad, W. Szyszkowski, W. Zhang, E. Haddad, J. Zou, W. Jamroz, and R. Kruzelecky).

Recently, some stress-responsive colloidal crystals have been proposed for tunable FBG (H. Ding, Y. Cheng, H. Gu, Y. Zhao, B. Wang, and Z. Gu: Tunable fiber Bragg grating based on responsive photonic crystals, Nanoscale Communication (RSCPublishing), 5, 11572, 2013).

However, none of the devices disclosed in prior art provide for the above indicated advantages.

SUMMARY OF THE INVENTION

It is an object of the present invention a tunable fiber Bragg grating device which comprises a stress responsive material suitable for fiber Bragg grating coupled to an inverse piezoelectric device.

This configuration provides an innovative way to implement a reconfigurable fiber Bragg grating device, since the inverse piezoelectric device may be easily controllable, and its coupling to the stress responsive material consequently and proportionally provides for dynamic reconfiguration of the operating wavelength range(s) of the fiber Bragg grating device. The change in the thickness of the inverse

piezoelectric device is proportional to, for example, an applied electric field. It is used to change the size of the stress responsive material, that is, to tune it.

Further, the innovative configuration of the present invention allows for a way to overcome the issue of temperature variation between the two ends of an optical fiber, since it provides a way to correspondingly reconfigure quickly the fiber Bragg grating device.

In an advantageous configuration of the tunable fiber Bragg grating device of the present invention, the inverse piezoelectric device has at least one changing dimension, being so positioned that the change in said changing dimension compresses said stress responsive material.

This tunable fiber Bragg grating device operates with an inverse piezoelectric device with one or more changing dimensions, and the changing dimension must compress the stress responsive material, so that the known variation of the dimension of the inverse piezoelectric device may be transferred to the stress responsive material.

It is also an object of the present invention a tunable superstructured fiber Bragg grating device which it comprises a plurality of tunable fiber Bragg grating devices as previously described.

The tunable superstructured fiber Bragg grating device benefits not only from the possibility of dynamic reconfiguration of codes / wavelength ranges, but also from the solution to the referred temperature variation issue, which is especially present in such devices.

In an advantageous configuration of the tunable superstructured fiber Bragg grating of the present invention, it is arranged in a star topology. Tunable superstructured fiber Bragg gratings constructed with a star topology and using, preferably, stress-responsive colloidal crystals, allow to overcome the prohibitive temperature variation of the current superstructured fiber Bragg gratings codecs and permit to write any code with different reconfigurable wavelengths.

A tunable superstructured fiber Bragg grating device benefits from a star topology since this arrangement provides for more available space to construct each tunable fiber Bragg grating device. Additionally, a star topology does not require impedance adaptation between each fibre Bragg grating device.

It is also an object of the present invention the use of the previously described tunable fiber Bragg grating device in a wavelength tunable optical encoder or decoder. A wavelength tunable optical encoder can easily tune the correct codes and compensate temperature drifts between an encoder and a decoder. In a FTTH (Fiber-to-the-Home) system, the encoder and the decoder can therefore be separated by many kilometers.

It is also an object of the present invention the use of the tunable superstructured fiber Bragg grating device previously described in a coherent time spreading optical code-division multiple-access system. This use enables that a unique code can be reused and mixed with different wavelengths to obtain a tunable wavelength-division multiplexing (WDM) system.

It is also an object of the present invention a method for encoding a signal in a fibre optic communication network, wherein the superstructured tunable fiber Bragg grating device previously described, in star topology, uses a code written in each of its extremity branches to encode a signal, each branch comprising the tunable fiber Bragg grating device previously described. This method is implementable by the superstructured tunable fiber Bragg grating device and the tunable fiber Bragg grating device as previously and subsequently described, in any of the described embodiments.

It is also an object of the present invention a method for decoding a signal in a fibre optic communication network, wherein the superstructured tunable fiber Bragg grating device previously described, in star topology, uses a code written in each of its extremity branches to decode a signal, each branch comprising the tunable fiber Bragg grating device previously described. This method is implementable by the superstructured tunable fiber Bragg grating device and the tunable fiber Bragg grating device as previously and subsequently described, in any of the described embodiments.

The previously described methods may be comprised in a method for communication in a fibre optic network. The method for communication in a fibre optic network comprises the previously described encoding method and the previously described decoding method, wherein the code used in decoding consists of (i) the code used in encoding or (ii) the conjugate of the code used in encoding, in a reverse order.

DESCRIPTION OF FIGURES

Figure 1 presents an embodiment of the present invention, not intending to be limitative, but only to better describe such embodiment.

Figure 1 contains a representation of a tunable superstructured fiber Bragg grating device with N branches, in a star topology. It contains a 3-port circulator (a), a splitter (b) with N outputs, and the referred N branches (c), wherein to each branch is connected a tunable fiber Bragg grating device which in constituted by a stress responsive material (d) and an inverse piezoelectric device (e). Each extremity branch (f) is a normal FGB. Where a cosine pattern is written with a specific wavelength.

Each inverse piezoelectric device contains two terminals which provide for its control, through the change of an electric variable, here represented as $\tilde{V}_N$.

DETAILED DESCRIPTION OF THE INVENTION

The main advantageous configurations of the present invention are described in the section Summary of the Invention, being subsequently described corresponding preferred embodiments.

In a preferred embodiment of the tunable fiber Bragg grating device of the present invention, combinable with the preceding described configurations, the stress-responsive colloidal crystals consist of monodisperse silica nanoparticles, preferably with a diameter of 180 nm. These nanoparticles may be synthesized by the Stober–Fink–Bohn method. The purified colloidal nanoparticles may be produced by dispersing in pure water and shaking with an excess of ion-exchange resin to form iridescent colors with the assistance of sonication (as of H. Ding, Y. Cheng, H. Gu, Y. Zhao, B. Wang, and Z. Gu: Tunable fiber Bragg grating based on responsive photonic crystals, Nanoscale Communication, RSCPublishing, 5, 11572, 2013).

In another preferred embodiment of the tunable fiber Bragg grating device of the present invention, combinable with any of the preceding, it further comprises means for the control of at least one electric variable electrically connected to said inverse piezoelectric device. Said means provide for local or remote control of the electric variable applied to the inverse piezoelectric device, varying, for example, its thickness and consequently compressing the stress-responsive material.

In a preferred embodiment of the tunable superstructured fiber Bragg grating device of the present invention, combinable with any of the preceding, each

branch consists of a monomode optical fibre, preferably consisting of a fiber Bragg grating, where a cosine pattern is written with a pre-defined wavelength.

In another preferred embodiment of the tunable superstructured fiber Bragg grating device of the present invention, combinable with any of the preceding, it further comprises a circulator and a splitter, wherein the splitter has at least *n*+1 inputs and outputs and interfaces the circulator and said n branches.

The several embodiments described are combinable.

Each of the claims of the following set of claims defines specific embodiments.

Lisboa, 28.07.2016

CLAIMS

1. A tunable fiber Bragg grating device **characterised in that** it comprises a stress responsive material suitable for fiber Bragg grating coupled to an inverse piezoelectric device.

2. A device according to the previous claims wherein the inverse piezoelectric device has at least one changing dimension, being so positioned that the change in said changing dimension compresses said stress responsive material.

3. A device according to any of the preceding claims wherein the stress responsive material comprises stress-responsive colloidal crystals.

4. A device according to the previous claim wherein the stress-responsive colloidal crystals consist of monodisperse silica nanoparticles, preferably with a diameter of 180 nm.

5. A device according to any of the preceding claims further comprising means for the control of at least one electric variable electrically connected to said inverse piezoelectric device.

6. A tunable superstructured fiber Bragg grating device **characterised in that** it comprises a plurality of tunable fiber Bragg grating devices as of any of the preceding claims.

7. A tunable superstructured fiber Bragg grating device according to the previous claim wherein it is arranged in a star topology with *n* branches.

8. A tunable superstructured fiber Bragg grating device according to the previous claim wherein each branch of the star topology comprises at least one tunable fiber Bragg grating devices.

9. A tunable superstructured fiber Bragg grating device according to the previous claim wherein each branch consists of a monomode optical fibre, preferably consisting of a fiber Bragg grating, where a cosine pattern is written with a pre-defined wavelength.

10. A tunable superstructured fiber Bragg grating device according to any of the claims 6-8 further comprising a circulator and a splitter, wherein the splitter has at least *n*+1 inputs and outputs and interfaces the circulator and said n branches.

11. Use of the tunable fiber Bragg grating device of any of the claims 1-5 in a wavelength tunable optical encoder or decoder.

12. Use of the tunable superstructured fiber Bragg grating device of any of the claims 6-10 in a coherent time spreading optical code-division multiple-access system.

13. A method for encoding a signal in a fibre optic communication network, wherein a superstructured tunable fiber Bragg grating device according to any of the claims 6-10 in star topology uses a code written in each of its extremity branches to encode a signal, each branch comprising a tunable fiber Bragg grating device according to any of the claims 1-5.

14. A method for decoding a signal in a fibre optic communication network, wherein a superstructured tunable fiber Bragg grating device according to any of the claims 6-10 in star topology uses a code written in each of its extremity branches to decode a signal, each branch comprising a tunable fiber Bragg grating device according to any of the claims 1-5.

15. A method for communication in a fibre optic network, comprising the encoding of claim 13 and the decoding of claim 14, wherein the code used in decoding consists of (i) the code used in encoding or (ii) the conjugate of the code used in encoding, in a reverse order.

Lisboa, 28.07.2016

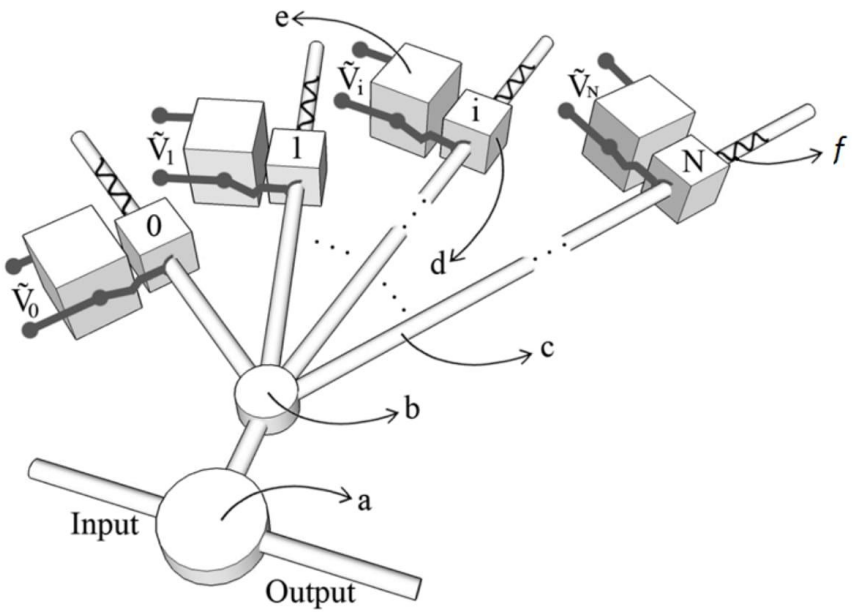

Figure 1

[P4] - J. Pereira, M.P.M. Ferreira, M. Gasparovic, Tunable Super-Structured Fiber Bragg Gratings with Perfect Sequences Based on m-Sequence, Journal of Electronic Science and Technology, JEST, Vol. 15, No. 4, pp. 358 - 363, December 2017.

Tunable Super-Structured Fiber Bragg Gratings with Perfect Sequences Based on *m*-Sequence

João S. Pereira, Marco P. M. Ferreira, and Marko Gasparovic

***Abstract*—Recently, a tunable fiber Bragg grating (FBG) was developed by using stress-responsive colloidal crystals. In this paper, we have simulated the application of these nanoparticles into the super-structured fiber Bragg grating (SSFBG) written with perfect sequences derived from a short maximal-length sequence. A tunable SSFBG will be available to overcome the prohibitive temperature variation of the optical codecs. Nevertheless, we presented a method to implement coherent time spreading optical code-division multiple-access (OCDMA) where a unique code (or perfect sequence) can be reused and mixed with different wavelengths to obtain a tunable wavelength-division multiplexing (WDM) system. In order to maximize the binary throughput, we have selected a unique short maximal-length sequence composed of 7 chips that can be tuned with 7 different optical wavelengths. We found thousands of different tunable combinations that presented power contrast ratios (*P*/*C*) higher than 12 dB. When a WDM-OCDMA system used 2 different combinations simultaneously, the perfect binary detection with error correction codes was achieved successfully. The tunable SSFBG with colloidal crystals will be a simple and good alternative choice for fiber-to-the-home (FTTH) communications.**

***Index Terms*—Optical code-division multiple-access (OCDMA), super-structured fiber Bragg grating (SSFBG), wavelength-division multiplexing OCDMA (WDM-OCDMA).**

1. Introduction

Optical fibers provide an enormous and unsurpassed transmission bandwidth with negligible latencies, and are now one of the transmission media for the long distance and high data rate transmission in telecommunication networks[1]-[4].

Manuscript received June 26, 2016; revised July 17, 2017.

J. S. Pereira (corresponding author) and M. Gaparovic are with the Instituto de Telecomunicações, Lisboa 1049-001, Portugal and are also with Institute Polytechnic of Leiria, Leiria 2411-901, Portugal (e-mail: joao.pereira@ipleiria.pt; marko1559@gmail.com).

M. P. M. Ferreira is with the Centro de Investigação em Informática e Comunicações, Institute Polytechnic of Leiria, Leiria 2411-901, Portugal (e-mail: marco.ferreira@ipleiria.pt).

Color versions of one or more of the figures in this paper are available online at http://www.journal.uestc.edu.cn.

Digital Object Identifier: 10.11989/JEST.1674-862X.70912063

Optical code-division multiple access (OCDMA) is a promising candidate for next-generation broadband access networks. Super-structured fiber Bragg gratings (SSFBGs) can be used as encoders/decoders on time spreading optical code-division multiple access (TS-OCDMA) communication, offering high performance, compactness, and compatibility with fiber-optic systems with a potential low cost[5]-[13].

The optical performance with high throughput passes through the use of optical codecs and decoders that can perform this task in optical domain and in real time. It is possible to find many kinds of optical codecs. Some of them are planar light wave circuits[14], spatial light wave phase modulators[15], and arrayed waveguide gratings[16]. However, all of them require a temperature stability. For example, if the temperature range between two optical network units (ONUs) of a fiber-to-the-home (FTTH) system is larger than 8.0 K, the temperature controller for the SSFBG should be installed in each ONU[3]. To avoid this problem, in this paper we will present a new optical SSFBG codec that is tunable and can, by this way, compensate the temperature drift. Nevertheless, the tunable SSFBG can also implement a simple wavelength multiplexing process between different users.

Fiber Bragg gratings (FBGs) are optical fibers which were developed by using stress-responsive colloidal crystals that can reflect particular wavelengths of light and transmit all others[1]. The FBG is a periodic perturbation of the refractive index along the fiber length which is formed by exposure of the core to an intense optical interference pattern[17]. An SSFBG, also called a sampled FBG, is a special FBG that consists of several small FBGs placed in close proximity to one another. SSFBGs have attracted much attention in recent years with the discovery of techniques allowing the creation of equivalent chirp or equivalent phase shifts. The biggest advantage of an SSFBG with equivalent chirp or equivalent phase shifts is the possibility to design and fabricate gratings with greatly varying phase and amplitude responses by adjusting the spatial profile of the superstructure[18]. The SSFBG technology has been shown to provide an attractive and highly flexible route to produce high-performance and potentially low-cost code generation and recognition components as required for direct sequence (DS) OCDMA systems[19]. In this paper, we present the integration of SSFBG with a tunable mechanism where the thickness of the nanomaterial can be adjusted to reduce the error probability in an optical communication system. A based

piezoelectric device can control this thickness with precision. Also, these FBGs are using stress-responsive colloidal crystals as their Bragg reflectors which have interesting optical properties, such as photonic band gaps (PBGs)[1]. This feature is responsible for making colloidal crystals optimal candidates for the construction of FBGs with a tunable filter or reflector, depending on the objective. It can also have the function of filtering multiple wavelengths by incorporating different colloidal crystal segments into the fiber[1]. The problem is that if we have fixed the colloidal crystal film, then the tuning ranges of the PBGs are mostly limited by their refractive index parameters. There is a necessity to alter the distance between neighboring colloidal crystals films to reduce the refractive index.

The main peak position (for a chip i) can be estimated by Bragg's equation[1] for a normal incident beam:

$$\lambda_i = 1.633 d_i n_{\text{average}} \tag{1}$$

where d_i is the distance between two adjacent nanoparticles and n_{average} is the average refractive index of the colloidal crystal films i. By definition, in digital communications a chip is a pulse of a pseudo-random noise (PN) code sequence used in DS code division multiple access (CDMA) techniques.

Based on (1), there are several protocols for tuning the PBGs of the films which are placed on the proximal end faces of two sections of optical fibers. A good example of tuning the PBG is changing the distance between neighboring colloidal crystals with mechanical stress. Its PBG can be tuned precisely by using different strengths of pressure.

Tunable FBGs, using responsive colloidal crystals, have characteristic reflection peaks of the FBG shifts when compression is applied to them. Furthermore, it has been found that the shift is linearly dependent with the compression ratio[1]. Let the compression ratio of the reflector R_i be defined as

$$R_i = 1 - (T_i / T_0) \tag{2}$$

with T_i being the compressed thickness of the colloidal crystal Bragg reflector and T_0 being its initial thickness. Then, the shifted center wavelength (λ_i) resulting from the compression can be approximated, with a 0.9899 correlation coefficient, as

$$\lambda_i = 603.1 - 385.3 R_i. \tag{3}$$

According to (3), the FBG with different Bragg reflectors could be customized precisely by quickly tuning the thicknesses of its Bragg reflectors.

In Section 2, we introduce a theoretical model for the tunable SSFBG. Section 3 presents a coherent wavelength-division multiplexing OCDMA (WDM-OCDMA) system with tunable SSFBG. The following Section 4 shows that it is possible to estimate the error probability of the tunable SSFBG, and main conclusions are gathered in the last section.

2. Theoretical Model for Tunable SSFBG

The SSFBG power reflection of the FBG i, with length L_i, is given by the following equation[17]:

$$r_i = \left| \frac{-\kappa \sinh\left(\sqrt{\kappa^2 - \hat{\sigma}^2} L_i\right)}{\hat{\sigma} \sinh\left(\sqrt{\kappa^2 - \hat{\sigma}^2} L_i\right) + \mathrm{j} \sqrt{\kappa^2 - \hat{\sigma}^2} \cosh\left(\sqrt{\kappa^2 - \hat{\sigma}^2} L_i\right)} \right|^2 \tag{4}$$

where j is the imaginary number, $\hat{\sigma} = (\lambda_{\max}/\lambda - 1)\pi N_G / L_i$, and $i = 0, 1, \cdots, N-1$. Here, $\lambda_{\max}$ is the wavelength of maximum reflectivity, that occurs when $\hat{\sigma} = 0$ and is given by $\lambda_{\max} = \left(1 + \overline{\delta n_{\text{eff}}} / n_{\text{eff}}\right)\lambda_i$. To simplify the study of SSFBG, it is possible to consider that $\lambda_{\max} \approx \lambda_i$. Here λ_i is the design wavelength of the FBG i for Bragg scattering by an infinitesimally weak grating[17]. n_{eff} is the refractive index. For a single-mode Bragg reflection with a uniform grating, the "dc" index change[17] spatially averaged over a grating period $\overline{\delta n_{\text{eff}}}$ is constant. Therefore, the coefficients $\hat{\sigma}$ and κ are also constants. κ is the "ac" coupling coefficient and $\hat{\sigma}$ is a general "dc" self-coupling coefficient used in the coupled-mode theory of uniform gratings, where N_G is the total number of grating periods[17].

The usage of responsive colloidal crystals in a SSFBG is represented in Fig. 1 with the R_i blocks, where Δz_i is the value of the separation between two chips. The N sections of length L_i have a tunable thickness T_i of colloidal crystals with a compression R_i. The N sections of length L_i are written by using the wavelength $\lambda_i = \lambda_0 + i\Delta\lambda$, where $\Delta\lambda$ is an incremental value of the wavelength ($\Delta\lambda << \lambda_0$). Each section of the grid represents a SSFBG chip that is etched with a phase ϕ_i, $i = 0, 1, \cdots, N-1$.

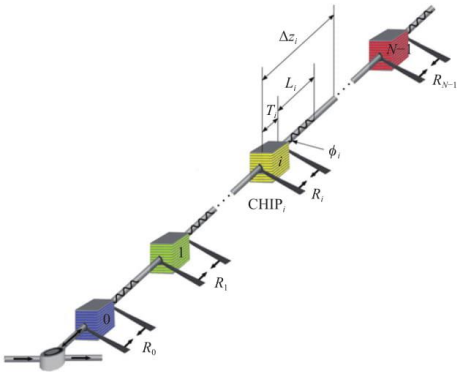

Fig. 1. Tunable SSFBG encoder structure.

For our SSFBG study (based on a selected family of codes) we considered that $\Delta z_i \geq \max(T_i + L_i)$. The power reflection (4) can be rewritten using a Taylor series for sinh(·) and cosh(·) when $\sqrt{\kappa^2 - \hat{\sigma}^2} L_i$, $i = 0, 1, \cdots, N-1$, assumes a low value.

Thus, the power reflection of a chip i has been derived and it is approximately[2]:

$$r_i(\lambda) \approx \left| \frac{-\kappa_1 L_i}{\pi N_G / L_i (\lambda_{\max}/\lambda - 1) + \mathrm{j}} \right|^2. \quad (5)$$

This expression is similar to the transfer function of a bandpass filter (BPF) centered on the wavelength $\lambda_{\max}$, with the amplitude $r_i(\lambda_{\max}) = |\kappa_1 L_i|^2$ and

$$r_i(\pm\infty) = \frac{|\kappa_1 L_i|^2}{1 + (\pi N_G / L_i)^2} = \varepsilon |\kappa_1 L_i|^2. \quad (6)$$

When $\pi N_G >> L_i$, then $r_i(\lambda_{\max}) >> r_i(\pm\infty)$ (because $\varepsilon << 1$), and therefore it is possible to associate a specific SSFBG i to a BPF.

In this scenario, it is considered that the N chips are written with the wavelength $\lambda_i = \lambda_0 + i\Delta\lambda$, for $0 \le i \le N-1$, and all chips will have the same value $\kappa = \kappa_1$. κ_1 is a constant and equals to the "ac" coupling coefficient of all colloidal crystals. For convenience, the transfer function of the 1st chip of the SSFBG, when $\phi_0 = 0$, may be modelled as a scaled version of the rectangular function defined by the following expression:

$$\mathrm{Rect}_\varepsilon\left(\frac{\lambda - \lambda_{\max}}{B}\right) = \begin{cases} 1 & \text{when} \quad \lambda_{\max} - B/2 \le \lambda \le \lambda_{\max} + B/2 \\ \varepsilon & \text{other} \quad \lambda \end{cases}. \quad (7)$$

This special rectangular function, centered at $\lambda_{\max}$, has a bandwidth equal to B and a minimum amplitude equal to $\varepsilon = 1/\left(1 + (\pi N_G / L_i)^2\right)$. When $\pi N_G >> L_i$, then $B \approx 2L_i\lambda_{\max}/\pi N_G$, and (7) is cut –3 dB at $\lambda = \lambda_{\max} \pm B/2$. Each grid of each SSFBG chip i, $i = 0, 1, \cdots, N-1$, acts as a specific BPF with a transfer function approximately equal to the following expression:

$$|\kappa_1 L_i|^2 \exp\{\mathrm{j}\phi_i\} \mathrm{Rect}_\varepsilon\left(\frac{\lambda - \lambda_0 - i\Delta\lambda}{B}\right). \quad (8)$$

It was considered that $\lambda_{\max} \approx \lambda_i$. The phase ϕ_i of the chip i is shown in Fig. 1. The power reflection of a series of N chips (a train of N FBGs) is given by

$$\prod_{i=1}^{N} |\kappa_1 L_i|^2 \exp\{\mathrm{j}\phi_i\} \mathrm{Rect}_\varepsilon\left(\frac{\lambda - \lambda_0 - i\Delta\lambda}{B}\right). \quad (9)$$

Considering the special case when $B/2 \le \Delta\lambda < B$, then the previous expression may be considered approximately equal to

$$\sum_{i=0}^{N-1} A^2 \exp\{\mathrm{j}(\phi_i + \phi_{i+1})\} \mathrm{Rect}_{\varepsilon_2}\left(\frac{\lambda - \lambda_0 - i\Delta\lambda - \Delta\lambda/2}{W}\right) \quad (10)$$

with $A^2 = \varepsilon^{N-2}|\kappa_1 L_i|^4$ and $\varepsilon_2 = \varepsilon/|\kappa_1 L_i|^2$.

This result of (10) is obtained when the product of two consecutive rectangular functions (of index i and index i+1) is equal to a rectangular function with a bandwidth $W = B - \Delta\lambda$, with $0 < W < B$, centered at $\lambda_0 + i\Delta\lambda + \Delta\lambda/2$. In this process, $\varepsilon_2 = \varepsilon/|\kappa_1 L_i|^2$ can be disregarded if (10) is sampled at the centers of rectangular pulses $\mathrm{Rect}_{\varepsilon_2}((\lambda - \lambda_0 - i\Delta\lambda - \Delta\lambda/2)/W)$. The sampling process is equivalent to considering that the bandwidth W is reduced to an infinitesimal value. This operation will convert (10) in a function approximately equal to a train of unit pulses. That is, the SSFBG power reflection of N chips (uniformly distributed) is approximately equal to (10) after the sampling procedure defined by

$$\sum_{i=0}^{N-1} A^2 \exp\{\mathrm{j}(\phi_i + \phi_{i+1})\} \delta\left(\lambda - \lambda_0 - i\Delta\lambda - \frac{\Delta\lambda}{2}\right). \quad (11)$$

The function $\delta(\cdot)$ is a unitary pulse. For convenience, it is considered that $\phi_N = \phi_0$. In other words, the power reflection has undergone a translation of one cycle. This simplification can be made if the codes written in SSFBGs are considered long ($N >> 2$). In this case, the inverse discrete Fourier transform (IDFT) of a normalized SSFBG power reflection (IDFT of (11) around $\lambda_0 + \Delta\lambda/2$) is approximately proportional to the following expression:

$$x_{\mathrm{SSFBG}}(t) \propto \sqrt{N}\,\mathrm{IDFT}\left\{\sum_{i=0}^{N-1} \exp[\mathrm{j}(\phi_i + \phi_{i+1})]\delta(\lambda - i\Delta\lambda)\right\} \quad (12)$$

when the input of the SSFBG is a unitary pulse with an amplitude $\sqrt{N}/A^2$. After the $\lambda_0 + \Delta\lambda/2$ translation of (11), this signal (12) can be considered as a baseband signal of the codes written in the SSFBG.

Each chip Δz_i of a SSFBG, when $B/2 \le \Delta\lambda < B$, has a phase $\theta_i = \phi_i + \phi_{i+1}$ defined by the cosine pattern (L_i of Fig. 1) and the stress-responsive colloidal crystals (T_i of Fig. 1). The amplitudes must be constant for all chips. This means that the SSFBG power reflection baseband signal, defined by the model (12), is the IDFT of a unimodular sequence. By definition, (12) is a perfect sequence[20]. This means that our tunable SSFBG codec will be immune of multipath interferences.

3. Coherent WDM-OCDMA System with Tunable SSFBG

Continuing the study, we simulated the usage of a coherent WDM-OCDMA system using a tunable SSFBG coded with a 7-chip *m*-sequence. The sequence used was [+1, +1, +1, –1, –1, +1, –1]. Because of the wavelength shifting properties of the compressed colloidal crystals, different wavelength channels can be chosen for each chip. Table 1 shows the 7 different channels that we used in our simulation, including the compression ratio R_i required to achieve the desired wavelength λ_i. Each channel has a bandwidth of B = 25 nm, $B/2 = \Delta\lambda$ = 12.5 nm.

By giving different tunings to each section of the SSFBG, different combinations of channels can be used to transmit the code. Our simulation includes three different scenarios of

channel configurations for the same code, which we called SSFBG1, SSFBG2, and SSFBG3. Table 2 shows the scenarios used. Notice that SSFBG3 uses only one channel. These multiple combination scenarios would also allow simultaneous users (each with a different WDM channel combination), or increase the throughput of the communications (sending multiple bits in parallel).

Table 1: Wavelength and compression ratio for the *m*-sequence of 7 chips

Channel i	Wavelength λ_i (nm)	Compression ratio R_i
0	512.5	0.235
1	525.0	0.203
2	537.5	0.170
3	550.0	0.138
4	562.5	0.105
5	575.0	0.073
6	587.5	0.040

Table 2: Different WDM combinations used to encode the *m*-sequence [+1, +1, +1, –1, –1, +1, –1].

Configuration name	WDM combination
SSFBG1	+Ch5, +Ch4, +Ch2, –Ch3, –Ch6, +Ch0, –Ch1
SSFBG2	+Ch1, +Ch0, +Ch6, –Ch4, –Ch5, +Ch2, –Ch3
SSFBG3	+Ch6, +Ch6, +Ch6, –Ch6, –Ch6, +Ch6, –Ch6

Figs. 2, 3, and 4 represent the power spectra of SSFBG1, SSFBG2 and SSFBG3 respectively. The *m*-sequence of 7 chips has been simulated by using 42 samples in the 100 nm that composes the entire 7-channels bandwidth, considering a SSFBG writing phase precision of $\pi/10$.

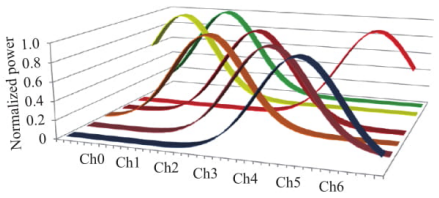

Fig. 2. Spectrum SSFBG1=+Ch5, +Ch4, +Ch2, –Ch3, –Ch6, +Ch0, –Ch1.

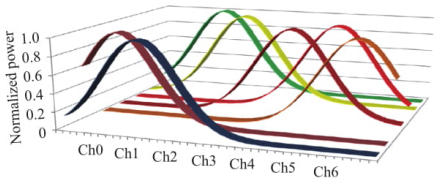

Fig. 3. Spectrum SSFBG2=+Ch1, +Ch0, +Ch6, –Ch4, –Ch5, +Ch2, –Ch3.

By analyzing the autocorrelation and cross-correlation properties of the SSFBGs, as shown in Figs. 5 and 6, respectively, we notice that all configurations present good autocorrelation and cross-correlation properties, with the configuration SSFBG3 presenting slightly worse autocorrelation, but still presenting a very distinctive in-phase peak. All configurations present a minimum power contrast ratio equal to 12.3 dB. The average power contrast ratio (defined as P/W=20log[Peak(Autocorrelation)/Average(Cross-correlation)]), is much larger and equal to 30.0 dB. P is the maximum value of the autocorrelation function of a signal and W is the average value of the cross-correlation function, using a logarithmic scale. The worst error probability has been found to be $\max\{P_e\}=5\times10^{-5}$.

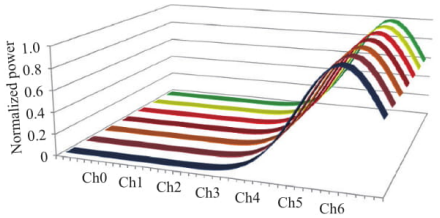

Fig. 4. Spectrum SSFBG3=+Ch6, +Ch6, +Ch6, –Ch6, –Ch6, +Ch6, –Ch6.

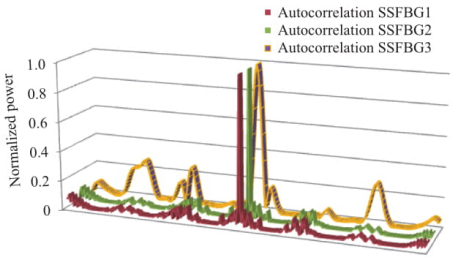

Fig. 5. Normalized autocorrelation, in time domain, with SSFBG1, SSFBG2, and SSFBG3.

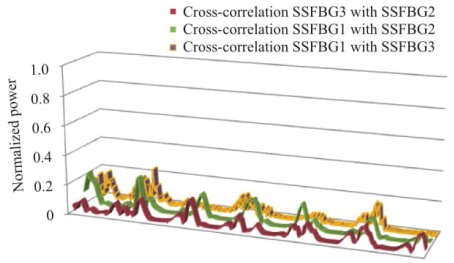

Fig. 6. Normalized cross-correlation, in time domain, with SSFBG1, SSFBG2, and SSFBG3.

4. Tunable SSFBG Error Probability

To simplify the study and analysis of the tunable SSFBG

error probability, we chose to consider only bipolar codes (with two phases: 0 and π). The chip +1 is coded with a phase 0 and the chip –1 is coded with the phase π. The worst case to be considered is when the 7 chips are coded in the same wavelength channel. Then, the phase modulation is simply a binary phase shift keying (BPSK) modulation and the system to be analyzed is a time-spreading optical-code-division multiple-access passive-optical-network (TS-OCDMA-PON) system with coherent coding and decoding making use of bipolar codes. The error probability P_e may be used to find an upper bound for an OCDMA system. This P_e upper bound $\max\{P_e\}$ can be a function of the cross-correlation power contrast ratio $P/C = 20\log[C_k(0)/\max\{C_{k,i}\}]$ (in dB), where $C_{k,i}$ is the cross-correlation and C_k is the autocorrelation[2]. P is the value of the autocorrelation function, centered in zero, and C is the maximum value of the cross-correlation function, using a logarithmic scale. Some P/C upper bounds, for periodic correlations, have been found. One of them is the Welch bound[21] of K perfect sequences of length N: $P/C = 20\log\sqrt{(KN-1)/(K-1)}$. For the aperiodic correlation case, the upper bound is $P/C = 20\log\sqrt{(2KN-K-1)/(K-1)}$.

For a good communication system, the code set selected should have a high P/C value. For example, it has been suggested that the SSFBG should have power contrast ratios higher than 17 dB for 127-chips Gold codes[22].

In this study, we consider the upper bound of the error probability[2] that is a function of the power contrast ratio P/C:

$$\max\{P_e\} \approx 1-\phi\left[\left(\frac{N_0}{2E_b}+(K-1)\left(1-\frac{1}{N}\right)10^{-P/10C}\right)^{-1/2}\right]. \quad (13)$$

Fig. 7 shows a 3D representation of the upper bound (13), for $K = 2$ users and the length is $N = 7\times7$ chips. For example, the error probability upper bound is lower than 10^{-5} when the two ratios P/C and E_b/N_0 are at least equal to 12.3 dB. E_b is the bit energy and N_0 is the spectral density of additive white Gaussian noise (AWGN). ϕ is the normalized cumulative distribution function of Gauss (with zero-mean and unit-variance). This situation requires a bit error correction method to guarantee an error free transmission. However, we should remember that (13) gives us the worst case error probability. Frequently, the error probability average is utilized and, of course, this average will be much lower than the worst case (13).

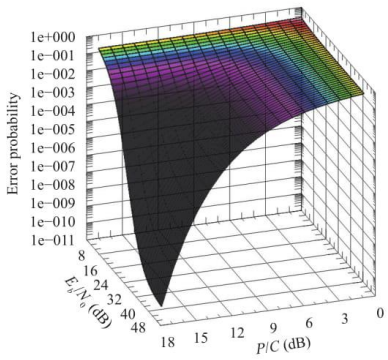

Fig. 7. 3D representation of the probability error upper bound with tunable SSFBG.

Finally, we should remember that the selection of the appropriate codes, the SSFBG ultraviolet light writing precision, and the precision of the optical communication synchronization (sampling operation) are important when we want to design a gigabit OCDMA-PON transmission system with a low bit error rate (BER) over more long distances.

5. Conclusions

In this paper, a new tunable SSFGB was developed by using stress-responsive colloidal crystals. A new SSFBG codec with nanoparticles has been simulated with a short maximal-length sequence. Using a mathematical model, we found that the novel tunable SSFBG is similar to a codec of perfect sequences. These sequences are, by definition, immune to multipath interferences.

Our proposed WDM-OCDMA system with coherent coding and decoding processes has been evaluated with an error probability based on the power contrast ratios of some code sets. The good results obtained allow the conclusion that the proposed tunable SSFBG, with colloidal crystals and perfect sequences, will be a simple solution for WDM-OCDMA communications, when the optical coding and decoding processes require the temperature stability and multiplexing capacity.

References

[1] H. Ding, Y. Cheng, H. Gu, Y. Zhao, B. Wang, and Z. Gu, "Tunable fiber Bragg grating based on responsive photonic crystals," *Nanoscale*, vol. 5, no. 23, pp. 11572:1-6, 2013.

[2] J. Pereira and H. A. Silva, "Error probability upper bound for perfect sequences implemented with super-structured fibre Bragg gratings," *IET Signal Processing*, vol. 8, no. 4, pp. 421-428, 2014.

[3] R. Matsumoto, T. Kodama, S. Shimizu, *et al.*, "40G-OCDMA-PON system with an asymmetric structure using a single multi-port and sampled SSFBG encoder/decoders," *Journal of Lightwave Technology*, vol. 32, no. 6, pp. 1132-1143, 2014.

[4] F. Idachaba, D. U. Ike, and O. Hope, "Future trends in fiber optics communication," *Lecture Notes in Engineering & Computer Science*, vol. 2211, no. 1, pp. 438-442, 2014.

[5] C. Lam, *Passive Optical Networks, Principles and Practice*, Elsevier, 2007.

[6] J. A. Salehi, A. M. Weiner, and J. P. Heritage, "Coherent ultrashort light pulse code division multiple access

communication schemes," *Journal of Lightwave Technology*, vol. 8, no. 3, pp. 478-491, 1990.

[7] P. Prucnal, M. Santoro, and T. Fan, "Spread spectrum fiber-optic local area network using optical processing," *Journal of Lightwave Technology*, vol. 4, no. 5, pp. 547-554, 1986.

[8] M. A. Santoro and P. R. Prucnal, "Asynchronous fiber optic LAN using CDMA and optical correlation," *Proc. of the IEEE*, vol. 75, no. 9, pp. 1336-1338, 1987.

[9] M. Hadi and M. R. Pakravan, "Analysis and design of adaptive OCDMA passive optical networks," *Journal of Lightwave Technology*, vol. 35, no. 14, pp. 2853-2863, 2017.

[10] H. S. Abbas and M. A. Gregory, "The next generation of passive optical networks," *Journal of Network and Computer Applications*, vol. 67, no. C, pp. 53-74, 2016.

[11] S. Ahmed, M. S. Kh. Abuhelala, and I. Glesk, "Managing dispersion-affected OCDMA auto-correlation based on PS multiwavelength code carriers using SOA," *IEEE/OSA Journal of Optical Communications and Networking*, vol. 9, no. 8, pp. 93-698, 2017.

[12] H. Mrabet, I. Dayoub, and Rabah Attia, "Comparative study of 2D-OCDMA-WDM system performance in 40-Gb/s PON context," *IET Optoelectronics*, vol. 11, no. 4, pp. 141-147, 2017.

[13] S. Nlend, T. G. Swart, and B. Twala, "An access optimization approach for FFH-OCDMA system's fiber Bragg gratings encoder," in *Proc. of 2017 IEEE AFRICON*, 2017, pp. 348-353.

[14] K. Okamoto, "Recent progress of integrated optics planar lightwave circuits," *Optical and Quantum Electronics*, vol. 31, no. 2, pp. 107-129, 1999.

[15] Z. Jiang, D. Seo, S. Yang, *et al*., "Four-user 10-Gb/s spectrally phase-coded O-CDMA system operating at ~30 fJ/bit," *IEEE Photonics Technology Letters*, vol. 17, no. 3, pp. 705-707, 2005.

[16] X. J. M. Leijtens, B. Kuhlow, and M. K. Smi. Arrayed waveguide gratings. [Online]. Available: http://alexandria.tue.nl/openaccess/Metis203741.pdf

[17] T. Erdogan, "Fiber grating spectra," *Journal of Lightwave Technology*, vol. 15, no. 8, pp. 1277-1294, 1997.

[18] S. Blais. Superstructured fiber Bragg gratings and applications in microwave signal processing. (2014). [Online]. Available: https://www.ruor.uottawa.ca/bitstream/10393/30358/3/Blais_Sebastien_2014_thesis.pdf

[19] P. C. Teh, M. Ibsen, L. B. Fu, J. H. Lee, Z. Yusoff, and D. J. Richardson, "A 16-channel OCDMA system (4 OCDM ×4 WDM) based on 16-chip, 20 Gchip/s superstructure fiber Bragg gratings and DFB fiber laser transmitters," in *Proc. of Optical Fiber Communication Conf.*, 2002, pp. 600-601.

[20] J. Pereira, *Sequências Perfeitas Para Sistemas de Comunicação*, Saarbrücken: Novas Edições Acadêmicas, 2015.

[21] D. Sarwate and M. Pursley, "Crosscorrelation properties of pseudorandom and related sequences," *Proc. of the IEEE*, vol. 68, no. 5, pp. 593-619, 1980.

[22] X. Wang, K. Matsushima, A. Nishiki, N. Wada, and K. Kitayama, "High reflectivity super structured FBG for coherent optical code generation and recognition," *Opt. Express*, vol. 12, no. 22, pp. 5457-5468, 2004.

João S. Pereira received the B.S., M.S., and Ph.D. degrees from University of Coimbra, Coimbra, Portugal in 1992, 2002, and 2013, respectively. Before 1987, he started the B.S. degree in higher mathematics at La Martinière Monplaisir, Lyon, France. After 1992, he worked for Ford Motor Company as a product engineer. Since 1997, he has been with the Polytechnic Institute of Leiria, Leiria, Portugal where currently, he is an assistant professor in network engineering. Simultaneously, he is an optical communication researcher at Instituto de Telecomunicações, Lisboa, Portugal. He is also an IEEE Senior Member. His last book (2015) is related to Perfect Sequences for Communication Systems. His research interests include signal processing, wireless and optical communication systems, and more recently internet of things (IoT) technologies.

Marco P. M. Ferreira received the B.S. degree in computer science from the Polytechnic Institute of Leiria in 2002. He is currently a Ph.D. student at Extremadura University, Badajoz, Spain. His research interests include metaheuristic algorithms and indoor positioning systems.

Marko Gasparovic received the B.S. degree in computer science from the Polytechnic Institute of Zagreb, Croatia in 2015. He is currently a master student in computer science with the Department of Mobile Computing, Polytechnic of Leiria, guided by Prof. J. S. Pereira. His current research as a part of master thesis work is based on indoor positioning system among others.

[P5] - J. Pereira, M.P.M. Ferreira, M. Gasparovic, Tunable super-structured fiber Bragg gratings with perfect sequences, OAHOST - Open Access Journal, Vol. 1, No. 1, pp. 1 - 15, October 2016.

OAHOST

ARTICLE Open Access

Tunable super-structured fiber Bragg gratings with perfect sequences

João S Pereira[1,2§], Marco PM Ferreira[2], Marko Gasparovic[1,2]

[1]*Instituto de Telecomunicações, Leiria, Portugal*
[2]*Escola Superior de Tecnologia e Gestão, Instituto Politécnico de Leiria, Leiria, Portugal*

[§]Corresponding author: email: joao.pereira@ipleiria.pt
marco.ferreira@ipleiria.pt
marko1559@gmail.com

Abstract

Recently, tunable fiber Bragg grating (FBG) was developed by using stress-responsive colloidal crystals [1]. In this paper, we have simulated the application of these nanoparticles into super-structured fiber Bragg grating (SSFGB) written with perfect sequences derived from a short Maximal-Length sequence [2]. A tunable SSFBG will be available to overcome the prohibitive temperature variation of these optical codecs [3]. Nevertheless, we present a method to implement a coherent time spreading optical code-division multiple-access (OCDMA) where a unique code (or perfect sequence) can be reused and mixed with different wavelengths to obtain a tunable wavelength-division multiplexing (WDM) system. In order to maximize the binary throughput, we have selected a unique short Maximal-Length sequence composed of 7 chips that can be tuned with 7 different optical wavelengths. We found thousands of different tunable combinations that present power contrast ratios (P/C) higher than 12 dB. When a WDM-OCDMA system uses 2 different combinations simultaneously, a perfect binary detection

with error correction codes is achieved successfully. The tunable SSFBG with colloidal crystals will be a simple and good alternative choice for Fiber-to-the-Home (FTTH) communications.

Introduction

Optical fibers provide enormous and unsurpassed transmission bandwidth with negligible latency, and are now the transmission medium of choice for long distance and high data rate transmission in telecommunication networks [4].

Optical Code-Division Multiple Access (OCDMA) is a promising candidate for next-generation broadband access networks. Super Structured Fiber Bragg Gratings (SSFBG) can be used as encoders/decoders on Time Spreading Optical Code-Division Multiple Access (TS OCDMA) communication, offering high-performance, compactness, and compatibility with fiber-optic systems with a potential low cost [5-8].

The optical performance with high throughput pass through the use of optical coders and decoders that can perform this task in optical domain and in real time. It is possible to find many kinds of optical Codecs. Some of them are planar lightwave circuits [9], spatial lightwave phase modulators [10], and arrayed waveguide gratings [11]. However, all of them require a temperature stability. For example, if the temperature range between two ONU (Optical Network Unit) of a Fiber-to-the-Home (FTTH) system is larger than 8.0 K, temperature controller for the SSFBG should be installed in each ONU [3]. To avoid this problem, in this paper we will present a new optical SSFBG codec that is tunable and can, by this way, compensate the temperature drift. Nevertheless, the tunable SSFBG can also implement a simple wavelength multiplexing process between different users.

Fiber Bragg gratings (FBG) are optical fibers which were developed by using stress-responsive colloidal crystals that can reflect particular wavelengths of light and transmit all others [1]. FBG is a periodic perturbation of the refractive index along the fiber length which is formed by exposure of the

core to an intense optical interference pattern [12]. A super structured fiber Bragg grating (SSFBG), also called a sampled fiber Bragg grating, is a special FBG that consists of several small FBGs placed in close proximity to one another. SSFBGs have attracted much attention in recent years with the discovery of techniques allowing the creation of equivalent chirp or equivalent phase shifts. The biggest advantage of an SSFBG with equivalent chirp or equivalent phase shifts is the possibility to design and fabricate gratings with greatly varying phase and amplitude responses by adjusting the spatial profile of the superstructure [13]. SSFBG technology has been shown to provide an attractive and highly flexible route to produce high performance, and potentially low cost, code generation and recognition components as required for Direct Sequence (DS-) OCDMA system [14]. In this paper, we present the integration of SSFBG with tunable mechanism where the thickness of nanomaterial can be adjusted to reduce error probability in an optical communication system. A based piezoelectric device can control this thickness with precision. Also, these FBG are using stress-responsive colloidal crystals as their Bragg reflectors which has interesting optical properties, such as photonic band gaps (PBG) [1]. This feature is responsible for making colloidal crystals optimal candidates for the construction of FBG with a tunable filter or reflector, depending on the objective. It can also have the function of filtering multiple wavelengths by incorporating different colloidal crystal segments into the fiber [1]. The problem is that if we have fixed colloidal crystal film, then the tuning ranges of PBG are mostly limited by their refractive index parameter. There is a necessity to alter the distance between neighboring colloidal crystals film to reduce refractive index.

The main peak position (for a chip i) can be estimated by Bragg's equation for a normal incident beam:

$$\lambda_i = 1.633 T_i n_{average}, \quad (1)$$

By definition, in digital communications a chip is a pulse of a Pseudo-random Noise (PN) code sequence used in direct-sequence code division multiple access (CDMA) techniques.

In (1), is the distance between two adjacent nanoparticles and $n_{average}$ is the average refractive index of the colloidal crystal film. Based on this equation, there are several protocols for tuning the PBG of the films which are placed on the proximal end faces of two sections of optical fibers. Good example of tuning the PBG is changing the distance between neighboring colloidal crystals with mechanical stress. Its PBG can be tuned precisely by using different strengths of pressure.

Tunable Fiber Bragg Gratings, using responsive colloidal crystals, has characteristic reflection peak of the FBG shifts when compression is applied to them. Furthermore, it has been found that the shift is linearly dependent with the compression ratio [1]. Let the compression ratio of the reflector, be defined as R_i,

$$R_i = 1-(T_i/T_0), \quad (2)$$

with being the compressed thickness of the colloidal crystal Bragg reflector and T_0 its initial thickness. Then, the shifted center wavelength (λ_i) resulting from the compression can be approximated, with a 0.9899 correlation coefficient, as

$$\lambda_i = 603.1-385.3R_i \ , (3)$$

According to (3), the FBG with different Bragg reflectors could be customized precisely by quickly tuning the thickness of its Bragg reflector.

In section II, we introduce a theoretical model for the tunable SSFBG. Section III presents a coherent WDM-OCDMA system with tunable SSFBG. The following section IV shows that it is possible to estimate the error probability of the tunable SSFBG, and main conclusions are gathered in the last section.

Methods Theoretical Model for Tunable SSFBG

The SSFBG power reflection of the fiber Bragg grating i is given by the following equation [12]

$$r_i = \left| \frac{-\kappa \sinh\left(\sqrt{\kappa^2 - \hat{\sigma}^2} L_i\right)}{\hat{\sigma} \sinh\left(\sqrt{\kappa^2 - \sigma^2} L_i\right) + j\sqrt{\kappa^2 - \hat{\sigma}^2} \cosh\left(\sqrt{\kappa^2 - \sigma^2} L_i\right)} \right|^2 , \quad (4)$$

With $\hat{\sigma} = \left(\frac{\lambda_{\max}}{\lambda} - 1\right)\pi \frac{N_G}{L_i}$ and $i = 0,1,...N-1$. Here, $\lambda_{\max}$ is the wavelength of maximum reflectivity, that occurs when $\hat{\sigma} = 0$ and is given by $\lambda_{\max} = \left(1 + \frac{\overline{\delta n_{eff}}}{n_{eff}}\right)\lambda_i$. To simplify the study of SSFBG, it is possible to consider that $\lambda_{\max} \approx \lambda_i$. Here λ_i is the design wavelength of fibre gratings i for Bragg scattering by an infinitesimally weak grating [12]. n_{eff} is the refractive index. For a single-mode Bragg reflection with a uniform grating, the "dc" index change [12] spatially averaged over a grating period $\overline{\delta n_{eff}}$ is constant. Therefore, the coefficients $\hat{\sigma}$ and κ are also constants. κ is the "ac" coupling coefficient and $\hat{\sigma}$ is a general "dc" self-coupling coefficient used in the coupled-mode theory of uniform gratings, where N_G is the total number of grating periods [12].

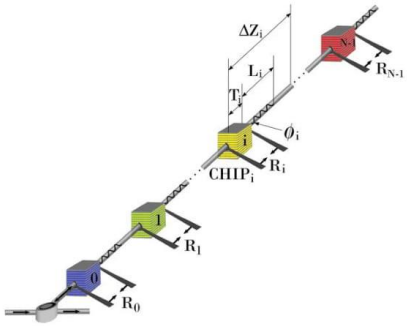

Fig. 1: The tunable SSFBG encoder structure.

Usage of responsive colloidal crystals in a SSFBG is represented in Fig. 1 with the R_i blocks, where Δz_i is the values of the separation between two chips. The N sections of length L_i have tunable thickness T_i of colloidal crystals with a compression R_i. The N sections of length L_i are written using the

wavelength $\lambda_i = \lambda_0 + i\Delta\lambda$. Where $\Delta\lambda$ is an incremental value of the wavelength ($\Delta\lambda << \lambda_0$). Each section of the grid represents a SSFBG chip that is etched with a phase ϕ_i, $i = 0,1,...N-1$.

For our SSFBG study (based on a selected family of codes) we considered that $\Delta z_i \geq \max(T_i + L_i)$. The power reflection (4) can be rewritten using a Taylor series for $sinh(\,)$ and $cosh(\,)$ when $\sqrt{\kappa^2 - \hat{\sigma}^2}L_i$ assumes a low value, $i = 0,1,...N-1$. Thus, the power reflection of a chip *i* has been derived and it is approximately [2]:

$$r_i(\lambda) \approx \left| \frac{-\kappa_1 L_i}{\pi \frac{N_G}{L_i}\left(\frac{\lambda_{\max}}{\lambda} - 1\right) + j} \right|^2 , (5)$$

This expression is similar to the transfer function of a bandpass filter (BPF) centered on the wavelength $\lambda_{\max}$, with the amplitude $r_i(\lambda_{\max}) = |\kappa_1 L_i|^2$ and:

$$r_i(\pm\infty) = \frac{|\kappa_1 L_i|^2}{1 + \left(\pi \frac{N_G}{L_i}\right)^2} = \varepsilon |\kappa_1 L_i|^2 , (6)$$

When $\pi N_G >> L_i$, then $r_i(\lambda_{\max}) >> r_i(\pm\infty)$ (because $\varepsilon << 1$), and therefore it is possible to associate a specific SSFBG *i* to a BPF filter.

In this scenario, it is considered that the *N* chips are written with the wavelengths $\lambda_i = \lambda_0 + i\Delta\lambda$, for $0 \leq i \leq N-1$, and all chips will have the same value $\kappa = \kappa_1$. For convenience, the transfer function of the 1st chip of the SSFBG, when $\phi_0 = 0$, may be modelled as a scaled version of the rectangular function defined by the following expression:

$$\mathrm{Rect}_{\varepsilon}\left(\frac{\lambda - \lambda_{\max}}{B}\right) = \begin{cases} 1 & when \quad \lambda_{\max} - \frac{B}{2} \leq \lambda \leq \lambda_{\max} + \frac{B}{2} \\ \varepsilon & other \quad \lambda \end{cases} , (7)$$

This special rectangular function, centered at $\lambda_{\max}$, has a bandwidth equal to B and a minimum amplitude equal to $\varepsilon = \frac{1}{1+\left(\pi \frac{N_G}{L_i}\right)^2}$. When $\pi N_G >> L_i$, then $B \approx \frac{2L_i}{\pi N_G}\lambda_{\max}$, and (7) is cut -3 dB at $\lambda = \lambda_{\max} \pm \frac{B}{2}$.

Each grid of each SSFBG chip *i*, $i = 0,1,...N-1$, acts as a specific BPF with a transfer function approximately equal to the following expression:

$$\left|\kappa_1 L_i\right|^2 \times \exp\{j\phi_i\} \times \mathrm{Rect}_{\varepsilon}\left(\frac{\lambda - \lambda_0 - i\Delta\lambda}{B}\right), \quad (8)$$

It was considered that $\lambda_{\max} \approx \lambda_i$. The phase ϕ_i of the chip *i* is shown in Fig. 1. The power reflection of a series of *N* chips (a train of *N* FBGs) is given by:

$$\prod_{i=1}^{N}\left|\kappa_1 L_i\right|^2 \times \exp\{j\phi_i\} \times \mathrm{Rect}_{\varepsilon}\left(\frac{\lambda - \lambda_0 - i\Delta\lambda}{B}\right), \quad (9)$$

Considering the special case when $\frac{B}{2} \le \Delta\lambda < B$, then the previous expression may be considered approximately equal to:

$$\sum_{i=0}^{N-1} A^2 \times \exp\{j(\phi_i + \phi_{i+1})\} \times \mathrm{Rect}_{\varepsilon_2}\left(\frac{\lambda - \lambda_0 - i\Delta\lambda - \frac{\Delta\lambda}{2}}{W}\right), \quad (10)$$

with $A^2 = \varepsilon^{N-2}\left|\kappa_1 L_i\right|^4$ and $\varepsilon_2 = \frac{\varepsilon}{\left|\kappa_1 L_i\right|^2}$.

This result (10) is obtained when the product of two consecutive rectangular functions (of index *i* and index *i* + 1) is equal to a rectangular function with a bandwidth $W = B - \Delta\lambda$, with $0 < W < B$, centered at $\lambda_0 + i\Delta\lambda + \frac{\Delta\lambda}{2}$. In this process, $\varepsilon_2 = \frac{\varepsilon}{\left|\kappa_1 L_i\right|^2}$ can be disregarded if (10) is sampled at the centers of rectangular pulses $\mathrm{Rect}_{\varepsilon_2}\left(\frac{\lambda - \lambda_0 - i\Delta\lambda - \frac{\Delta\lambda}{2}}{W}\right)$. The sampling process is equivalent to considering that the bandwidth W is reduced to an infinitesimal value. This operation will convert (10) in a function

approximately equal to a train of unit pulses. That is, the SSFBG power reflection of *N* chips (uniformly distributed is approximately equal to (10) after the sampling procedure defined by:

$$\sum_{i=0}^{N-1} A^2 \times \exp\left\{ j\left(\phi_i + \phi_{i+1}\right)\right\} \times \delta\left(\lambda - \lambda_0 - i\Delta\lambda - \frac{\Delta\lambda}{2}\right), \quad (11)$$

The function $\delta(\ )$ is a unitary pulse. For convenience, it is considered that $\phi_N = \phi_0$. In other words, the power reflection has undergone a translation of one cycle. This simplification can be made if the codes written in SSFBGs are considered long ($N >> 2$). In this case, the IDFT (Inverse Discrete Fourier Transform) of a normalized SSFBG power reflection (IDFT of (11) around $\lambda_0 + \frac{\Delta\lambda}{2}$), is approximately proportional to the following expression:

$$x_{SSFBG}(t) \propto \sqrt{N} \times IDFT\left\{ \sum_{i=0}^{N-1} \exp\left[j\left(\phi_i + \phi_{i+1}\right)\right] \times \delta\left(\lambda - i\Delta\lambda\right)\right\}, \quad (11)$$

When the input of the SSFBG is a unitary pulse with an amplitude $\frac{\sqrt{N}}{A^2}$. After the $\lambda_0 + \frac{\Delta\lambda}{2}$ translation of (11), this signal (12) can be considered as a baseband signal of the codes written in the SSFBG. Each chip Δz_i of a SSFBG, when $\frac{B}{2} \le \Delta\lambda < B$, has a phase $\theta_i = \phi_i + \phi_{i+1}$ defined by the cosine pattern (L_i of Fig. 1) and the stress-responsive colloidal crystals (T_i of Fig. 1). The amplitudes must be constant for all chips. This means that the SSFBG power reflection baseband signal, defined by the model (12), is the IDFT of a unimodular sequence. By definition, (12) is a perfect sequence [15]. This mean that our tunable SSFBG codec will be immune of multipath interferences.

Coherent WDM-OCDMA System with Tunable SSFBG

Continuing the study, we simulated the usage of a coherent WDM-OCDMA system using a Tunable SSFBG coded with a 7-chip m-sequence. The sequence used was [+1, +1, +1, -1, -1, +1, -1]. Because of

the wavelength shifting properties of the compressed colloidal crystals, different wavelength channels can be chosen for each chip. Table 1 shows the 7 different channels that we used in our simulation, including the compression ratio R_i required to achieve the desired wavelength λ_i. Each channel has a bandwidth of B = 25 nm. $\frac{B}{2} = \Delta\lambda$ = 12.5 nm.

By giving different tunings to each section of the SSFBG, different combinations of channels can be used to transmit the code. Our simulation includes three different scenarios of channel configurations for the same code, which we called SSFBG1, SSFBG2 and SSFBG3. Table 2 shows the scenarios used. Notice that SSFBG3 uses only one channel. These multiple combination scenarios would also allow simultaneous users (each with a different WDM channel combination), or increasing the throughput of the communication (sending multiple bits in parallel).

Channel Ch i	Wavelength λ_i [nm]	Compression ratio R_i
0	512,5	0,235
1	525,0	0,203
2	537,5	0,170
3	550,0	0,138
4	562,5	0,105
5	575,0	0,073
6	587,5	0,040

Table 1: Wavelength and compression ratio for the m-sequence of 7 chips.

Configuration Name	WDM Combination
SSFBG1	+Ch5, +Ch4, +Ch2, -Ch3, -Ch6, +Ch0, -Ch1
SSFBG2	+Ch1, +Ch0, +Ch6, -Ch4, -Ch5, +Ch2, -Ch3
SSFBG3	+Ch6, +Ch6, +Ch6, -Ch6, -Ch6, +Ch6, -Ch6

Table 2: Different WDM combinations used to encode the m-sequence [+1, +1, +1, -1, -1, +1, -1].

Figures 2, 3 and 4 represent the power spectrum of SSFBG1, SSFBG2 and SSFBG3 respectively. The m-sequence of 7 chips has been simulated using 42 samples in the 100 nm that composes the entire 7-channels bandwidth and considering a SSFBG writing phase precision of $\frac{\pi}{10}$.

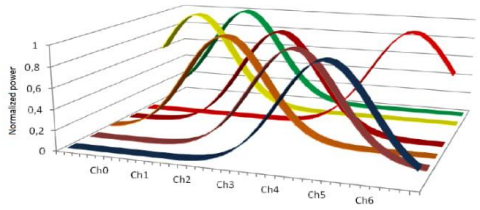

Figure 2: Spectrum SSFBG1="+Ch5,+Ch4,+Ch2,-Ch3,-Ch6,+Ch0,-Ch1".

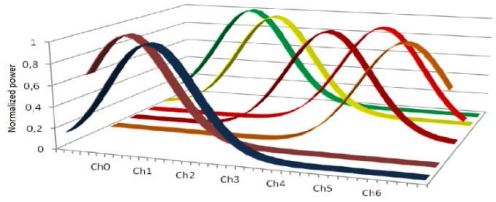

Figure 3: Spectrum SSFBG2="Ch1,Ch0,Ch6,-Ch4,-Ch5,+Ch2,-Ch3".

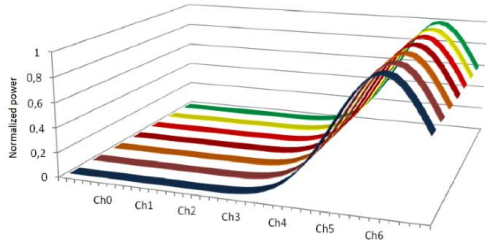

Figure 4: Spectrum SSFBG3="+Ch6,+Ch6,+Ch6,-Ch6,-Ch6+Ch6,-Ch6".

Analyzing the autocorrelation and cross-correlation properties of the SSFBG, (Figures 5 and 6 respectively), we notice that all configurations present good autocorrelation and cross-correlation properties, with configuration SSFBG3 presenting slightly worse autocorrelation, but still presenting a very distinctive in-phase peak. All configurations present a minimum power contrast ratio equal to 12.3 dB. The average power contrast ratio (defined as P/W=20*log[Peak(Correlation)/Average(Correlation)]), is much larger and equal to 30.0 dB. The Worst Error Probability has been found to be $\max\{P_e\} = 5*10^{-5}$.

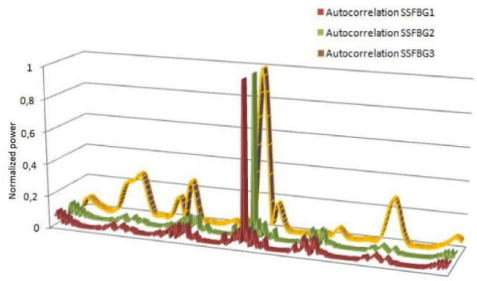

Figure 5: Normalized autocorrelation, in time domain, with SSFBG1, SSFBG2, and SSFBG3.

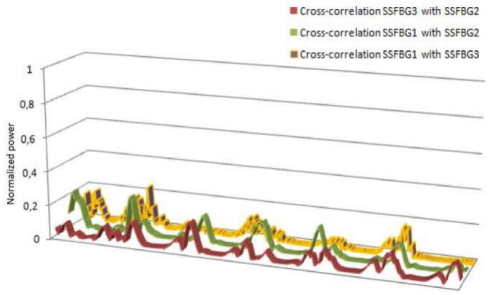

Figure 6: Normalized cross-correlation, in time domain, with SSFBG1, SSFBG2, and SSFBG3.

Tunable SSFBG Error Probability

To simplify the study and analysis of the tunable SSFBG error probability, we chose to consider only bipolar codes (with two phases: 0 and π). The chip +1 is coded with a phase 0 and the chip -1 is coded with the phase π. The worst case to be considered is when the 7 chips are coded in the same wavelength channel. Then, the phase modulation is simply a BPSK modulation and the system to be analyzed is a TS-OCDMA-PON system with coherent coding and decoding making use of bipolar codes. The error probability P_e may be used to find an upper bound for an OCDMA system. This P_e upper bound $\max\{P_e\}$ can be a function of the cross-correlation power contrast ratio $P/C = 20\log\left[C_k(0)/\max\{C_{k,i}\}\right]$ (in dB), where $C_{k,i}$ is the cross-correlation and C_k is the autocorrelation [2]. Some P/C upper bounds, for

periodic correlations, have been found. One of them is the Welch bound [16] of *K* perfect sequences of length *N*: $P/C = 20\log\sqrt{\frac{KN-1}{K-1}}$. For the aperiodic correlation case, the upper bound is

$P/C = 20\log\sqrt{\frac{2KN-K-1}{K-1}}$.

For a good communication system, the code set selected should have a high P/C value. For example, it has been suggested that the SSFBG should have power contrast ratios higher than 17 dB for 127-chips Gold codes [17].

In this study, we consider the upper bound of the error probability [2] that is a function of the power contrast ratio P/C:

$$\max\{P_e\} \approx 1-\phi\left[\left(\frac{N_0}{2E_b}+(K-1)\left(1-\frac{1}{N}\right)10^{-\frac{P/C}{10}}\right)^{-1/2}\right], \quad (13)$$

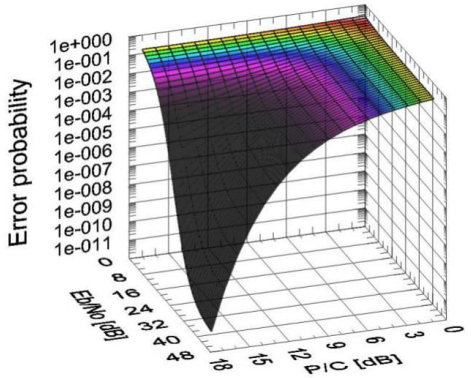

Figure 7: 3D representation of the probability error upper bound with tunable SSFBG.

Figure 7 shows a 3D representation of the upper bound (13), for K = 2 users and the length is N = 7 x 7 chips. For example, the error probability upper bound is lower than 10^{-5} when the two ratios P/C and E_b/N_o are at least equal to 12.3 dB. E_b is the bit energy and N_o is the spectral density of additive white Gaussian noise (AWGN). This situation requires a bit error correction method to guarantee an error free

transmission. However, we should remember that (13) gives us the worst case error probability. Frequently, the error probability average is utilized and, of course, this average will be much lower than the worst case (13).

Finally, we should remember that the selection of the appropriate codes, the SSFBG ultraviolet light writing precision, and the precision of the optical communication synchronization (sampling operation) are important when we want to design a gigabit OCDMA-PON transmission system with low BER over more long distances.

Conclusions

In this paper, a new tunable super-structured fiber Bragg grating (SSFGB) was developed by using stress-responsive colloidal crystals. A new SSFBG codec with nanoparticles has been simulated with short Maximal-Length sequence. Using a mathematical model, we found that the novel tunable SSFBG is similar to a codec of perfect sequences. These sequences are, by definition, immune to multipath interferences.

Our proposed WDM-OCDMA system with coherent coding and decoding process has been evaluated with an error probability based on the power contrast ratios of some code sets. The good results obtained allow the conclusion that the new tunable SSFBG, with colloidal crystals and perfect sequences, will be a simple solution for WDM-OCDMA communications, when the optical coding and decoding processes require temperature stability and multiplexing capacity.

References

1. Shuman S: **Structure, mechanism, and evolution of the mRNA capping apparatus.** *Prog. Nucleic Acid Res. Mol. Biol* 2000, **66**:1-40

2. Chomczynski P, Sacchi N: **Single-step method of RNA isolation by acid guanidinium thiocyanate-phenol-chloroform extraction.** *Anal Biochem* 1987, **162**:156-159
3. Sambrook J, Fitsch EF, Maniatis T: *Molecular Cloning: A Laboratory Manual.* Cold Spring Harbor, Cold Spring Harbor Press 1989
4. Wessely S, Wood F: **Peer review of grant applications: a systematic review.** In: *Peer review in Health Sciences.* Edited by Godlee F, Jefferson T. London, BMJ Books 1999, 14-31
5. Advisory Committee on Genetic Modification: *Annual Report.* London; 1999.
1. H. Ding, Y. Cheng, H. Gu, Y. Zhao, B. Wang, and Z. Gu: **Tunable fiber Bragg grating based on responsive photonic crystals**, *Nanoscale Communication (RSCPublishing)*, 5, 11572 (2013).
2. J. Pereira, H. A. Silva: **Error probability upper bound for perfect sequences implemented with super-structured fibre Bragg gratings**, *IET Signal Processing*, 8, 4, 421-428 (June, 2014).
3. R. Matsumoto, T. Kodama, S. Shimizu, R. Nomura, K. Omichi, N. Wada, and K. Kitayama: **40G-OCDMA-PON System With an Asymmetric Structure Using a Single Multi-Port and Sampled SSFBG Encoder/Decoders**, *Journal of Lightwave Technology*, 32, 6 (March 15, 2014).
4. Francis Idachaba, Dike U. Ike, and Orovwode Hope: **Future Trends in Fiber Optics Communication**, *Proceedings of the World Congress on Engineering 2014*, Vol I, WCE 2014, July 2 - 4, 2014.
5. Cedric Lam: **Passive Optical Networks, Principles and Practice**, *Elsevier*, 2007.
6. Salehi, J. A., Weiner, A. M., and Heritage, J. P.: **Coherent Ultrashort Light Pulse Code Division Multiple Access Communication Schemes**, *IEEE J. Lightwave Technol.*, Mar. 1990, 8, (3), pp. 478-491
7. Prucnal, P., Santoro M., and Fan T.: **Spread spectrum fiber-optic local area network using optical processing**, *IEEE J. Lightwave Technol.*, May 1986, 4, (5)

8. Santoro, M. A., and Prucnal, P. R.: **Asynchronous fiber optic LAN using CDMA and optical correlation**, *Proc. IEEE*, Sept. 1987, 75, (9)
9. Katsunari Okamoto: **TUTORIAL REVIEW Recent progress of integrated optics planar lightwave circuits**, *Optical and Quantum Electronics*, 1999, 31, pp. 107-129
10. Z. Jiang, et al.: **Four-User 10-Gb/s Spectrally Phase-Coded O-CDMA System Operating at ~30fJ/bit**, *IEEE Photon. Tech. Lett.*, 2005, 17, pp. 705-707
11. Xaveer J. M. Leijtens, Berndt Kuhlow, and Meint K. Smi: **Arrayed Waveguide Gratings**, pp. 1-63, http://alexandria.tue.nl/openaccess/Metis203741.pdf, accessed April 2013
12. Erdogan T.: **Fiber grating spectra**, *IEEE J. Lightwave Technol.*, Aug. 1997, 15, (8), pp. 1277-1294
13. Sebastien Blais: **Superstructured Fiber Bragg Gratings and Applications in Microwave Signal Processing**, Ottawa, Canada, 2014. https://www.ruor.uottawa.ca/bitstream/10393/30358/3/Blais_Sebastien_2014_thesis.pdf
14. Teh, P.C., Ibsen, M., Fu, L. B., Lee, J. H., Yusoff, Z., and Richardson, D. J.: **A 16-channel OCDMA system (4 OCDM x4WDM) based on 16-chip, 20 Gchip/s superstructure fiber Bragg gratings and DFB fiber laser transmitters**, *Proc. Optical Fiber Communication Conf. (OFC'2002)*, Los Angeles, CA, ThEE1, pp. 600–601
15. J. Pereira: **Sequências perfeitas para sistemas de comunicação**, *Novas Edições Acadêmicas*, Saarbrücken, 2015.
16. Sarwate, D., Pursley, M.: **Crosscorrelation Properties of Pseudorandom and Related Sequences**, *Proceedings of the IEEE*, May 1980, 68, (5), pp. 593 – 619.
17. Wang, X., Matsushima, K., Nishiki, A., Wada, N., and Kitayama, K.: **High reflectivity super structured FBG for coherent optical code generation and recognition**, *Opt. Express*, Nov. 2004, 12, (22), pp. 5457- 5468.

[P6] - J. Pereira, M.P.M. Ferreira, M. Gasparovic, Tunable Super-Structured Fibre Bragg Gratings with Perfect Sequences, Energy Material Nanotechnology, Beijing, China, Vol. 1, pp. 29 - 29, April 2016.

Tunable super-structured fiber Bragg gratings with perfect sequences

João S. Pereira[1,2], Marco Ferreira[2] and Marko Gasparovic[1,2]

[1] Instituto de Telecomunicações, Leiria, Portugal
[2] Escola Superior de Tecnologia e Gestão do Instituto Politécnico de Leiria, Portugal
E-mails: joao.pereira@ipleiria.pt.

Abstract — **Recently, tunable fiber Bragg grating (FBG) was developed by using stress-responsive colloidal crystals [1]. In this paper, we have simulated the application of these nanoparticles into super-structured fiber Bragg grating (SSFGB) written with perfect sequences derived from a short Maximal-Length sequence [2]. A tunable SSFBG will be available to overcome the prohibitive temperature variation of these optical codecs [3]. Nevertheless, we present a method to implement a coherent time spreading optical code-division multiple-access (OCDMA) where a unique code (or perfect sequence) can be reused and mixed with different wavelengths to obtain a tunable wavelength-division multiplexing (WDM) system. In order to maximize the binary throughput, we have selected a unique short Maximal-Length sequence composed of 7 chips that can be tuned with 7 different optical wavelengths. We found thousands of different tunable combinations that present power contrast ratios (P/C) higher than 12 dB. When a WDM-OCDMA system uses 2 different combinations simultaneously, a perfect binary detection with error correction codes is achieved successfully. The tunable SSFBG with colloidal crystals will be a simple and good alternative choice for Fiber-to-the-Home (FTTH) communications.**

Index Terms **– *M*-sequences, Nanomaterial, OCDMA, SSFBG, and Stress-responsive Colloidal Crystals.**

I. Introduction

Optical fibers provide enormous and unsurpassed transmission bandwidth with negligible latency, and are now the transmission medium of choice for long distance and high data rate transmission in telecommunication networks [4].

Optical Code-Division Multiple Access (OCDMA) is a promising candidate for next-generation broadband access networks. Super Structured Fiber Bragg Gratings (SSFBG) can be used as encoders/decoders on Time Spreading Optical Code-Division Multiple Access (TS OCDMA) communication, offering high-performance, compactness, and compatibility with fiber-optic systems with a potential low cost [5-8].

The optical performance with high throughput pass through the use of optical coders and decoders that can perform this task in optical domain and in real time. It is possible to find many kinds of optical Codecs. Some of them are planar lightwave circuits [9], spatial lightwave phase modulators [10], and arrayed waveguide gratings [11]. However, all of them require a temperature stability. For example, if the temperature range between two ONU (Optical Network Unit) of a Fiber-to-the-Home (FTTH) system is larger than 8.0 K, temperature controller for the SSFBG should be installed in each ONU [3]. To avoid this problem, in this paper we will present a new optical SSFBG codec that is tunable and can, by this way, compensate the temperature drift. Nevertheless, the tunable SSFBG can also implement a simple wavelength multiplexing process between different users.

Fiber Bragg gratings (FBG) are optical fibers which were developed by using stress-responsive colloidal crystals that can reflect particular wavelengths of light and transmit all others [1]. FBG is a periodic perturbation of the refractive index along the fiber length which is formed by exposure of the core to an intense optical interference pattern [12]. A super structured fiber Bragg grating (SSFBG), also called a sampled fiber Bragg grating, is a special FBG that consists of several small FBGs placed in close proximity to one another. SSFBGs have attracted much attention in recent years with the discovery of techniques allowing the creation of equivalent chirp or equivalent phase shifts. The biggest advantage of an SSFBG with equivalent chirp or equivalent phase shifts is the possibility to design and fabricate gratings with greatly varying phase and amplitude responses by adjusting the spatial profile of the superstructure [13]. SSFBG technology has been shown to provide an attractive and highly flexible

route to produce high performance, and potentially low cost, code generation and recognition components as required for Direct Sequence (DS-) OCDMA system [14]. In this paper, we present the integration of SSFBG with tunable mechanism where the thickness of nanomaterial can be adjusted to reduce error probability in an optical communication system. Also, these FBG are using stress-responsive colloidal crystals as their Bragg reflectors which has interesting optical properties, such as photonic band gaps (PBG) [1]. This feature is responsible for making colloidal crystals optimal candidates for the construction of FBG with a tunable filter or reflector, depending on the objective. It can also have the function of filtering multiple wavelengths by incorporating different colloidal crystal segments into the fiber [1]. The problem is that if we have fixed colloidal crystal film, then the tuning ranges of PBG are mostly limited by their refractive index parameter. There is a necessity to alter the distance between neighboring colloidal crystals film to reduce refractive index.

The main peak position λ_i (for a chip i) can be estimated by Bragg's equation for a normal incident beam:

$$\lambda_i = 1.633 T_i n_{average} . \quad (1)$$

In (1), T_i is the distance between two adjacent nanoparticles and $n_{average}$ is the average refractive index of the colloidal crystal film. Based on this equation, there are several protocols for tuning the PBG of the films which are placed on the proximal end faces of two sections of optical fibers. Good example of tuning the PBG is changing the distance between neighboring colloidal crystals with mechanical stress. Its PBG can be tuned precisely by using different strengths of pressure.

Tunable Fiber Bragg Gratings, using responsive colloidal crystals, has characteristic reflection peak of the FBG shifts when compression is applied to them. Furthermore, it has been found that the shift is linearly dependent with the compression ratio [1]. Let the compression ratio of the reflector R_i, be defined as

$$R_i = 1 - (T_i / T_0), \quad (2)$$

with T_i being the compressed thickness of the colloidal crystal Bragg reflector and T_0 its initial thickness. Then, the shifted center wavelength (λ_i) resulting from the compression can be approximated, with a 0.9899 correlation coefficient, as

$$\lambda_i = 603.1 - 385.3 R_i , \quad (3)$$

According to (3), the FBG with different Bragg reflectors could be customized precisely by quickly tuning the thickness of its Bragg reflector.

In section II, we introduce a theoretical model for the tunable SSFBG. Section III presents a coherent WDM-OCDMA system with tunable SSFBG. The following section IV shows that it is possible to estimate the error probability of the tunable SSFBG, and main conclusions are gathered in the last section.

II. Theoretical Model for Tunable SSFBG

The SSFBG power reflection of the fiber Bragg grating i is given by the following equation [12]

$$r_i = \left| \frac{-\kappa \sinh\left(\sqrt{\kappa^2 - \hat{\sigma}^2} L_i\right)}{\hat{\sigma} \sinh\left(\sqrt{\kappa^2 - \hat{\sigma}^2} L_i\right) + j\sqrt{\kappa^2 - \hat{\sigma}^2} \cosh\left(\sqrt{\kappa^2 - \hat{\sigma}^2} L_i\right)} \right|^2 \quad (4)$$

with $\hat{\sigma} = \left(\frac{\lambda_{\max}}{\lambda} - 1\right)\pi \frac{N_G}{L_i}$ and $i = 0,1,...N-1$. Here, $\lambda_{\max}$ is the wavelength of maximum reflectivity, that occurs when $\hat{\sigma} = 0$ and is given by $\lambda_{\max} = \left(1 + \frac{\overline{\delta n_{eff}}}{n_{eff}}\right)\lambda_i$.

To simplify the study of SSFBG, it is possible to consider that $\lambda_{\max} \approx \lambda_i$. Here λ_i is the design wavelength of fibre gratings i for Bragg scattering by an infinitesimally weak grating [12]. n_{eff} is the refractive index. For a single-mode Bragg reflection with a uniform grating, the "dc" index change [12] spatially averaged over a grating period $\overline{\delta n_{eff}}$ is constant. Therefore, the coefficients $\hat{\sigma}$ and κ are also constants. κ is the "ac" coupling coefficient and $\hat{\sigma}$ is a general "dc" self-coupling coefficient used in the coupled-mode theory of uniform gratings, where N_G is the total number of grating periods [12].

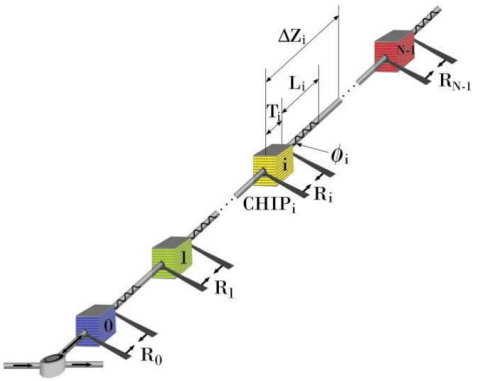

Fig. 1: The tunable SSFBG encoder structure.

Usage of responsive colloidal crystals in a SSFBG is represented in Fig. 1 with the R_i blocks, where Δz_i is the values of the separation between two chips. The N sections of length L_i have tunable thickness T_i of colloidal crystals with a compression R_i. The N sections of length L_i are written using the wavelength $\lambda_i = \lambda_0 + i\Delta\lambda$. Where $\Delta\lambda$ is an incremental value of the wavelength ($\Delta\lambda \ll \lambda_0$). Each section of the grid represents a SSFBG chip that is etched with a phase ϕ_i, $i = 0,1,...N-1$.

For our SSFBG study (based on a selected family of codes) we considered that $\Delta z_i \geq \max(T_i + L_i)$. The power reflection (4) can be rewritten using a Taylor series for sinh( ) and cosh( ) when $\sqrt{\kappa^2 - \hat{\sigma}^2}L_i$ assumes a low value, $i = 0,1,...N-1$. Thus, the power reflection of a chip i has been derived and it is approximately [2]:

$$r_i(\lambda) \approx \left| \frac{-\kappa_1 L_i}{\pi \frac{N_G}{L_i}\left(\frac{\lambda_{\max}}{\lambda} - 1\right) + j} \right|^2 . \quad (5)$$

This expression is similar to the transfer function of a bandpass filter (BPF) centered on the wavelength $\lambda_{\max}$, with the amplitude $r_i(\lambda_{\max}) = |\kappa_1 L_i|^2$ and:

$$r_i(\pm\infty) = \frac{|\kappa_1 L_i|^2}{1 + \left(\pi \frac{N_G}{L_i}\right)^2} = \varepsilon |\kappa_1 L_i|^2 . \quad (6)$$

When $\pi N_G >> L_i$, then $r_i(\lambda_{\max}) >> r_i(\pm\infty)$ (because $\varepsilon << 1$), $i = 0,1,...N-1$ and therefore it is possible to associate a specific SSFBG i to a BPF filter.

In this scenario, it is considered that the N chips are written with the wavelengths $\lambda_i = \lambda_0 + i\Delta\lambda$, for $0 \leq i \leq N-1$, and all chips will have the same value $\kappa = \kappa_1$. For convenience, the transfer function of the 1st chip of the SSFBG, when $\phi_0 = 0$, may be modelled as a scaled version of the rectangular function defined by the following expression:

$$\mathrm{Rect}_\varepsilon\left(\frac{\lambda - \lambda_{\max}}{B}\right) = \begin{cases} 1 & when \quad \lambda_{\max} - \frac{B}{2} \leq \lambda \leq \lambda_{\max} + \frac{B}{2} \\ \varepsilon & other \quad \lambda \end{cases} . \quad (7)$$

This special rectangular function, centered at $\lambda_{\max}$, has a bandwidth equal to B and a minimum amplitude equal to $\varepsilon = \frac{1}{1 + \left(\pi \frac{N_G}{L_i}\right)^2}$. When $\pi N_G >> L_i$, then $B \approx \frac{2L_i}{\pi N_G}\lambda_{\max}$, and (7) is cut -3 dB at $\lambda = \lambda_{\max} \pm \frac{B}{2}$. Each grid of each SSFBG chip i, $i = 0,1,...N-1$, acts as a specific BPF with a transfer function approximately equal to the following expression:

$$|\kappa_1 L_i|^2 \times \exp\{j\phi_i\} \times \mathrm{Rect}_\varepsilon\left(\frac{\lambda - \lambda_0 - i\Delta\lambda}{B}\right). \quad (8)$$

It was considered that $\lambda_{\max} \approx \lambda_i$. The phase ϕ_i of the chip i is shown in Fig. 1. The power reflection of a series of N chips (a train of N FBGs) is given by:

$$\prod_{i=1}^{N} |\kappa_1 L_i|^2 \times \exp\{j\phi_i\} \times \mathrm{Rect}_\varepsilon\left(\frac{\lambda - \lambda_0 - i\Delta\lambda}{B}\right) \quad (9)$$

Considering the special case when $\frac{B}{2} \leq \Delta\lambda < B$, then the previous expression may be considered approximately equal to:

$$\sum_{i=0}^{N-1} A^2 \times \exp\{j(\phi_i + \phi_{i+1})\} \times \mathrm{Rect}_{\varepsilon_2}\left(\frac{\lambda - \lambda_0 - i\Delta\lambda - \frac{\Delta\lambda}{2}}{W}\right) \quad (10)$$

with $A^2 = \varepsilon^{N-2}|\kappa_1 L_i|^4$ and $\varepsilon_2 = \frac{\varepsilon}{|\kappa_1 L_i|^2}$.

This result (10) is obtained when the product of two consecutive rectangular functions (of index i and index $i + 1$) is equal to a rectangular function with a bandwidth $W = B - \Delta\lambda$, with $0 < W < B$, centered at $\lambda_0 + i\Delta\lambda + \frac{\Delta\lambda}{2}$. In this process, $\varepsilon_2 = \frac{\varepsilon}{|\kappa_1 L_i|^2}$ can be disregarded if (10) is sampled at the centers of rectangular pulses $\mathrm{Rect}_{\varepsilon_2}\left(\frac{\lambda - \lambda_0 - i\Delta\lambda - \frac{\Delta\lambda}{2}}{W}\right)$. The sampling process is equivalent to considering that the bandwidth W is reduced to an infinitesimal value. This operation will convert (10) in a function approximately equal to a train of unit pulses. That is, the SSFBG power reflection of N chips (uniformly distributed is approximately equal to (10) after the sampling procedure defined by:

$$\sum_{i=0}^{N-1} A^2 \times \exp\{j(\phi_i + \phi_{i+1})\} \times \delta\left(\lambda - \lambda_0 - i\Delta\lambda - \frac{\Delta\lambda}{2}\right). \quad (11)$$

The function $\delta(\ )$ is a unitary pulse. For convenience, it is considered that $\phi_N = \phi_0$. In other words, the power reflection has undergone a translation of one cycle. This simplification can be made if the codes written in SSFBGs are considered long ($N >> 2$). In this case, the IDFT (Inverse Discrete Fourier Transform) of a normalized SSFBG power reflection (IDFT of (11) around $\lambda_0 + \frac{\Delta\lambda}{2}$), is approximately proportional to the following expression:

$$x_{SSFBG}(t) \propto \sqrt{N} \times IDFT\left\{\sum_{i=0}^{N-1} \exp\left[j(\phi_i + \phi_{i+1})\right] \times \delta(\lambda - i\Delta\lambda)\right\} \quad (12)$$

when the input of the SSFBG is a unitary pulse with an amplitude $\frac{\sqrt{N}}{A^2}$. After the $\lambda_0 + \frac{\Delta\lambda}{2}$ translation of (11), this signal (12) can be considered as a baseband signal of the codes written in the SSFBG.

Each chip Δz_i of a SSFBG, when $\frac{B}{2} \le \Delta\lambda < B$, has a phase $\theta_i = \phi_i + \phi_{i+1}$ defined by the cosine pattern (L_i of Fig. 1) and the stress-responsive colloidal crystals (T_i of Fig. 1). The amplitudes must be constant for all chips. This means that the SSFBG power reflection baseband signal, defined by the model (12), is the IDFT of a unimodular sequence. By definition, (12) is a perfect sequence [15]. This mean that our tunable SSFBG codec will be imune multipath interferences.

III. Coherent WDM-OCDMA system with tunable SSFBG

Continuing the study, we simulated the usage of a coherent WDM-OCDMA system using a Tunable SSFBG coded with a 7-chip m-sequence. The sequence used was [+1, +1, +1, -1, -1, +1, -1]. Because of the wavelength shifting properties of the compressed colloidal crystals, different wavelength channels can be chosen for each chip. Table 1 shows the 7 different channels that we used in our simulation, including the compression ratio R_i required to achieve the desired wavelength λ_i. Each channel has a bandwidth of B = 25 nm. $\frac{B}{2} = \Delta\lambda = 12.5$ nm.

By giving different tunings to each section of the SSFBG, different combinations of channels can be used to transmit the code. Our simulation includes three different scenarios of channel configurations for the same code, which we called SSFBG1, SSFBG2 and SSFBG3. Table 2 shows the scenarios used. Notice that SSFBG3 uses only one channel. These multiple combination scenarios would also allow simultaneous users (each with a different WDM channel combination), or increasing the throughput of the communication (sending multiple bits in parallel).

Channel Ch i	Wavelength λ_i [nm]	Compression ratio R_i
0	512,5	0,235
1	525,0	0,203
2	537,5	0,170
3	550,0	0,138
4	562,5	0,105
5	575,0	0,073
6	587,5	0,040

Table 1: Wavelength and compression ratio for the m-sequence of 7 chips.

Configuration Name	WDM Combination
SSFBG1	+Ch5, +Ch4, +Ch2, -Ch3, -Ch6, +Ch0, -Ch1
SSFBG2	+Ch1, +Ch0, +Ch6, -Ch4, -Ch5, +Ch2, -Ch3
SSFBG3	+Ch6, +Ch6, +Ch6, -Ch6, -Ch6, +Ch6, -Ch6

Table 2: Different WDM combinations used to encode the m-sequence [+1, +1, +1, -1, -1, +1, -1].

Figures 2, 3 and 4 represent the power spectrum of SSFBG1, SSFBG2 and SSFBG3 respectively. The m-sequence of 7 chips has been simulated using 42 samples in the 100 nm that composes the entire 7-channels bandwidth and considering a SSFBG writing phase precision of $\frac{\pi}{10}$.

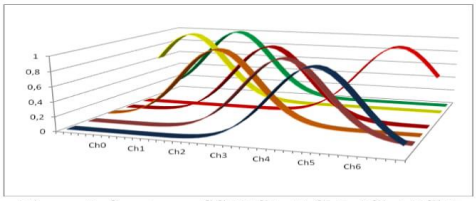

Figure 2: Spectrum SSFBG1="+Ch5,+Ch4,+Ch2,-Ch3,-Ch6,+Ch0,-Ch1".

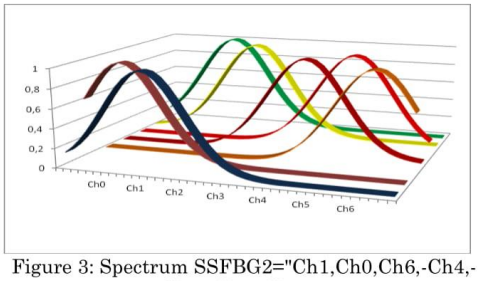

Figure 3: Spectrum SSFBG2="Ch1,Ch0,Ch6,-Ch4,-Ch5,+Ch2,-Ch3".

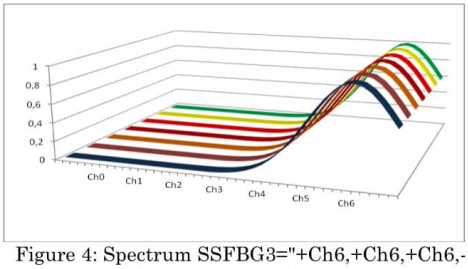

Figure 4: Spectrum SSFBG3="+Ch6,+Ch6,+Ch6,-Ch6,-Ch6+Ch6,-Ch6".

Analyzing the autocorrelation and cross-correlation properties of the SSFBG, (Figures 5 and 6 respectively), we notice that all configurations present good autocorrelation and cross-correlation properties, with configuration SSFBG3 presenting slightly worse autocorrelation, but still presenting a very distinctive in-phase peak. All configurations present a minimum power contrast ratio equal to 12.3 dB. The average power contrast ratio (defined as P/W=20.log[Peak(Correlation)/Average(Correlation)]), is much larger and equal to 30.0 dB. The Worst Error Probability has been found to be $\max\{P_e\} = 5.10^{-5}$.

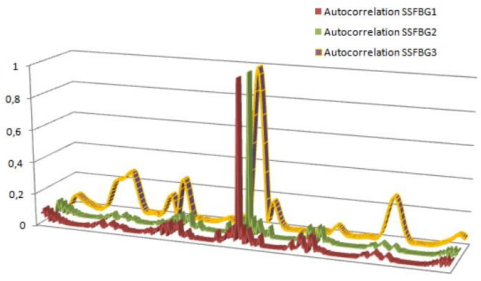

Figure 5: Normalized autocorrelation, in time domain, with SSFBG1, SSFBG2, and SSFBG3.

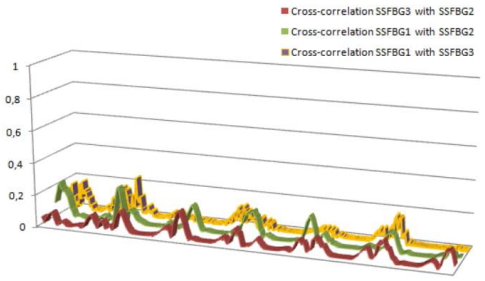

Figure 6: Normalized cross-correlation, in time domain, with SSFBG1, SSFBG2, and SSFBG3.

IV. TUNABLE SSFBG ERROR PROBABILITY

To simplify the study and analysis of the tunable SSFBG error probability, we chose to consider only bipolar codes (with two phases: 0 and π). The chip +1 is coded with a phase 0 and the chip -1 is coded with the phase π. The worst case to be considered is when the 7 chips are coded in the same wavelength channel. Then, the phase modulation is simply a BPSK modulation and the system to be analyzed is a TS-OCDMA-PON system with coherent coding and decoding making use of bipolar codes. The error probability P_e may be used to find an upper bound for an OCDMA system. This P_e upper bound $\max\{P_e\}$ can be a function of the cross-correlation power contrast ratio $P/C = 20\log\left[C_k(0)/\max\{C_{k,i}\}\right]$ (in dB), where $C_{k,i}$ is the cross-correlation and C_k is the autocorrelation [2]. Some P/C upper bounds, for periodic correlations, have been found. One of them is the Welch bound [16] of K perfect sequences of length N: $P/C = 20\log\sqrt{\frac{KN-1}{K-1}}$. For the aperiodic correlation case, the upper bound is $P/C = 20\log\sqrt{\frac{2KN-K-1}{K-1}}$.

For a good communication system, the code set selected should have a high P/C value. For example, it has been suggested that the SSFBG should have power contrast ratios higher than 17 dB for 127-chips Gold codes [17].

In this study, we consider the upper bound of the error probability [2] that is a function of the power contrast ratio P/C:

$$\max\{P_e\} \approx 1-\phi\left[\left(\frac{N_0}{2E_b}+(K-1)\left(1-\frac{1}{N}\right)10^{-\frac{P/C}{10}}\right)^{-1/2}\right]. \quad (13)$$

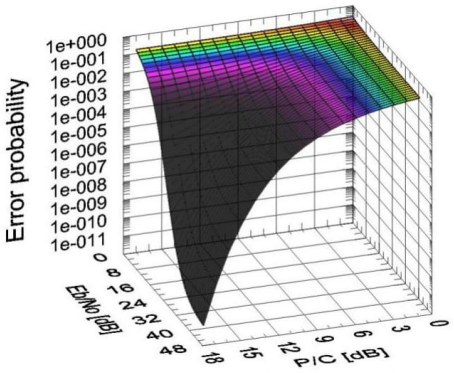

Figure 7: 3D representation of the probability error upper bound with tunable SSFBG.

Figure 7 shows a 3D representation of the upper bound (13), for K = 2 users and the length is N = 7 x 7 chips. For example, the error probability upper bound is lower than 10^{-5} when the two ratios P/C and E_b/N_o are at least equal to 12.3 dB. E_b is the bit energy and N_o is the spectral density of additive white Gaussian noise (AWGN). This situation requires a bit error correction method to guarantee an error free transmission. However, we should remember that (13) gives us the worst case error probability. Frequently, the error probability average is utilized and, of course, this average will be much lower than the worst case (13).

Finally, we should remember that the selection of the appropriate codes, the SSFBG ultraviolet light writing precision, and the precision of the optical communication synchronization (sampling operation) are important when we want to design a gigabit OCDMA-PON transmission system with low BER over more long distances.

V. Conclusions

In this paper, a new tunable super-structured fiber Bragg grating (SSFGB) was developed by using stress-responsive colloidal crystals. A new SSFBG codec with nanoparticles has been simulated with short Maximal-Length sequence. Using a mathematical model, we found that the novel tunable SSFBG is similar to a codec of perfect sequences. These sequences are, by definition, immune to multipath interferences.

Our proposed WDM-OCDMA system with coherent coding and decoding process has been evaluated with an error probability based on the power contrast ratios of some code sets. The good results obtained allow the conclusion that the new tunable SSFBG, with colloidal crystals and perfect sequences, will be a simple solution for WDM-OCDMA communications, when the optical coding and decoding processes require temperature stability and multiplexing capacity.

References

1. H. Ding, Y. Cheng, H. Gu, Y. Zhao, B. Wang, and Z. Gu: Tunable fiber Bragg grating based on responsive photonic crystals, *Nanoscale Communication* (RSCPublishing), 5, 11572 (2013).
2. J. Pereira, H. A. Silva, Error probability upper bound for perfect sequences implemented with super-structured fibre Bragg gratings, *IET Signal Processing*, 8, 4, 421-428 (June, 2014).
3. R. Matsumoto, T. Kodama, S. Shimizu, R. Nomura, K. Omichi, N. Wada, and K. Kitayama, 40G-OCDMA-PON System With an Asymmetric Structure Using a Single Multi-Port and Sampled SSFBG Encoder/Decoders, *Journal of Lightwave Technology*, 32, 6 (March 15, 2014).
4. Francis Idachaba, Dike U. Ike, and Orovwode Hope, 'Future Trends in Fiber Optics Communication' *Proceedings of the World Congress on Engineering 2014*, Vol I, WCE 2014, July 2 - 4, 2014.
5. Cedric Lam: 'Passive Optical Networks, Principles and Practice' (*Elsevier*, 2007).
6. Salehi, J. A., Weiner, A. M., and Heritage, J. P.: 'Coherent Ultrashort Light Pulse Code Division Multiple Access Communication Schemes', *J. Lightwave Technol*., Mar. 1990, 8, (3), pp. 478-491
7. Prucnal, P., Santoro M., and Fan T.: 'Spread spectrum fiber-optic local area network using optical processing', *IEEE J. Lightwave Technol*., May 1986, 4, (5)
8. Santoro, M. A., and Prucnal, P. R.: 'Asynchronous fiber optic LAN using CDMA and optical correlation', *Proc. IEEE*, Sept. 1987, 75, (9)
9. Katsunari Okamoto, 'TUTORIAL REVIEW Recent progress of integrated optics planar lightwave circuits ', *Optical and Quantum Electronics*, 1999, 31, pp. 107-129
10. Z. Jiang, et al., 'Four-User 10-Gb/s Spectrally Phase-Coded O-CDMA System Operating at ~30fJ/bit', *IEEE Photon. Tech. Lett.*, 2005, 17, pp. 705-707
11. Xaveer J. M. Leijtens, Berndt Kuhlow, and Meint K. Smi, 'Arrayed Waveguide Gratings', pp. 1-63, http://alexandria.tue.nl/openaccess/Metis203741.pdf, accessed April 2013.
12. Erdogan T.: 'Fiber grating spectra', *J. Lightwave Technol.*, Aug. 1997, 15, (8), pp. 1277-1294
13. Sebastien Blais, 'Superstructured Fiber Bragg Gratings and Applications in Microwave Signal Processing', Ottawa, Canada, 2014. https://www.ruor.uottawa.ca/bitstream/10393/30358/3/Blais_Sebastien_2014_thesis.pdf
14. Teh, P.C., Ibsen, M., Fu, L. B., Lee, J. H., Yusoff, Z., and Richardson, D. J.: 'A 16-channel OCDMA system (4 OCDM x4WDM) based on 16-chip, 20 Gchip/s superstructure fiber Bragg gratings and DFB fiber laser transmitters', *Proc. Optical Fiber Communication Conf.* (OFC'2002), Los Angles, CA, ThEE1, pp. 600–601
15. J. Pereira, Sequências perfeitas para sistemas de comunicação, *Novas Edições Acadêmicas*, Saarbrücken, 2015.
16. Sarwate, D., Pursley, M.: 'Crosscorrelation Properties of Pseudorandom and Related Sequences', *Proceedings of the IEEE*, May 1980, 68, (5), pp. 593 – 619.
17. Wang, X., Matsushima, K., Nishiki, A., Wada, N., and Kitayama, K.: 'High reflectivity super structured FBG for coherent optical code generation and recognition', *Opt. Express*, Nov. 2004, 12, (22), pp. 5457- 5468.

[P7] - M. Gasparovic, P. Nicolau, A. Marques, C. Silva, L. Marcelino, On Privacy in User Tracking Mobile Applications, Information Systems and Technologies (CISTI), 2016 11th Iberian Conference, 16191805, 5-18 June 2016.

On Privacy in User Tracking Mobile Applications

Marko Gašparović[1], Pedro Nicolau[1], Ana Marques[1], Catarina Silva[1], Luis Marcelino[1]

[1]Polytechnic Institute of Leiria School of Technology and Management Leiria, Portugal

{2152124, 2150119, 2151668}@my.ipleiria.pt, {catarina, luis.marcelino}@ipleiria.pt

Abstract: In mobile applications, tracking a user with Global Positioning System (GPS) can be very beneficial, making life easier for the user, by e.g. finding points of interest around the user, such as gas stations, super markets, restaurants etc. Nevertheless, the location of the user can be misused and hence privacy issues can become a relevant problem in mobile application development. Technically, location is determined either internally by the device or externally by interacting systems and networks. The resultant location information may be stored and used under various conditions and applications can track the position of the user without his/her consent and eventually misuse it for instance with the intent of sending redirected publicity or even getting logs of the user's location. However, the user's location may not always be obtained using the most precise location function available. In this work we discuss and propose different options to choose how accurate geo localization in an application can be and uphold that it is up to the developer to decide what is the appropriate method to choose or give the user the freedom to define his/her privacy thresholds. These thresholds can be extremely variable both between users and scenarios, and we present a survey to approach this issue. best mode to work with is. Results show that users are concerned with privacy issues, but they are necessarily acting accordingly to keep their privacy at a high level of protection. Finally we point out that developers shouldn't misuse possibilities of tracking and users should be more cautious with application permissions as will be shown in a real case study.

Key words: **GPS, geo-localization, positioning system, geo-localization, user tracking, privacy.**

I. Introduction

In today's world users are greatly dependent on their smartphones, at a point that sometimes they forget about privacy and how much data they make available to others by accepting permissions, privacy policies etc. This can be a big problem considering that in the near future, by 2020, it is predicted to be nearly 50 billion devices connected to internet [1]. In such a mobile world, this means users will not be obliged to accept application permissions just on their smartphones, it is going to be on smart TVs, smart watches and smart glasses among others. Sometimes, these permissions do not respond to a real need for the application to function, but serve to create an advertising environment that adapts the location and user's interests. The users take several risks when they systematically accept these permissions. They are exposing their location or their internet habits, and the final destination of this data sometimes is not clear. We made testing with different geo-location precision test which we set programmatically and we will compare and examine obtained results. We also report on a user study in which we investigate how much different users of mobile applications care about their privacy.

In the next section we will present state of the art and introduce what different privacy issues in the field of mobile application's permissions as well as geo-localization. Afterwards in the third section, we will talk about location services precisions, how to get user's location and different accuracy options. In the fourth section we will present user test on user privacy and compare them. Finally, we will discuss the results obtained from the location services precision tests and based on the result present final conclusions.

II. State of the art

Since the application market drastically extended, there have been many problems related to malicious application that leak user's private information stored in own smart device [2]. In 2012 it was revealed that *Path* application automatically uploaded smartphone users' entire address books to its servers. This resulted in public outcry that led the platform provider to revise their permission model [3]. Other prior work has found that many Android and iOS applications share the user's location with third parties and expose the device identifier to trackers [4]. This behaviour is part of everyday applications rather than malware, and it occurs in spite of the existing permission architecture. From the 2010, unfortunately, the growth in the Android platform has triggered the interest of unscrupulous application developers. Android grayware collects excessive amounts of

personal information (e.g., for aggressive marketing campaigns), and malware harvests data or sends premium SMS messages for profit. Grayware and malware have both been found in the Android Market, and the rate of new malware is increasing over time [5]. Since we are becoming surrounded by applications on a different devices, it is becoming obvious that high technology products are not the only thing users' wants to have. With a good product user is also interested in how much privacy does device provides. Application privacy research has produced many useful tools to analyse the privacy-related behaviours of mobile apps. However, these automated tools cannot assess people's perceptions of whether a given action is legitimate, or how that action makes them feel with respect to privacy. Application permission differentiate between iOS and Android. In the older versions of Android users had to accept all the permissions in order to install application. If the permissions are not accepted it was not possible to install the application. Users of iOS devices have always had possibility to install application without accepting any permissions and when some permission needs to be used alerts the user. User could then accept that permission or reject it. In the newest version of Android OS 6.0 – Marshmallow, users have also this option and more, they can choose which permission they never want to share with the application.

III. Location services precision

In order to get the position of the users by taking the data internally from the GPS or externally by systems and networks it is developers duty to decide what is the best precision for application to work. In the programming languages for iOS and Android there are particular levels of precisions to get the best information for the application and yet to reduce privacy issues, as well as save phones battery.

A. Getting the user's location

There are two options for configuring location-related services [6]:

- Use the standard location service, which allows you to specify the desired accuracy of the location data and receive updates as the location changes.
- Use the significant location change service, which provides a more limited set of tracking options but offers significant power savings over the standard location services.

There are several specific functionalities when programming mobile applications for iOS or Android where developer can set the different precisions of the location services. The Location Manager class is the central point for configuring the delivery of location and heading-related events. A Location Manager object provides tracking large or small changes in the user's current location with a configurable degree of accuracy [7] [8]. This configurable degree of accuracy is explained more detailed in the chapter III.C where we will see the difference between degrees of accuracy.

B. Ways of getting user location

There are different ways of getting the users position depending on amount of accuracy application needs to use.

a) Network – based
Location can be determined using the service provider's network infrastructure. The accuracy of network-based techniques varies, such as cell identification and triangulation. [9]

b) Handset-based
This technique determines the location of the handset by putting its location by cell identification, signal strengths of the home and neighbouring cells, which is continuously sent to the carrier. [9]

c) Wi-Fi
Typical parameters useful to geo-locate device is getting the Wi-Fi hotspot's the SSID and the MAC address of the access point where the device is currently connected. [10]

d) GPS
The best and most precise technique of getting users' location. It uses a network of about 30 satellites orbiting the Earth and each one transmits information about its position and the current time at regular intervals. These signals, travelling at the speed of light, are intercepted by GPS receiver. [11]

C. Desired accuracy

Some of generic function both in iOS and Android:

a) Best For Navigation
b) Hundred Meters
c) Kilometer
d) Three Kilometers

Developers should assign one of these values to the desired accuracy property for usage in certain scenario. Depending on the information about user's location needed developers should use corresponding value and this is where some of the developers misuse this option. If the high accuracy is not needed, then developer should specify accuracy *Kilometer* and not accuracy *BestForNavigation*. Determining a location with greater accuracy requires more time, more power and less privacy for the end user.

IV. SURVEY ON USER PRIVACY

When it comes to privacy one big part have the users themselves. It is important to see how much people care about their private information and how comfortable they are with revealing that data to the application. We performed a privacy study with 40 participants of which 21 males and 19 females. In this test our main goal was to determine what the amount of concern is among people when it comes to privacy related to a user location. In this study we wanted to cover the real purpose of the test which is privacy about user location and set up the questions related to privacy in general so the participant is not aware of the fact that main goal of the test is about location privacy, therefore, study is much more secure of having the correct and satisfying results. Additionally we found out some other interesting facts that we presented later in this paper.

A. Internet survey – results and discussion

This internet survey about mobile application was consisted of 10 questions where 8 questions regarding mobile privacy. In the first two questions we wanted to find out the gender of the participant and the group age where they match. Question regarding how comfortable users are about revealing certain data were about:

- Favorite TV show
- Full name
- Age
- Phone number
- Precise location
- Do they check application permissions
- Are the application permissions important do them
- Are they concerned about their privacy

We had 40 participants of which 52.5% were males and 47.5% females. As we can see on the Figure 1 the most substantial age group was between ages 24 and 29 where we have 21 users. Second largest group was between ages 18 and 23 and after that follows 30 – 35 group and we had no one who was more than 40 years old. Since we are dealing here most with the young age groups this is not a representation of all age groups, but it is a rather representation of the users between ages 18 and 35.

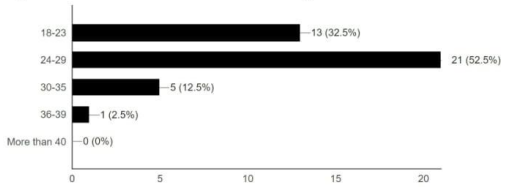

Figure 1 – Age groups

In this research our gudline was the graph from AT&T Labs-Research Technical Report from year 1999 concerning what is the procentage of comfort zones for the person and for the person's child [12]. As shown in the Figure 2 we can see that comfort levels for insensitive data such as Favorite TV show or Favorite snack has reasnobly high percentage, whereas for sensitive data such as social security and credit card people tend to care much more and to reveal that data they don't feel as much as safe.

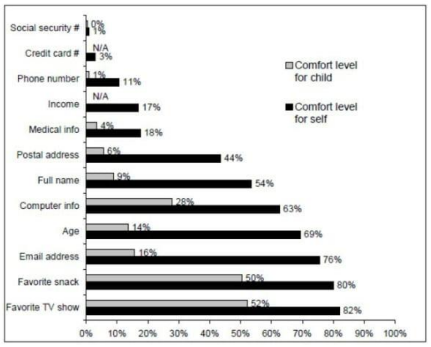

Figure 2 - Comfort levels

In our reseach we wanted to compare this graph on the Figure 2 with the new data which we would get and the results are explained further in the section. We also emphasize that all the survey presented is about mobile application privacy and how comfortable they are about revealing certain data to the application if they need to use it. For all the questions regarding how comfortable they are we had 5 levels of comfort.

a) Very comfortable
b) Comfortable
c) Neither
d) Uncomfortable
e) Very uncomfortable

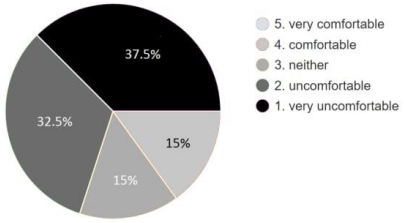

Figure 3 - Comfort of revealing precise location to the app

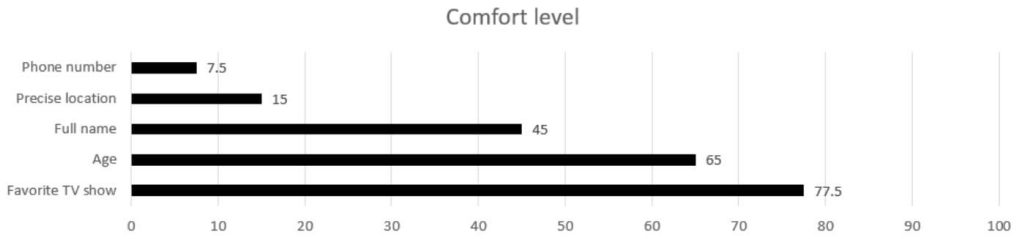

Figure 4 - Levels of comfort

Concering favorite TV show our results showed us that results in two research are consistant and that people are not over concerned about reveling this kind od data - 77.5%, but some of the particapants responded they are not comfortable matching the results with the Figure 2. Revealing their age most of the people 67.5% said that they have nothing against revealing their age to the app. Regarding the question about users reveling their own full name we got devided opinions. Most of them, 45% declared as comforbale, 35% not comfortable and 20% were neither comfortable or uncomfortable. With the revealing their phone number people are not comfortable. 45% said that they are very uncomfortable and 32.5% uncomfortable and that makes high 77.5% of people would not feel comfortable about revealing their phone number.

As we can see in the Figure 3 most of the participants, 37.5% are very uncomfortable and 32.5% uncomfortable about revealing their precise location to an app. Just 15% said that they are comfortable.

Of all the questions made, precise location was one of the most delicat one and concering privacy about the geo-locating topic particapants would almost not reveal their location with ease. Since this was our main goal of the research we wanted to find out how much users actually care when it comes to actual applications. We can see that the some of the problems comes from the users themselves since we didn't get so satisfying results when it comes to checking application permissions before installing one.

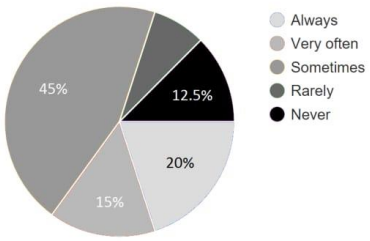

Figure 5 - Application permission checking

In the Figure 5 we see that percentage of people who never, rarely and sometimes check application permission is veryhigh, making it together 62%. But on the other hand when we asked are they concerend about their privecy when thinking about mobile application, 30% of them responded how they are very concerned and 17.5% extremely concerned and yet most of them don't check permissions.

If we look at Figure 4 we see levels of comforts of participants from our survey. We took percentage of *Very comfortable* and *Comfortable* summed them and put them in the Table 1 column '*Our survey'* to compare it with Figure 2 that is, with column *'AT&T report'*. Privacy concerns with phone number, full name, age and favorite TV show are fairly the same with some minor differences. In all fields mentioned above, our survey shows slight decrease of the level of comfort, hence people are slightly more concerned about their privacy. We made a comparison between users' postal address (AT&T report, year 1999) and precise location (Our survey, year 2016) but they are rather distinct values. We considered that we could compare these two values since in that time postal address was important as precise location today, but from the AT&T report we see that users are far less worried about revealing their postal address than precise location from our survey.

Table 1 - Comparison between our survey and AT&T report

Different information	Levels of comfort	
	Our survey	AT&T report
Phone number	7.5%	11%
Precise location / postal address	15%	44%
Full name	45%	54%
Age	65%	69%
Favorite TV show	77.5%	82%

B. Geo-location percision tests and discussion (iOS device)

In this chapter we present the tests for a different geo-location precision levels within the programming language Swift. Since iOS always uses the best precision possible if the location services are on, we had to programmatically set random values in the area of chosen precision, i.e. if we set a precision *HunderdMeters* iOS will always get the best precision, only thing that changes is radius around the user,

so we generated a random position within that area (radius) to imitate users' location to reduce location services precision therefore mitigate privacy issues. In these testings' we have used an iPhone 4S with its different location services precisions with application about finding nearest bars around users' position. From our testing we used three different localization precisions:

a) Best
b) Hundred Meters
c) Three Kilometers

Precision best is the standard GPS based position system for getting the most accurate position of the user. For options hundred meters we have a radius of hundred meters where the application gets the position of the user as explained above and also Three Kilometers with the same characteristics, but different radius value. This testing showed us that if location services are on, phone will always use the best one, so we forced localization to be 'more inaccurate' where this precision value can be set in the settings of the application with the precision as user needs. However, when set on Three Kilometers option we sometimes got imprecise values of the user location missing for around two kilometers and more so based on that application gave us bars in that area, which is not a useful information for the user.

V. Conclusions

In the field of mobile application privacy concerning the position of the user it is hard to have a satisfactory defined rules, but it is important to establish satisfying relation between how much accuracy certain application use and how much does it actually need. As we can see in the performed testing with the users the most privacy troubles comes from the user itself since they do not spend enough time on questioning certain application permissions. If certain application does not require precise geo-localization, developers should not misuse the data gotten from the phone of the users for other purposes. From our geo-location tests we found out that it is not always required to use high precision accuracy all the time and most of the applications can work with the same functionalities even when the geo-localization is not the most precise one.

VI. Bibliography

[1] Cisco, "Internet Of Things Will Deliver $1.9 Trillion Boost To Supply Chain And Logistics Operations," 2015. [Online]. Available: http://newsroom.cisco.com/press-release-content?articleId=1621819. [Accessed: 01-Jan-2015].

[2] S. Kim, J. I. Cho, H. W. Myeong, and D. H. Lee, *A study on static analysis model of mobile application for privacy protection*, vol. 114. Dordrecht: Springer Netherlands, 2012.

[3] Cnet, "Path to pay $800,000 to settle privacy issues with FTC," 2013. [Online]. Available: http://www.cnet.com/news/path-to-pay-800000-to-settle-privacy-issues-with-ftc/. [Accessed: 01-Jan-2015].

[4] G. Egele, M., Kruegel, C., Kirda, E., Vigna, "PiOS Detecting privacy leaks in iOS applications," *Proc. 18th Annu. Netw. Distrib. Syst. Secur. Symp. NDSS 2011*, p. 11, 2011.

[5] A. P. Felt, M. Finifter, E. Chin, S. Hanna, and D. Wagner, "A survey of mobile malware in the wild," *Proc. 1st ACM Work. Secur. Priv. smartphones Mob. devices - SPSM '11*, pp. 3 – 14, 2011.

[6] Apple, "CLLocationManager Class Reference." [Online]. Available: https://developer.apple.com/library/mac/documentation/CoreLocation/Reference/CLLocationManager_Class/. [Accessed: 12-Feb-2016].

[7] Android, "LocationManager | Android Developers," 2016. [Online]. Available: http://developer.android.com/reference/android/location/LocationManager.html. [Accessed: 17-Feb-2016].

[8] Apple, "CLLocationManager Class Reference," 2015. [Online]. Available: https://developer.apple.com/library/ios/documentation/CoreLocation/Reference/CLLocationManager_Class/. [Accessed: 17-Feb-2016].

[9] eTutorials.org, "Mobile Positioning Techniques :: Chapter 17: Location-Based Services :: Part Four: Beyond Enterprise Data :: Mobile and wireless design essentials :: Mobile devices :: eTutorials.org." [Online]. Available: http://etutorials.org/Mobile+devices/mobile+wireless+design/Part+Four+Beyond+Enterprise+Data/Chapter+17+Location-Based+Services/Mobile+Positioning+Techniques/. [Accessed: 17-Feb-2016].

[10] about tech, "How Does a Wi-Fi Positioning System Work?" [Online]. Available: http://gps.about.com/od/glossary/g/wifi_position.htm. [Accessed: 17-Feb-2016].

[11] physics.org, "How does GPS work?| Explore | physics.org." [Online]. Available: http://www.physics.org/article-questions.asp?id=55. [Accessed: 17-Feb-2016].

[12] AT&T Labs, "Beyond Concern: Understanding Net Users' Attitudes About Online Privacy," 1999.